Final Technical Report

April 1992

Optical Computing and Optical Signal Processing

(Phase I)

Contract Number: F49620-91-C-0090

DTIC
ELECTE
MAY 1 9 1992
S A D

Performed For

AFOSR/NC

Bolling Air Force Base, DC 20332-6448

E-Tek Dynamics, Inc.

1885 Lundy Avenue

San Jose, California 95131

COMPLETED PROJECT SUMMARY

TITLE: Optical Computing and Optical Signal Processing

PRINCIPAL INVESTIGATOR: J.J. Pan

INCLUSIVE DATES: October 1991 to April 1992

CONTRACT/GRANT NUMBER: F49620-91-C-0090

SENIOR RESEARCH PERSONNEL:

JUNIOR RESEARCH PERSONNEL:

PUBLICATIONS: A technical paper has been prepared for publication.

ABSTRACT OF OBJECTIVES AND ACCOMPLISHMENTS:

Highly efficient nonlinear optical materials (NOMs) are required for optical computing and optical signal processing. However, currently, no such NOMs are practically available. In this project, new organic NOMs have been researched and developed. New organic NOM design principles and approaches have been reviewed and investigated to optimize the nonlinear optical performance. Four newly home-designed organic materials, namely, CMVI, DVDA, MOHNS and HOMNS have been synthesized and purified. Nonlinear optical responses, such as second-order and third-order nonlinearities, optical transparencies and melting points have been measured and characterized. Device fabrication and application of organic NOMs for optical computing and optical signal processing have also been investigated.

In this Phase I period, E-Tek has successfully demonstrated the capability of research and developing new organic NOMs for optical computing and optical signal processing. Four preliminarily selected and newly home-designed NOMs have been developed. In the next period, we would like to continue to put emphasis on optimizing the organic NOMs. Device fabrication of, NOMs, such as polymer, thin film, single crystal, will be investigated and developed for the application of optical computing and optical signal processing.

REPORT DOCUMENTATION PAGE

Public reporting burden for this collection of information is estimated to average 1 hour per response, including the time for reviewing instructions, searching existing data sources, gathering and maintaining the data needed, and completing and reviewing the collection of information. Send comments regarding this burden estimate or any other aspect of this collection of information, including suggestions for reducing this burden, to Washington Headquarters Services, Directorate for Information Operations and Reports, 1215 Jefferson Davis Highway, Suite 1204, Arlington, VA 22202-4302, and to the Office of Management and Budget, Paperwork Reduction Project (0704-0188), Washington, DC 20503.

1. AGENCY USE ONLY (Leave blank)	2. REPORT DATE 05/01/92	3. REPORT TYPE AND DATES COVERED Final Technical Report (10/91 – 04/92)

4. TITLE AND SUBTITLE Optical Computing and Optical Signal Processing	5. FUNDING NUMBERS 63218C 1602 01
6. AUTHOR(S) J.J. Pan	

7. PERFORMING ORGANIZATION NAME(S) AND ADDRESS(ES) E-Tek Dynamics Incorporated 1885 Lundy Avenue, Suite 103 San Jose, CA 95131	8. PERFORMING ORGANIZATION REPORT NUMBER

9. SPONSORING/MONITORING AGENCY NAME(S) AND ADDRESS(ES) AFOSR/NC Building 410 lling AFB DC 203326448	10. SPONSORING/MONITORING AGENCY REPORT NUMBER F49620-91-C-0090

11. SUPPLEMENTARY NOTES

12a. DISTRIBUTION/AVAILABILITY STATEMENT APPROVED FOR PUBLIC RELEASE; DISTRIBUTION IS UNLIMITED.	12b. DISTRIBUTION CODE

13. ABSTRACT (Maximum 200 words)

High efficient nonlinear optical materials (NOMs) are highly required for optical computing and optical signal processing. However, currently no such practical NOMs are available. In this project, new organic NOMs have been researched and developed. New organic NOM design principle and approach have been reviewed and investigated. Four new organic NOMs, namely, CMVI, DVDA, MOHNS and HMONS have been synthesized and purified. Nonlinear optical responses of these four samples have been demonstrated and preliminary been characterized. Device fabrication and application for optical computing and optical signal processing have been investigated.

14. SUBJECT TERMS Nonlinear optics, organic materials, conjugation, polymer, transparency, nonlinear response device.	15. NUMBER OF PAGES 130
	16. PRICE CODE

17. SECURITY CLASSIFICATION OF REPORT Unclassified	18. SECURITY CLASSIFICATION OF THIS PAGE Unclassified	19. SECURITY CLASSIFICATION OF ABSTRACT Unclassified	20. LIMITATION OF ABSTRACT

Table of Contents

Table of Contents
(Continued)

Table of Contents
(Continued)

List of Figures

List of Figures
(Continued)

ah-64444FR-LF

List of Figures
(Continued)

ah-64444FR-LF

List of Figures
(Continued)

List of Figures
(Continued)

ah-64444FR-LT

List of Tables
(Continued)

1.0 Introduction

This report presents the Phase I research and development (R&D) result of new organic materials as third-order nonlinear Optical materials other than reported. The work described here was performed over the period of October, 1991 through April, 1992.

The description of 1990 Small Business Innovative Research (SBIR) research topic number SDIO 91-011 entitled "Optical Computing and Optical Signal Processing" is stated in SBIR solicitation announcement as:

> Description: Dense computing capability is sought in all architectural variation, from all optic to hybrid computers. Specific examples of areas to be addressed include, but are not limited to, high speed multiplexing, monolithic optoelectronic transmitters, holographic methods, reconfigurable interconnects, optoelectronic circuits, and any other technology contributing to advance in intracomputer communications, optical logic gates, bistable memories, optical transistors, and power limiters. In particular, nonlinear optical materials advancements and new bistable optical device configuration are of interest.

Many nonlinear optical materials of large second-order susceptibility have been developed for use of second-harmonic generation and optical modulation. Although the studies of the third-order nonlinear optical materials have been extensively carried out. Still less highly third-order nonlinear materials

responding in the femto-second time region and nonabsorbing in red-to-green wavelength region have been investigated and developed.

Semiconductors, ferroelectric oxides, cubic oxides (sillenites) and organic materials are the most types of nonlinear optical materials that provide third-order optical nonlinearities.

Ferroelectric oxide crystals, such as $LiNbO_3$, $LiTaO_3$, $KTa_{1-x}Nb_xO_3$ (KTN), $BaTiO_3$, $KNbO_3$, $Sr_{1-x}Ba_xNb_2O_3$ (SBN), $Ba_2NaNb_5O_{15}$ (BNN), and $Ba_{1-x}Sr_xK_{1-y}Na_yNb_5O_{15}$ (BSKNN), crystallographic structures varies considerably from one group of materials to another.

$LiNbO_3$	Ilmenite
SBN	Tungsten Bronze
$BaTiO_3$	Perorskite

However, ferroelectric oxides have several properties in common. They are transparent from the band gap (~ 350 nm) to the intrinsic absorption edge around 4.5 μm. They are most sensitive at visible wavelengths and their quadratic electro-optic coefficients are lower than semiconductors and organic compounds.

Ferroelectric oxides are hard (7 mohs and higher), non-hygroscopic materials, and these properties are highly advantageous for the preparation of optical quality surfaces. Their linear and nonlinear dielectric properties are inherently

ah-44FR-TX

temperature dependent because of their ferroelectric nature.

Cubic oxides of the sillenites family, consist of $Bi_{12}SiO_{20}$, $Bi_{12}GeO_{20}$, and $Bi_{12}TiO_{20}$ (BSO, BGD, and BTO) are cubic with the point group symmetry 23 (or T). Thus, in the absence of electric fields, sillenites exhibit no linear birefringence. But, since the 23 space group lacks a center of inversion symmetry, the sillenites exhibit electrically induced birefringence. These three materials are very similar. Electro-optic coefficients range from 4 to a little over 5 $pm.V^{-1}$ at visible wavelengths. The linear electro-optic effect in the sillenites is characterized by three equal coefficients γ_{41}, γ_{52}, and γ_{63}. Careful measurements in BSO yield γ_{41} = 4.5 pmV^{-1} at $450\mu m$.

Optical nonlinearity in semiconductors and organic compound has been studied extensively because some of these materials have very high third-order nonlinearities. Optical bistability has been observed in many organics, mainly in dyes and liquid crystals, as well as in series of semiconductors, such as GaAs, InSb, GaAs/AlGaAs multiple quantum well structure (MQWS), InAs, CdS, ZnSe and CuCl. The optical Kerr coefficient n_2, defined by $n = n_1 + n_2I$, where I is the optical intensity

Although semiconductors are known to have higher third-order effects than those of organics, some organic and polymer materials have demonstrated large third-order susceptibilities and may find some special applicants. The third-order susceptibilities of some organics are listed in Table 1.1, together with data for GaAs and

3

Table 1.1

Third-Order Susceptibilities of Some Organics and Semiconductors

Molecule	$\gamma(10^{-36} esu)$	$x^{(3)}(10^{-14} esu)$
aniline	7.78	32
nitrobenzene	43.3	1.67×10^2
m-nitroaniline	85	3.32×10^2
o-nitroaniline	123	4.83×10^2
p-nitroaniline	496	1.97×10^3
polydiacetylene-PTS		1.6×10^4 [a]
polydiacetylene-TCDU		3.7×10^3 [a]
trans-retinal	100 [b]	
cis-trans bixine	300 [b]	
dodecapreno-beta-carotene	1.7×10^4 [b]	
trans-beta-carotene	1.4×10^3 [b]	
paradimethylamine-1-pheny 1,4-nitrobutadiene (DAM-PNB)	2.8×10^4 [c]	
GaAs		1.2×10^3 [d]
InSb		5×10^3 [d]

[a] At 2.62μm, [b] At 1.89μm, [c] At 1.06μm, [d] Far from the band gap

InSb taken far from the absorption edge, where γ is the third-order polarizability of the molecule and $\chi^{(3)}$ is the third-order susceptibility. The values of the $\chi^{(3)}$ measured in polydiacedylene polymers are comparable to those of the inorganic semiconductors. The one-dimensional delocalization that results from the polymerization of diacetylenes produces a dramatic enhancement of the optical nonlinearities of these compounds. TCDU polymer shows an effect about 600 times that of TCDU monomer.

One way to enhance the third-order effect in organics is to extend the conjugated π-bond length. However, the large $\chi^{(3)}$ of those material is due to the resonance effect, which may prevent rapid response time. Additionally, increasing conjugated-chain length results in a red-shift of transparency range. In order to overcome these disadvantages, E-Tek proposed to design new organic materials, other than those reported to data, with high nonlinearity, fast response time and blue-shift of transparency range. These E-Tek newly designed materials are:

- 2-Cyanoethylmethan-Oatevinylindole (CMVI)
- P-1, 1-Dicyanoviny-Dincethylarininoaniline (DVDA)
- 2-Methoxy-5-Nitrophenol (MNP)
- 4-Aminobenzophenone (ABP)
- 3-Acetamido-4-Methoxy-4[1]-Nitrostibene (ACMONS)
- 3-Amino-4-Methoxy-4[1]-Nitrostibene (AMMONS)
- 3-Hydroxy-4-Methoxy-4[1]-Nitrostilbene (HMONS)
- 3-Methoxy-4-Hydroxy-4[1]-Nitrostilbene (MHONS)

5

See Table 1.2. These candidates may have large nonlinearities $\chi^{(3)}$ and fast response time because:
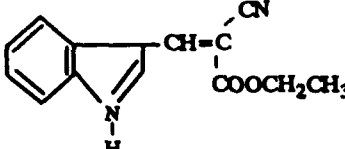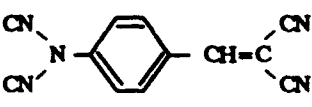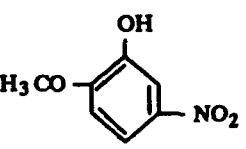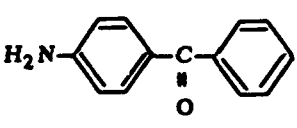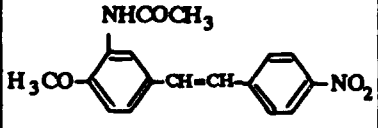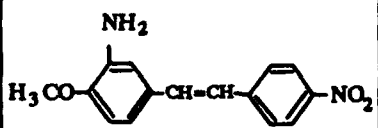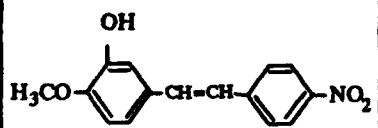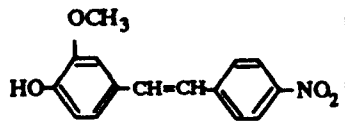
(1) They have polarizable electro configuration, electron donor groups and electron acceptor groups.

(2) They are delocalized π electrode system, charge transfer provides π electron dipole moment.

(3) They are short π conjugated molecules, that lead to broad optical transparence band and fast response time.

(4) High molecular force results in high melting point.

1.1 Phase I R&D Objectives

Phase I technical objective of the research and development of organic materials with high third-order nonlinearities and fast response time are:

- Theoretical studies and design, investigate new organic compounds.

- Investigate the approaches to synthesize those newly designed organic compounds.

- Measure physical chemistry parameters of new materials.

- Demonstrate the second-order and third-order optical nonlinearities by SHG powder effect measurement and Z-scan technique.

- Polymeric form, thin film and device studies and investigation.

Table 1.2
E-Tek Newly Designed Organic Nonlinear Optical Materials

Name	Formula	Absorption Edge (nm)	Powder SHG at 1064 nm Urea = 1	M.P.°C or Damage Threshold
2-Cyanoethylmethan-oatevinylindole (CMVI)	(indole with $CH=C$ substituent bearing CN and $COOCH_2CH_3$)	388 ~ (Calculated)	25	165
P-1, 1-dicyanovinyl-dimethylaminoaniline (DVDA)	$(CN)_2N$—C$_6$H$_4$—$CH=C(CN)_2$	436 ~ (Calculated)	45	180
2-Methoxy-5-nitrophenol (MNP)	H_3CO—(phenol, OH)—NO_2	414 ~ (Calculated)	High	105
4-Aminobenzophenone (ABP)	H_2N—C$_6$H$_4$—$\overset{O}{\underset{}{C}}$—C$_6H_5$	400 ~ 2000 (Measured)	132 x (Urea = 1)	123 30 Gw cm^{-2} (30 PSC Pulse)
3-Acetanido-4-methoxy-4'-nitrostilbene (ACMONS)	H_3CO—(ring, $NHCOCH_3$)—$CH=CH$—C$_6$H$_4$—NO_2			205
3-Amino-4-methoxy-4'-nitrostilbene (AMMONS)	H_3CO—(ring, NH_2)—$CH=CH$—C$_6$H$_4$—NO_2			186
3-Hydroxy-4-methoxy-4'-nitrostilbene (HMONS)	H_3CO—(ring, OH)—$CH=CH$—C$_6$H$_4$—NO_2			
3-Methoxy-4-hydroxy-4'-nitrostilbene (MHONS)	HO—(ring, OCH_3)—$CH=CH$—C$_6$H$_4$—NO_2			

- Phase II proposal.

The R&D investigation results of these objectives will be presented and discussed in the next chapters.

1.2 E-Tek Phase I R&D Project Approach

E-Tek Phase I R&D Project Approach is listed in Figure 1.1.

Theoretical Studies and Design New Organic Materials

Investigate Apporaches To Synthesize These Newly Designed Organic Materials

Synthesize And Purify New Organic Materials

New NOMs

Measure Physicochemistry Properties Of New Materials

Demonstrate The Optical Nonlinearities $x^{(2)}$ and $x^{(3)}$

Device Fabrication Studies And Application Investigation
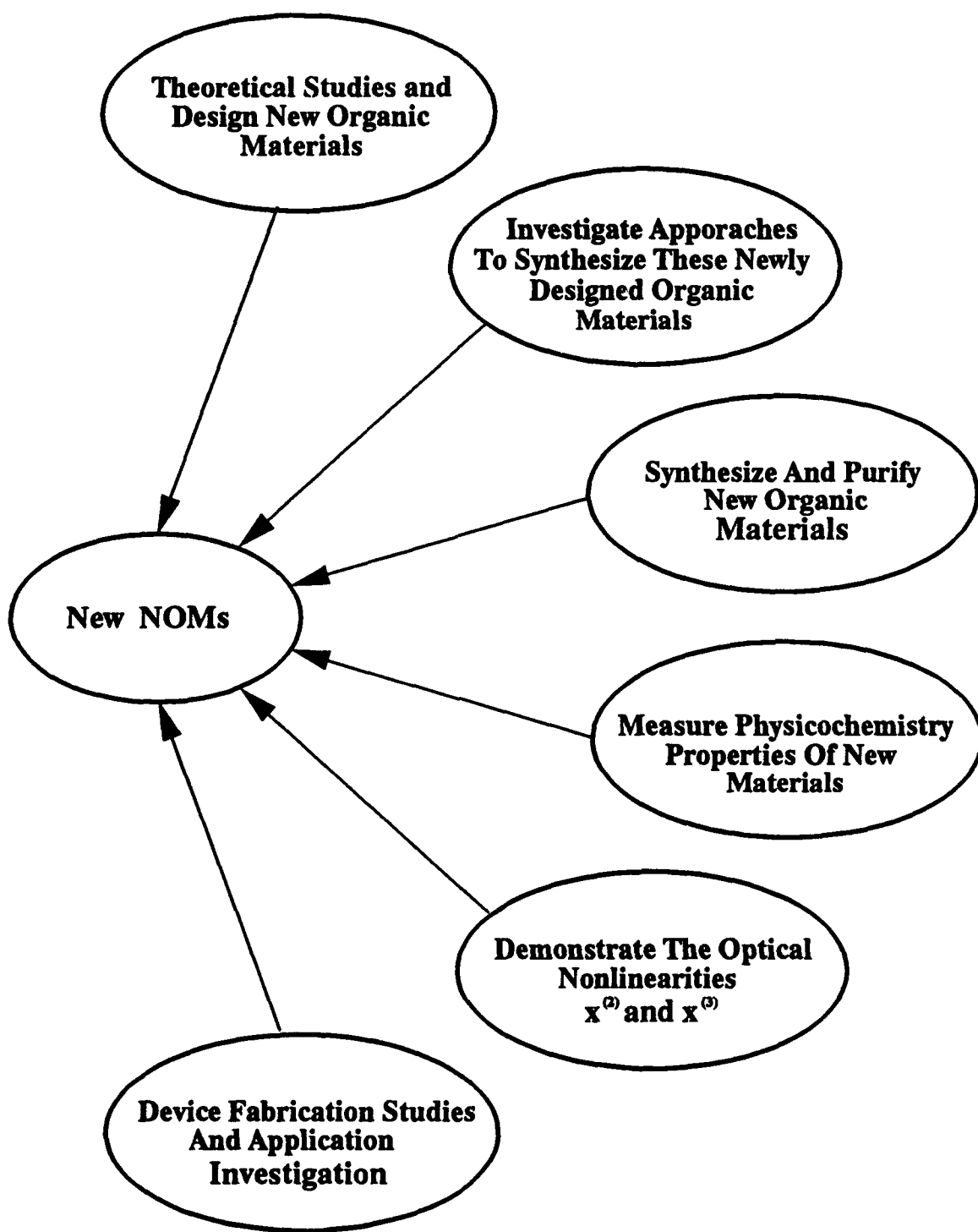
Figure 1.1 E-TEK Phase I R&D Project Approach

61-44pst

2.0 Nonlinear Organic Materials

2.1 Theoretical Concepts of Third-Order Optical Nonlinearities

In this section, the theoretical foundation of the third-order optical nonlinearities and its applications are briefly reviewed to distinguish the key physical parameters of nonlinear materials.

The propagation of optical radiation in a crystal can be described completely in terms of the impermeability tensor η_{ij}, $\eta = \varepsilon_o \varepsilon^{-1}$. The two directions of polarization as well as the corresponding indices of refraction (i.e., velocity of propagation) of the normal modes are found most easily by using the index ellipsoid. The index ellipsoid assumes its simplest form in the principal coordinate system:

$$\frac{x^2}{n_x^2} + \frac{y^2}{n_y^2} + \frac{z^2}{n_z^2} = 1 \qquad (2.1)$$

Where the directions x, y and z are the principal axes - that is, the directions in the crystal along which D and E are parallel. $1/n_x^2$, $1/n_y^2$ and $1/n_z^2$ are the principal values of the impermeability tensor η_{ij}.

According to the quantum theory of solids, the optical dielectric impermeability tensor depends on the distribution of charges in the crystal. The application of an electric field will result in a redistribution of the bond charges and possibly a slight deformation of the ion lattice. The net result is a change

in the optical impermeability tensor. This is known as the electro-optic effect. The electro-optic coefficients are defined traditionally as:

$$\eta_{ij}(E) - \eta_{ij}(0) \equiv \Delta\eta_{ij} = r_{ijk}E + s_{ijkl}E_kE_l$$

$$= f_{ijk}P_k + g_{ijkl}P_kP_l \qquad (2.2)$$

Where E is the applied electric field and P is the polarization field vector. The constants r_{ijk} and f_{ijk} are the linear (or Pockels) electro-optic coefficients. These coefficients are related by the following equations:

$$f_{ijk} = \frac{r_{ijk}}{\varepsilon_k - \varepsilon_o} \qquad (2.3)$$

$$g_{ijkl} = \frac{s_{ijkl}}{(\varepsilon_k - \varepsilon_o)(\varepsilon_l - \varepsilon_o)} \qquad (2.4)$$

Where ε_k, ε_l are the principal optical dielectric constants. Thus the index ellipsoid of a crystal in the presence of an applied electric field is given by:

$$\eta_{ij}(E) \; \chi_i\chi_j = 1 \qquad (2.5)$$

When the electric field vanishes, the index ellipsoid reduces to (2.1.1) since the dielectric tensor ε_{ij} is a symmetric tensor, provided the medium is lossless and optically inactive. η_{ij} must also be a symmetric tensor, provided the medium is lossless and

11

optically inactive. Consequently, the indices i and j in Equation (2.2) can be permuted. The quadratic electro-optic coefficient is given, according to Equation (2.2), by:

$$S_{ijkl} = \frac{1}{2}\left(\frac{\partial^2 \eta_{ij}}{\partial E_k\, \partial E_l}\right)\ E = 0 \qquad (2.6)$$

Since the order of partial differentiation is immaterial, the indices k and l can be permuted. These permutation symmetries are summarized in the following equations:

$$r_{ijk} = r_{jik} \qquad (2.7)$$

$$S_{ijkl} = S_{jikl} \qquad (2.8)$$

$$S_{ijkl} = S_{ijlk} \qquad (2.9)$$

Because of these permutation symmetries, it is convenient to introduce contracted indices to abbreviate the notation. They are defined as:

$$
\begin{aligned}
1 &= (11), \\
2 &= (22), \\
3 &= (33), \\
4 &= (23) = (32), \\
5 &= (13) = (31), \\
6 &= (12) = (21)
\end{aligned}
\qquad (2.10)
$$

ah-44FR-TX1

Using these contracted indices, we can write:

$$r_{1k} = r_{11k},$$

$$r_{2k} = r_{22k},$$

$$r_{3k} = r_{33k},$$

$$r_{4k} = r_{23k} = r_{32k}$$

$$r_{5k} = r_{13k} = r_{31k},$$

$$r_{6k} = r_{12k} = r_{21k},$$

$$k = 1, 2, 3 \qquad (2.11)$$

It is important to remember that the contraction of the indices is just a matter of convenience. These matrix elements (6 x 3) do not have the usual tensor transformation or multiplication properties. The permutation symmetry reduces the number of independent elements of r_{ijk} from 27 to 18, and the number of elements of S_{ijkl} from 81 to 36.

Unlike the linear electro-optic effect, the second order electro-optical effect exists in a medium with any symmetry by using contracted indices (2.11), the equation of the index ellipsoid in the presence of an electric field can be written:

$$x^2 \left(\frac{1}{n_x^2} + s_{11}E_x^2 + s_{12}E_y^2 + s_{13}E_z^2 + 2s_{14}E_yE_z + 2s_{15}E_zE_x + 2s_{16}E_xE_y \right)$$

$$+ y^2 \left(\frac{1}{n_y^2} + s_{21}E_x^2 + s_{22}E_y^2 + s_{23}E_z^2 + 2s_{24}E_yE_z + 2s_{25}E_zE_x + 2s_{26}E_xE_y \right)$$

$$+ z^2 \left(\frac{1}{n_z^2} + s_{31}E_x^2 + s_{32}E_y^2 + s_{33}E_z^2 + 2s_{34}E_yE_z + 2s_{35}E_zE_x + 2s_{36}E_xE_y \right)$$

$$+ 2yz \left(s_{41}E_x^2 + s_{42}E_y^2 + s_{43}E_z^2 + 2s_{44}E_yE_z + 2s_{45}E_zE_x + 2s_{46}E_xE_y \right)$$

$$+ 2zx \left(s_{51}E_x^2 + s_{52}E_y^2 + s_{53}E_z^2 + 2s_{54}E_yE_z + 2s_{55}E_zE_x + 2s_{56}E_xE_y \right)$$

$$+ 2xy \left(s_{61}E_x^2 + s_{62}E_y^2 + s_{63}E_z^2 + 2s_{64}E_yE_z + 2s_{65}E_zE_x + 2s_{66}E_xE_y \right) = 1$$

$$(2.12)$$

The coefficients s_{ij} are usually given in the principal coordinate axes. This new ellipsoid (2.12) reduces to the unperturbed ellipsoid (2.1) when the electric field vanishes. The electric field, in general, changes the the dimensions and orientation of the index ellipsoid. This change is dependent upon the direction of the applied electric field as well as the 6 x 6 matrix elements s_{ij}.

Table 2.1 gives the form of the quadratic electro-optic coefficients for all the crystal classes. The quadratic electro-optic coefficients of some crystals are given in Table 2.2.

ah-44FR-TX1

Table 2.1 Quadratic Electro-Optic Coefficients in Contracted Notation for All Crystal Symmetry Classes

Triclinic:

$$1,\bar{1}$$

$$\begin{pmatrix} s_{11} & s_{12} & s_{13} & s_{14} & s_{15} & s_{16} \\ s_{21} & s_{22} & s_{23} & s_{24} & s_{25} & s_{26} \\ s_{31} & s_{32} & s_{33} & s_{34} & s_{35} & s_{36} \\ s_{41} & s_{42} & s_{43} & s_{44} & s_{45} & s_{46} \\ s_{51} & s_{52} & s_{53} & s_{54} & s_{55} & s_{56} \\ s_{61} & s_{62} & s_{63} & s_{64} & s_{65} & s_{66} \end{pmatrix}$$

Monoclinic:

$$2,m,2/m$$

$$\begin{pmatrix} s_{11} & s_{12} & s_{13} & 0 & s_{15} & 0 \\ s_{21} & s_{22} & s_{23} & 0 & s_{25} & 0 \\ s_{31} & s_{32} & s_{33} & 0 & s_{35} & 0 \\ 0 & 0 & 0 & s_{44} & 0 & s_{46} \\ s_{51} & s_{52} & s_{53} & 0 & s_{55} & 0 \\ 0 & 0 & 0 & s_{64} & 0 & s_{66} \end{pmatrix}$$

Orthohombic:

$$2mm,222,mmmm$$

$$\begin{pmatrix} s_{11} & s_{12} & s_{13} & 0 & 0 & 0 \\ s_{21} & s_{22} & s_{23} & 0 & 0 & 0 \\ s_{31} & s_{32} & s_{33} & 0 & 0 & 0 \\ 0 & 0 & 0 & s_{44} & 0 & 0 \\ 0 & 0 & 0 & 0 & s_{55} & 0 \\ 0 & 0 & 0 & 0 & 0 & s_{66} \end{pmatrix}$$

Tetragonal:

$$4,\bar{4},4/m$$

$$
\begin{pmatrix}
s_{11} & s_{12} & s_{13} & 0 & 0 & s_{16} \\
s_{12} & s_{11} & s_{13} & 0 & 0 & -s_{16} \\
s_{31} & s_{32} & s_{33} & 0 & 0 & 0 \\
0 & 0 & 0 & s_{44} & s_{45} & 0 \\
0 & 0 & 0 & -s_{45} & s_{44} & 0 \\
s_{61} & -s_{61} & 0 & 0 & 0 & s_{66}
\end{pmatrix}
$$

$$422,4mm,\bar{4}2m,4/mm$$

$$
\begin{pmatrix}
s_{11} & s_{12} & s_{13} & 0 & 0 & 0 \\
s_{12} & s_{11} & s_{13} & 0 & 0 & 0 \\
s_{31} & s_{31} & s_{33} & 0 & 0 & 0 \\
0 & 0 & 0 & s_{44} & 0 & 0 \\
0 & 0 & 0 & 0 & s_{44} & 0 \\
0 & 0 & 0 & 0 & 0 & s_{66}
\end{pmatrix}
$$

Trigonal:

$$3,\bar{3}$$

$$
\begin{pmatrix}
s_{11} & s_{12} & s_{13} & s_{14} & s_{15} & -s_{61} \\
s_{12} & s_{11} & s_{13} & -s_{14} & -s_{15} & s_{61} \\
s_{31} & s_{31} & s_{33} & 0 & 0 & 0 \\
s_{41} & -s_{41} & 0 & s_{44} & s_{45} & -s_{51} \\
s_{51} & -s_{51} & 0 & -s_{45} & s_{44} & s_{41} \\
s_{61} & -s_{61} & 0 & -s_{15} & s_{14} & \frac{1}{2}(s_{11}-s_{12})
\end{pmatrix}
$$

$$32,3m,\bar{3}m$$

$$
\begin{pmatrix}
s_{11} & s_{12} & s_{13} & s_{14} & 0 & 0 \\
s_{12} & s_{11} & s_{13} & -s_{14} & 0 & 0 \\
s_{13} & s_{13} & s_{33} & 0 & 0 & 0 \\
s_{41} & -s_{41} & 0 & s_{44} & 0 & 0 \\
0 & 0 & 0 & 0 & s_{44} & s_{41} \\
0 & 0 & 0 & 0 & s_{14} & \frac{1}{2}(s_{11}-s_{12})
\end{pmatrix}
$$

16

Hexagonal:

$$6,\bar{6},6/m$$

$$
\begin{pmatrix}
s_{11} & s_{12} & s_{13} & 0 & 0 & -s_{61} \\
s_{12} & s_{11} & s_{13} & 0 & 0 & s_{61} \\
s_{31} & s_{31} & s_{33} & 0 & 0 & 0 \\
0 & 0 & 0 & s_{44} & s_{45} & 0 \\
0 & 0 & 0 & -s_{45} & s_{44} & 0 \\
s_{61} & -s_{61} & 0 & 0 & 0 & \frac{1}{2}(s_{11} - s_{12})
\end{pmatrix}
$$

$$622,6mm,\bar{6}m2,6/mmm$$

$$
\begin{pmatrix}
s_{11} & s_{12} & s_{13} & 0 & 0 & 0 \\
s_{12} & s_{11} & s_{13} & 0 & 0 & 0 \\
s_{31} & s_{31} & s_{33} & 0 & 0 & 0 \\
0 & 0 & 0 & s_{44} & 0 & 0 \\
0 & 0 & 0 & 0 & s_{44} & 0 \\
0 & 0 & 0 & 0 & 0 & \frac{1}{2}(s_{11} - s_{12})
\end{pmatrix}
$$

Cubic:

$$23,m3$$

$$
\begin{pmatrix}
s_{11} & s_{12} & s_{13} & 0 & 0 & 0 \\
s_{13} & s_{11} & s_{12} & 0 & 0 & 0 \\
s_{12} & s_{13} & s_{11} & 0 & 0 & 0 \\
0 & 0 & 0 & s_{44} & 0 & 0 \\
0 & 0 & 0 & 0 & s_{44} & 0 \\
0 & 0 & 0 & 0 & 0 & s_{44}
\end{pmatrix}
$$

$$432, m3m, \bar{4}3m$$

$$
\begin{pmatrix}
s_{11} & s_{12} & s_{12} & 0 & 0 & 0 \\
s_{12} & s_{11} & s_{12} & 0 & 0 & 0 \\
s_{12} & s_{12} & s_{11} & 0 & 0 & 0 \\
0 & 0 & 0 & s_{44} & 0 & 0 \\
0 & 0 & 0 & 0 & s_{44} & 0 \\
0 & 0 & 0 & 0 & 0 & s_{44}
\end{pmatrix}
$$

Isotropic:

$$
\begin{pmatrix}
s_{11} & s_{12} & s_{12} & 0 & 0 & 0 \\
s_{12} & s_{11} & s_{12} & 0 & 0 & 0 \\
s_{12} & s_{12} & s_{11} & 0 & 0 & 0 \\
0 & 0 & 0 & \frac{1}{2}(s_{11} - s_{12}) & 0 & 0 \\
0 & 0 & 0 & 0 & \frac{1}{2}(s_{11} - s_{12}) & 0 \\
0 & 0 & 0 & 0 & 0 & \frac{1}{2}(s_{11} - s_{12})
\end{pmatrix}
$$

For example, when an optically isotropic medium is placed in a static electric field, it becomes birefringent. This effect is associated mostly with the alignment of the molecules in the presence of the field. The medium then behaves optically as if it were a uniaxial medium in which the electric field defines the optic axis. Since the medium is isotropic, we may choose the z axis to be in the direction of the electric field. Then Equation (2.12), the index ellipsoid is then given by:

$$x^2 \left(\frac{1}{n^2} + s_{12}E^2 \right) + y^2 \left(\frac{1}{n^2} + s_{12}E^2 \right) + z^2 \left(\frac{1}{n^2} + s_{11}E^2 \right) = 1,$$

$$(2.13)$$

Where E is the magnitude of the applied electric field, and

18

Table 2.2
Quadratic Electro-Optic Coefficients

Substance	Symmetry	Wavelength λ (μm)	Electr-Optic Coefficients S_{ij} (10^{-18} m^2/V^2)	Index of Refraction n_1	Temperature* T(°C)
BaTiO$_3$ (T$_0$ = 120 °C)	m3m	0.633 0.500	$s_{11} - s_{12} = 2290$ $n_0^3(s_{11} - s_{12}) = 72{,}000$ $n_0^3 s = 44{,}000$	n = 2.42	T > T$_0$ T ≈ T$_0$
K(Nb$_{0.37}$Ta$_{0.63}$)O$_3$ KTaO$_3$	m3m m3m	0.633 0.633	$s_{11} - s_{12} = 2890$ $s_{11} - s_{12} = 10$	n = 2.29 n = 2.24	20 -226
SrTiO$_3$	m3m	0.633	$s_{11} - s_{12} = 31 (-126°C)$ $s_{44} > 500/n^3 (-153°C)$	n = 2.38	
Pb$_{0.88}$La$_{0.88}$ (Ti$_{0.35}$Zr$_{0.35}$)O$_3$ (PLZT) (T$_0$ = 63 °C)	m∞m	0.550	$s_{33} - s_{13} = 26000/n^3 (63°C)$	n = 2.450	RT
KH$_2$PO$_4$ (KDP)	42m	0.540	$n_e^3(s_{33} - s_{13}) = 31$ $n_0^3(s_{31} - s_{11}) = 13.5$ $n_0^3(s_{12} - s_{11}) = 13.5$ $n_0^3 s_{66} = 3.0$	n$_0$ = 1.5115** n$_e$ = 1.4698**	RT
(NH$_4$)H$_2$PO$_4$ (ADP)	42m	0.540	$n_e^3(s_{33} - s_{13}) = 24$ $n_0^3(s_{31} - s_{11}) = 16.5$ $n_0^3(s_{12} - s_{11}) = 5.8$ $n_0^3 s_{66} = 2.0$	n$_0$ = 1.5266** n$_e$ = 1.4808**	RT

* RT = Room Temperature

** AT 0.546 μm.

ah-64444FL-T22

we have used $s_{13} = s_{23} = s_{12}$ and $s_{33} = s_{11}$. This index ellipsoid can be written as:

$$\frac{x^2 + y^2}{n_o^2} + \frac{z^2}{n_e^2} = 1 \tag{2.14}$$

with

$$n_o = n - \frac{1}{2} n^3 s_{12} E^2$$

$$\tag{2.15}$$

$$n_e = n - \frac{1}{2} n^3 s_{11} E^2$$

The birefringence $(n_e - n_o)$ is given by:

$$n_e - n_o = \frac{1}{2} n^3 (s_{12} - s_{11}) E^2, \tag{2.16}$$

Where n_o is the index of refraction for light polarized at right angles to the electric field E, and n_e is the index of refraction for light polarized in the direction of E. Equation (2.16) can also be written:

$$n_e - n_o = -n^3 s_{44} E^2 \tag{2.17}$$

By using the relationship $s_{44} = \frac{1}{2} (s_{11} - s_{12})$ for isotropic media (see Table 2.1). Equations (2.16) and (2.17) are often written as:

$$n_e - n_o = K\lambda E^2, \tag{2.18}$$

20

Where K is the so-called Kerr constant and λ is the vacuum wavelength. Table 2.3 lists the Kerr constants of several materials. The Kerr constant and the quadratic electro-optic coefficients of an isotropic medium are related by:

$$s_{44} = - \frac{K\lambda}{n^3}$$

In any real atomic system, polarization induced in the medium is not proportional to the optical electric field, but can be expressed in a Taylor series expansion as:

$$P_i = \varepsilon_o \chi_{ij} E_j + 2\chi_{ijk}^{(2)} E_j E_k + 4\chi_{ijke}^{(3)} E_j E_k E_e + \ldots \qquad (2.19)$$

where:

P_i is the ith component of the instantaneous polarization and E_i is the component of the instantaneous field. Summations over repeated indices are assumed. χ_{ij} is the linear susceptibility, while $\chi_{ijk}^{(2)}$ and $\chi_{ijkl}^{(3)}$ are the second and third nonlinear optical susceptibilities respectively.

The electro-optic coefficients r_{ijk} and s_{ijkl} defined in Equation (2.2) depend, in general, on the wavelength of light, the modulation frequency, and the temperature of the crystal. These coefficients are related directly to the nonlinear susceptibility tensors $\chi_{ijk}^{(2)}$, $\chi_{ijkl}^{(3)}$, and can be calculated by

Table 2.3   Kerr Constant of Some Selected Substances

Substance	λ (μm)	n	K (m/V^2)
Benzene	0.546	1.503	4.9×10^{-15}
	0.633	1.496	4.14×10^{-15}
CS_2	0.546	1.633	3.88×10^{-14}
	0.633	1.619	3.18×10^{-14}
	0.694	1.612	2.83×10^{-14}
	1.000	1.596	1.84×10^{-14}
	1.600	1.582	1.11×10^{-14}
CCl_4	0.633	1.456	7.4×10^{-16}
	0.546	1.460	8.6×10^{-16}
Water	0.589		5.1×10^{-14}
Nitrotoluene	0.589		1.37×10^{-12}
Nitrobenzene	0.589		2.44×10^{-12}

ah-44FR-TX1

using quantum theory, the third-order nonlinear susceptibility $\chi_{ijk\ell}$ is related to the quadratic electro-optic coefficients $s_{ijk\ell}$ defined by Equation (2.2), by:

$$\chi_{ijk\ell}^{(3)} = -\frac{\varepsilon_{ii}\varepsilon_{jj}}{12\varepsilon_o} s_{ijk\ell} \qquad (2.20)$$

When the tensor components are again defined in the principal coordinate system.

Some materials have been listed in terms of $\chi^{(3)}$, the third-order nonlinearities (see Table 2.4).

2.2 Organic Materials and Molecule Engineering

Some organic materials possess high third-order optical nonlinearity. These materials could be in the forms of single crystal, polymer and thin film. More recent recognition is that organic and polymeric materials with large delocalized π-electron system may exhibit extremely large nonlinear response, in many cases much larger than their inorganic counterparts. Of particular importance for conjugated organic system is the fact that the origin of the nonlinear effects is the polarization of the π-electron cloud as opposed to displacement or rearrangement of nuclear coordinates found in inorganic materials.

Development of new organic nonlinear optical materials have relied on knowledge of molecular nonlinear polarizability and the

ah-44FR-TX1

Table 2.4 $\chi_{xyyx}(-\omega, \omega, \omega, -\omega)$ of Some Materials at $\lambda = 694$nm

Material	n	$\chi_{xyyx}(-\omega, \omega, \omega, -\omega)$ $(10^{-34}$ MKS$)$
CS_2	1.612	441
CCl_4	1.454	6.2
Fused Quartz	1.455	1.5
YAG	1.829	7.41
Benzene	1.493	68.9
LSO Glass	1.505	2.26
ED-4 Glass	1.631	9.8
BK-7 Glass	1.513	2.26
LaSF-7 Glass	1.91	12.4

ah-44FR-TX1

relationship between nonlinear optic fundamental concepts and chemical structure. In the dipolar approximation, the polarization induced in an atom or molecule by external field E can be written as:

$$P = \alpha.E + \beta..EE + \gamma...EEE + ... \qquad (2.21)$$

Where the vector quantities P and E are related by the tensor quantities α, β, and γ, which are often referred to as the polarizability, hyperpolarizability, and second hyperpolarizability, respectively. Similarly the polarization induced in macroscopic or bulk media can be expressed as:

$$P = \chi^{(1)}.E + \chi^{(2)}..EE + \chi^{(3)}...EEE + ... \qquad (2.22)$$

Where the coefficients $\chi^{(1)}$, $\chi^{(2)}$, and $\chi^{(3)}$ are similar in meaning to their microscopic counterparts. In this formalism the even order tensors β and $\chi^{(2)}$ are zero in centrosymmetric media, whereas the odd order tensors do not have symmetry restrictions associated with them. The molecular quantities α and γ are related to their macroscopic counterparts through summations over the number of contributing atoms or molecules per unit volume and are corrected for local contributions from neighboring molecular fields. Conversely, a molecule with an asymmetric charge distribution on a nonzero β may therefore exist in a centrosymmetric crystal or orientationally averaged molecular environment such as a liquid or amorphous polymer. Therefore, it

25

may exhibit a vanishingly small value of $\chi^{(2)}$. To determine $\chi^{(2)}$ experimentally, the detailed nature of the propagation of the incident field and induced fields in the medium of interest must be carefully considered. For instance, conditions may exist where orientational averaging may not lead to zero $\chi^{(2)}$ (e.g., when the size of a noncentrosymmetric domain in an ensemble of orientationally averaged domains approaches or exceeds the wavelength of light).

The nonlinear coefficients are determined by the detailed nature of the electronic environment of the medium, its symmetry for even order coefficients, and the exact nature of the interacting field components. For instance, molecules and molecular solids with delocalized π systems exhibit much larger coefficients than covalently bonded molecules and solids. The ability to tailor charge asymmetry, control the enhancement of the nonlinear polarization from electronic dispersion, and provide optical transparency in regions of the spectrum compatible with useful light sources are convenient tools of the physical organic chemist. These factors represent enormous potential for designing materials with specific properties for certain applications.

The situation for $\chi^{(3)}$ becomes complicated very quickly because the odd order coefficients can produce responses at the input frequencies as well as resonant effects like two-proton absorption and various Raman active resonances. At least 20 different processes occurring through $\chi^{(3)}$ have been observed.

26

2.2.1 Nonlinear Optical Susceptibilities

In this section, we shall discuss the behavior of the nonlinear optical susceptibilities for both small-size and infinite-extension systems and we will set up here their general expressions. For small-size systems (zero dimensionality), much smaller than the optical wavelength, the relevant quantity is the induced dipole p, whose dependence on the applied local field is expressed in terms of the dipolar polarizabilities α, β, γ, etc. Using standard time-dependent perturbation theory in the transparency region (or static perturbation theory), these are:

$$\alpha = 2\sum_{n}{}' \frac{\mu_{gn}\mu_{ng}}{E_{ng}} \tag{2.23}$$

$$\beta = 3\left[\sum_{n,n'}{}' \frac{\mu_{gn}\mu_{nn'}\mu_{n'g}}{E_{ng}E_{n'g}} - \mu_{gg}\sum_{n}{}' \frac{\mu_{gn}\mu_{ng}}{E_{ng}^2} \right] \tag{2.24}$$

$$\gamma = 4\left[\sum_{n,n'n''}{}' \frac{\mu_{gn}\mu_{nn'}\mu_{n'n''}\mu_{n''g}}{E_{ng}E_{n'g}E_{n''g}} - \sum_{n}{}' \frac{\mu_{gn}\mu_{ng}}{E_{ng}} \sum_{n'}{}' \frac{\mu_{gn'}\mu_{n'g}}{E_{n'g}^2} \right] \tag{2.25}$$

Where $\sum_{m}{}'$ means that terms with $E_{mg} = 0$ will be excluded, m labels the electronic states of the molecule (g is the ground state), and we limit ourselves to the x components; μ is the electronic dipole moment operator. The calculation of these expressions is quite involved, but useful information about size effects and scaling laws can be obtained with the help of the Unsold approximation (Flytzanis, 1975).

27

ah-44FR-TX1

For extended periodic systems, the relevant quantity is now the induced dipole density or polarization P, whose dependence on the applied macroscopic field is expressed in terms of the nonlinear susceptibilities $\chi^{(1)}$, $\chi^{(2)}$, $\chi^{(3)}$, etc., and the electron states are represented in terms of Bloch band states. For the derivation of the scaling laws for extended systems that can be related to the ones for small-size systems, the choice of the appropriate expressions of $\chi^{(n)}$ is crucial. This point has been mostly tackled using the Genkin Mednis approach (Genkin and Mednis, 1968; Flytzanis, 1975), and one obtains:

$$\chi_{xx}^{(1)} = \frac{4e^2}{hV} \int_{B.Z.} \Omega_{vc} S_{cv} dk \tag{2.26}$$

$$\chi_{xxxx}^{(3)} = \frac{8e^4}{h^3 V} \int_{B.Z.} \left[\frac{1}{\omega_{ve}} \left(\frac{\partial S_{ev}}{\partial k} \right) \left(\frac{\partial S_{ev}}{\partial k} \right) - \Omega_{vc} S_{cv} S_{vc} S_{cv} \right] dk \tag{2.27}$$

Where $h\omega_{cv} = \varepsilon_c - \varepsilon_y$, Ω_{vc} is the transition dipole-moment matrix element between the highest valence (v) and lowest conduction (c) bands, $S_{vc} = \Omega_{vc}/\omega_{vc}$, and ε_v and ε_c are the band energies for the v and c band, respectively; in Equations (2.26) and (2.27) are the two-band approximation. Furthermore, we have assumed that the system posse ses inversion symmetry so that in particular $\chi^{(2)} = 0$; for noncentrosymmetric systems, the expression of $\chi^{(3)}$ is slightly more lengthy (Agrawal et al., 1978) and the second-order susceptibility is:

ah-44FR-TX1

$$\chi^{(2)} = \left(\frac{6e^3}{h^2v}\right)\frac{i}{2\pi}\int_{B.Z.}\left[S_{ev}S_{ev}(\Omega_{vv}\Omega_{cc}) - \frac{1}{2}\left(S_{vc}\frac{\partial S_{ev}}{\partial k} - \frac{\partial S_{vc}}{\partial k}S_{ev}\right)\right]dk$$

$$(2.28)$$

where Ω_{vv} and Ω_{cc} are intraband transition dipole-moment matrix elements. One may formally define also polarizabilities $\alpha^{(n)}$ for such infinitely extended systems by the relation:

$$\chi^{(n)} = \frac{\alpha^{(n)}}{v}\qquad\qquad(2.29)$$

Where v is the repeat unit-cell volume. By simple inspection and comparison of Equations (2.23), (2.24) and (2.25) with (2.26), (2.27) and (2.28) respectively, one may easily see the similarity between these two sets of expressions; as a matter of fact, Equations (2.23) to (2.25) change over to Equations (2.26) to (2.28) for extended systems with localized electron states.

It is stressed here the fact that the behavior of the nonlinear optical susceptibilities $\chi^{(n)}$ is determined by the competition of two terms, intraband ones that arise from field mixing of Bloch band states within a band and interband ones that arise from mixing of states across the gap (with wave-vector conservation); in contrast, the linear susceptibility $\chi^{(1)}$ only involves interband terms. For highly delocalized systems (strong overlap between wave functions), the quantities ω_{cv} and Ω_{cv} vary strongly over the Brillouin zone and therefore the intraband term in $\chi^{(3)}$ becomes the dominant one.

29

As can be seen from Equations (2.26), (2.27), and (2.28), the susceptibilities are expressed as integrals over the Brillouin zone. The main contribution to these integrals is in general expected to come from some few nonoverlapping critical regions in the joint density of states (see, for instance, Ashcroft and Mermin, 1981); these are points, lines, and the surfaces depending on the spatial extension of the electronic density distribution and are defined by the condition:

$$\nabla_k \omega_{cv}(k) = 0 \qquad (2.30)$$

This is indeed the case for $\chi^{(1)}$ (see, for instance, Cardona and Pollack, 1971) and was found also to be the case for odd-order susceptibilities $\chi^{(2n+1)}$, as will be shown. This directly establishes a relation between the optical susceptibilities $\chi^{(2n+1)}$ and the topology and dimensionality of the joint density of states. More importantly, it allows one to express $\chi^{(2n+1)}$ in terms of the values of Ω_{vc} and ω_{cv} at these critical regions; the latter can also be related to the characteristics of the electron distribution. This functional dependence is precisely the origin of the scaling laws to be given below and also strongly reflects the dimensionality of the electron distribution. The critical point analysis of the even-order susceptibilities $\chi^{(2n)}$ is not as straightforward as for the odd-order ones, as will be cursorily exemplified below for $\chi^{(2)}$, and will not be pursued to any extent here.

30

2.2.1.1 Zero-Dimensionality System

Under this headline we loosely include isolated molecular systems of finite extension in all directions and of size much less than the wavelength λ. We shall restrict our discussion to linear centrosymmetric conjugated molecules like polyenes etc. The case of a linear conjugated carbon chain without bond alternation will be tackled first, as it affords almost complete analytical solution using a method initially applied for the investigation of the so called Stark ladder level configuration (Wannier, 1962; Fukuyama et al., 1973); subsequently, the case of bond alternation will also be considered, but the analysis will rely on numerical results.

A. Carbon Chains Without Bond Alternation

We use the Huckel approximation (Murrell, 1963) so that the coefficients c_n of the wave functions $\psi = \sum_c c_n \phi$ and their eigenvalues ε for a finite conjugated chain containing 2N equally spaced carbon atoms, in the presence of a static electric field E, are determined through

$$c_n(- \varepsilon + nw) + \beta(c_{n+1} + c_{n-1}) = 0 \qquad (2.31)$$

with the boundary conditions $c_0 = c_{2N+1} = 0$; in Equation (2.31), $w = eaE$, where a is the interatomic distance; β is the resonance (hopping) energy between neighboring carbon atoms; ε is measured with respect to the Coulomb energy of the carbon chain;

ah-44FR-TX1

and the Huckel approximations, $\langle\phi_n|X|\phi_n\rangle = na$ and $\langle\phi_n|\phi_m\rangle = \delta_{nm}$, were used. The solution of Equation (2.31) is:

$$c_n = AJ_{\gamma-\varepsilon/w}(-2w/\beta) + BY_{n-\varepsilon/w}(-2w/\beta) = 0$$

Where J_γ and Y_γ are the Bessel and von Newman functions, related (Abramovitz and Stegun, 1964) by:

$$Y_\gamma(x)\sin\gamma\pi = J(x)\cos\nu\pi - J_{-\gamma}(x)$$

The boundary conditions $c_0 = c_{2N+1} = 0$ give

$$J_{-\gamma\xi}(2\gamma)Y_{1-\gamma\xi}(2\gamma) - J_{\gamma/\bar{\gamma}-\gamma\xi}Y_{-\gamma\xi}(2\gamma) = 0$$

where $\gamma = -\beta/w, \xi = -\delta/\beta$, and $\bar{\gamma} = (N+1)\gamma$

The roots of this equation give the 2N eigenvalues ε_n, which for the case of E = 0 reduce to $\varepsilon_n^0 = 2\beta\cos\theta_n^0$ with $\theta_n^0 = n\pi/(N+1)$, while at the high field intensity limit ($\gamma \ll 1$) one obtains the Stark ladder spectrum $\varepsilon_n = nw$ (Wannier, 1962), and the same is true for intermediate field intensities $\bar{\gamma} \ll 1$ but $\gamma \gg 1$. For low field intensities where perturbation theory can be used — namely, $\gamma \gg 1$ and $\bar{\gamma} \gg 1$ — using the double asymptotic development of Bessel functions (Abramovitz and Stegun, 1964) and rearranging the expressions one obtains for the total energy of the electron system (Agrawal et al., 1978).

32

$$W = \sum_{n=1}^{\infty} \varepsilon_n = W_0 - N\beta \sum_{k=0}^{\infty} \frac{\lambda^{(k)}}{\bar{\gamma}^{2k}} \qquad (2.32)$$

Where the $\lambda^{(k)}$ are constants that in principle can be calculated. Inserting $\bar{\gamma} = - (N + 1)\beta/eaE$, using the definition of the polarizabilities for a symmetric molecule,

$$W = W_0 - \sum_{k=1}^{\infty} \frac{1}{2k - 1} \alpha^{(2k-1)} E^{2k-1} \qquad (2.33)$$

and identifying terms of the same order in E in Equations (2.32) and (2.13), respectively, one obtains (Agrawal et al., 1978).

$$\alpha^{(2n-1)} \approx N^{2n+1} e^{2n} a^{2n}/\beta^{2n-1} = L^{2n+1} e^{2n}/\alpha\beta^{2n-1} \qquad (2.34)$$

valid for large N, and L = Na is the half-length of the chain. In particular for the linear and third order polarizabilities one has:

$$\alpha \approx N^3 e^2 a^2/\beta = L^3 e^2/a\beta \qquad (2.35)$$

$$\gamma \approx N^5 e^4 a^4/\beta^3 = L^5 e^4/a\beta^3 \qquad (2.36)$$

These expressions clearly show how the odd-order polarizabilities for linear molecules with equidistant atoms scale with the molecular extension L and resonance energy β and they constitute scaling laws; Equation (2.35) was initially derived by Davies (1952) and Equation (2.36) by Rustagi and Ducuing (1972)

using the free electron model to describe such chains (Kuhn, 1948).

These scaling laws should in principle apply for cyanine dyes; however, it is difficult to rigorously test the fifth-power dependence of γ on N. Indeed, as N increases, so does the wavelength of the first absorption peak (Murrell, 1963), and the frequency dependence of γ cannot be overlooked; it may mask any N dependence (Hermann and Ducuing, 1974).

B. Chains with Bond Alternation

These chains are characterized by two resonance energies, β_1 and β_2, and the situation is drastically different from the previous case as bond alternation stabilizes the main absorption peak to a fixed value $2|\beta_1 - \beta_2|$ as the chain length increases (Murrell, 1963); on the other hand, the analytical treatment of the polarizabilities becomes prohibitingly difficult, and meaningful trends can only be extracted numerically. These can be cast in a very simple form if we introduce the delocalization parameter:

$$N_d = \frac{\beta_1 + \beta_2}{\beta_1 - \beta_2} \qquad (2.37)$$

We present next the main conclusions regarding the third-order polarizability γ_{2N} for a chain 2N atoms when plotted as a function of N_d for different values of N (Agrawal and

Flytzanis, 1976).

For a given N, γ_{2N} shows a maximum at $N_d = 2N$; for $N_d > N$, γ_{2N} decreases monotonically with increasing N_d (and N fixed) and for $N_d \to \infty$ (or $\beta_1 = \beta_2$) one recovers expression (15), namely, a fifth-power dependence of γ_{2N} on N.

For $N_d < N$, γ_{2N} decreases monotonically as:

$$\gamma_{2N} \sim N_d^6 \qquad (2.38)$$

independently of N for N_d not too close to unity. For $N_d \approx 1$, or $\beta_2 \approx 0$, γ becomes negative and we reach the expression $\gamma_0 = - Ne^4a^4/\beta_1^3$ for $\beta_2 = 0$, which corresponds to the value of γ_{2N} for N independent bonds represented by two-level systems; this limiting behavior (bond additivity) clearly must be modified, since the chain group contributions must also be included now and may even dominate the actual value of γ.

The above trend is a clear example of size effect and indicates that the third-order polarizability γ exhibits distinctly different scaling laws depending on whether the electron delocalization length $L_d = N_d a$ is smaller or larger than molecular length $L = Na$; in particular, we expect that the scaling law [Equation (2.38)] should be independent of N as long as $N_d < N$, and this is strikingly corroborated by the analytical results of infinite bond-alternated chains (Agrawal and Flytzanis, 1976).

ah-44FR-TX1

2.2.1.2 One-Dimensional Systems

We consider now the case of infinite one-dimensional crystals, which can be either one-dimensional organic semiconductors (like polyacetylene or polydiacetylene) or inorganic ones (like SbSI). To gain insight into the scaling laws that prevail here, we exemplify this class of systems with the infinite simply bond-alternated carbon chain and adopt the Huckel approximation to describe the electronic density; within the Huckel approximation two resonance integrals β_1 and β_2 are introduced to characterize the bond alternation as in Section 2.2.1.1.B.

It turns out that the scaling laws for $\chi^{(2n+1)}$ derived for this simple system are quite universal and valid for all one-dimensional systems and can be cast in the form of power laws of the electron delocalization length $L_d = N_d a$ where N_d is given by Equation (2.37) (Agrawal and Flytzanis, 1976; Agrawal et al., 1978); for the case of $\chi^{(3)}$ it reduces to a sixth-power dependence on N_d, the same one found numerically for finite chains when $N > N_d$ [Equation. (2.38)].

We assume complete separation between σ and π electrons and we concentrate only on the π-electron contribution. The electron states for such bond-alternated chain can be obtained analytically in the form of Bloch band states. One has in particular:

36

$$\hbar\omega_{cv} = 2\beta_2 \sqrt{(1 + \nu^2 + 2\nu\cos ka)} \equiv 2\beta_2\zeta_0 \qquad (2.39)$$

$$e\Omega_{cv} = ea \ (1 - \nu^2)/4\zeta_0^2 \qquad (2.40)$$

Where $\nu = \beta_1/\beta_2$. Inserting the Equation (2.39) for $\hbar\omega_{cv}$ in Equation (2.30), we see that the joint density of states becomes infinite at the edge of the Brllouin zone, $ka = \pi$, and this constitutes the critical point where also the matrix element Ω_{cv} (ka) attains its maximum values,

$$|\Omega_{cv}(\pi)| = a \left| \frac{\beta_1 + \beta_2}{\beta_1 - \beta_2} \right| = L_d \qquad (2.41)$$

which is the optical delocalization length, and the energy difference $\hbar\omega_{cv}$ becomes smallest,

$$\hbar\omega_{cv} \ (\pi) = 2|\beta_2 - \beta_1| = E_0 \qquad (2.42)$$

which also is the optical gap where the main absorption peak is located. The coincidence of these three features at a single point of the Brillouin zone — namely, (1) infinite joint density of states, (2) maximum transition dipole moment, and (3) smallest energy gap — is an essential characteristic of the one-dimensional semiconductors, reminiscent of a metallic-type behavior (this point is the only one preserved from the metallic case when bond alternation sets in), and is the origin of the enhanced contribution of the π electrons over the σ electrons in

ah-44FR-TX1

the optical susceptibilities. Indeed, inserting Equations
(2.39) and (2.40) in Equations (2.26) and (2.27) one finds
for strong electron delocalization, $N_d = 4L_d/a > 1$,

$$\chi_\pi^{(1)} = \frac{2}{3\pi} \chi_\sigma^{(1)} N_d^2 \tag{2.43}$$

$$\chi_\pi^{(3)} = \frac{2}{3\pi} \chi_\sigma^{(3)} N_\sigma^6 \tag{2.44}$$

and quite generally one can show that

$$\chi_\pi^{(2n-1)} \approx \chi_\sigma^{(2n-1)} N_d^{4n-2} \tag{2.45}$$

where $\chi_\sigma^{(2n-1)}$ is the expression of the susceptibility for a chain
of saturated bonds (σ electrons), which corresponds to setting
$\beta_2 = 0$ in Equations (2.39) and (2.40) or

$$\chi_\sigma^{(2n-1)} \sim (ea)^{2n}/\beta_2^{2n-1} \tag{2.46}$$

Equation (2.44) and the more general one of Equation (2.45) are
valid for a large electron delocalization $N_d > 1$; it was found
that the main contribution in the odd-order nonlinear
susceptibilities comes from the intraband terms, which have
opposite sign to the interband ones (Agrawal et al., 1978). Since
$N_d > 1$, comparison of Equations (2.45) and (2.46) shows that
indeed the nonlinear susceptibilities for π-electron systems are
greatly enhanced by many orders of magnitude over those of the σ
electrons (for the same electron density), and in particular this
justifies the neglect of the side-group contributions in these

ah-44FR-TX1

chains, since these usually are saturated molecular systems.

The detailed analysis of Agrawal et al.(1978) showed that the scaling law of Equation (2.45) is not restricted to simply bond-alternated chains but is valid for all one-dimensional systems, with or without inversion symmetry, bond super-alternation, coupled chains, etc., and similarly one expects that the scaling law of Equation (2.46) for higher-order susceptibilities is universally valid for all one-dimensional systems with delocalized electron states (Flytzanis, 1983).

Clearly the universality of the scaling law of Equation (2.47) or the more general one of Equation (2.45) has only been proven within the one-electron approach where electron correlation is altogether neglected (Ovchinnikov, 1973); when the latter is taken into account, the expressions of Ω_{cv} and $\chi^{(n)}$ become too exceedingly complex to allow any analytical or even numerical treatment , and no conclusions can be drawn yet.

In practice, one-dimensional conjugated chains are seldom of infinite extension; they are more usually interrupted by different types of defects, extrinsic (impurities etc.) or intrinsic (conjugation or Pople-Wamsley defects, solutions, etc.). The question arises then as to what extent the scaling laws of Equation (2.45) or (2.46) obtained for an infinite chain are still valid for chains formed by segments of 2N atoms. For $\chi^{(3)}$, the answer is contained in Section 2.2.1.1.B, where it was found that indeed that the third-order polarizability of such a segment

ah-44FR-TX1

still exhibits the sixth-power dependence in dependence on N_d as long as $N_d > 1$, and this independently of N as long as $N_d < N$; thus the scaling law of Equation (2.45) is still valid, and similarly we expect this to be the case for the scaling law of Equation (2.46).

For the subsequent discussion it is convenient to cast the scaling law of Equation (2.46) in a form more closely related to solid-state terminology. Indeed, we note that for the simply bond-alternated chain, when considered as a one-dimensional semiconductor, the Fermi energy $E_F = |\beta_2 + \beta_1|$ and the energy gap $E_0 = 2|\beta_1 + \beta_2|$ so that $N_d \approx E_F/E_0$ or

$$\chi^{(3)} \approx \chi_\sigma^{(3)} \left(\frac{E_F}{E_0} \right)^6 \qquad (2.47)$$

and more generally

$$\chi^{(2n-1)} \approx \chi_\sigma^{(2n-1)} \left(\frac{E_F}{E_0} \right)^{4n-2} \qquad (2.48)$$

which contains quantities directly accessible to measurement, the Fermi energy and the energy gap. This form in particular allows one to compare organic with inorganic semiconductors (like SbSI), and more importantly it directly relates $\chi^{(2n-1)}$ to the critical-point energy E_0; the sixth-power dependence of $\chi^{(3)}$ on E_F/E_0 was first derived by Cardona and Pollack (1971) using critical-point analysis and also by Sauteret et al. (1976) using a simple model of a one-dimensional semiconductor.

ah-44FR-TX1

Before moving into the case of higher-dimensionality systems, we wish to say a few words about the second-order susceptibility $\chi^{(2)}$, given by Equation (2.28). Here the interband and intraband terms can each have either sign, so that they may add or subtract. Careful analysis of Equation (2.28) reveals that contributions to the integrand only come from regions were Ω_{cv} is complex (Agrawal et al., 1978); it vanishes whenever Ω_{vc} becomes real or pure imaginary, and this is precisely what happens at the edge of the Brillouin zone of a one-dimensional system. Thus, in contrast to $\chi^{(3)}$, $\chi^{(2)}$ does not take full advantage of the infinite densities of states there and the highly delocalized character of these states; in particular, the critical-point analysis for the derivation of scaling laws is not as straightforward as for $\chi^{(3)}$.

2.2.1.3 Two- and Three-Dimensional Systems

For two- and three-dimensional crystalline systems, the electronic band states and energies cannot be obtained easily in a closed analytical form over the whole Brillouin zone, and the calculation of the susceptibilities using Equations (2.26 to 2.28) can only be conducted numerically. However as pointed previously, the main contribution to the integrals in Equations (2.26 to 2.28) comes from some few nonoverlapping critical regions in the density of states, and one then may use the approach of Cardona and Pollack (1971) based on a model density of states to obtain the contributions to $\chi^{(2n-1)}$ from the different critical points.

A. Two-Dimensional Systems

Here the critical regions are of two kinds: a point, at energy E_0 at the edge of the Brillouin zone, reminiscent of one-dimensional patterns in the electron density distribution, with their contribution to $\chi^{(2n-1)}$ given by Equation (2.47); and a line, at energy E_1, intrinsic to the two-dimensional character of the system. In general, $E_1 < E_0$, and furthermore the impact of E_0 is now reduced as E_1 attracts a large density of states. Cardona and Pollack (1971), using plausible simplifications in their model density of states, show that the contribution to $\chi^{(1)}$ and $\chi^{(3)}$ from the critical points on E_1 are

$$\chi^{(1)} \sim P^2/E_1^2 \qquad (2.49)$$

$$\chi^{(3)} \sim P^2/E_1^5 \qquad (2.50)$$

respectively, and by induction we make the conjecture that

$$\chi^{(2n-1)} \sim P_0^2 /E_1^{3n-1} \qquad (2.51)$$

where P is an average transition dipole moment matrix element.

As in the one-dimensional semiconductor case, the scaling law of Equation (2.50) arises from competition of field mixing of states within each band (intraband terms) and k-conserving coupling across the gap (interband terms). This competition can

42

also be interpreted as displacement of opposite sign of the band gap at the critical points when an electric field is applied (Cardona and Pollack, 1971).

B. Three-Dimensional Systems

Here, besides contributions from critical points E_0 and lines E_1 of the form of Equations (2.48) and (2.51), respectively, $\chi^{(2n-1)}$ will also contain contributions from critical surfaces at energy E_2, and in general $E_2 < E_1 < E_0$, so that for a given electron density the impact of E_0 is further reduced.

In particular, since ω_{cv} and Ω_{cv} vary much more rapidly as we move from E_0 to E_2, the corresponding intraband terms also become more dominant.

Again using simple considerations for the model density of states, one obtains (Cardona and Pollack, 1971).

$$\chi^{(1)} = P^2/E_2^{5/2} \tag{2.52}$$

$$\chi^{(3)} = P^2/E_2^{9/2} \tag{2.53}$$

and by induction we make the conjecture that

$$\chi^{(2n-1)} \sim P^2/E_2^{2n+1/2} \tag{2.54}$$

Clearly these scaling laws are subject to large uncertainties, as

ah-44FR-TX1

they were derived from a very approximate model for the density of states.

Summarizing the previous three sections, the scaling laws were derived for systems with infinite extension in one, two, or three dimensions. For many important applications of nonlinear optics, however, systems with reduced extension will increasingly be used; accordingly, size effects will be crucial and some modifications must be introduced. This has been extensively discussed for the one-dimensional systems, where it was shown that as long as the electron delocalization length L_d is smaller than the chain length L, the scaling laws have the same form as for the infinite one-dimensional systems given by Equations (2.44) and (2.45).

For two- and three-dimensional systems, the validity range of the scaling laws of Equations (2.50) and (2.53) or the more general ones of Equations (2.51) and (2.54), respectively, cannot be obtained as easily, and the whole problem has to be reconsidered carefully.

In addition, we may also consider the case where systems of finite extension are imbedded in a different medium of infinite extension, usually amorphous or glass; these are the so-called composite materials, like metal inclusions in glasses (Peremboom and Wyder, 1981) or semiconductor-doped glasses. Here, local field effects mediated through the surrounding medium can play a crucial role under certain resonance conditions and lead to an

ah-44FR-TX1

enhancement of the nonlinear susceptibilities. The effective medium approach (Maxwell-Garnett theory) has been extended to the nonlinear case to take into account these effects (Rustagi and Flytzanis, 1984; Ricard et al., 1985), but more work must be done on these systems to clearly understand the origin of the nonlinear response and the scaling laws that prevail there. More recently, Hache et al. (1986) have discussed quantum size effects in the third-order polarizability of small metallic particles and derived the expression of the third-order susceptibility of the corresponding composite material; the dielectric confinement of the electrons in these metallic particles leads to a strong dependence of the magnitude of $\chi^{(3)}$ on the size of the particles. The case of the semiconductor-doped glasses provides another class of composite materials where size effects play an important role in the nonlinear optical properties. Here, too, the dielectric confinement drastically modifies the nature of the electronic states, the oscillator strength as well as the response time of the nonlinearity [Roussignol et al. (1986)]. This in particular leads to an intensity dependence, of the optical Kerr effect and the optical-phase-conjugated reflectivity in these materials, that was termed "frustrated saturation". [Roussignol et al. (1986)].

The study of the nonlinear optical properties of composite materials is interesting in a number of other aspects as it is related to that of small aggregates that are of paramount importance in many areas in chemistry and metallurgy. From a more fundamental point of view, the physics of such a low-dimensionality system throws a new light on some basic

ah-44FR-TX1

physical principles, which are suppressed when we deal with infinitely large systems. These heterogeneous materials present a lot of advantages when compared to the homogeneous ones, since one can artificially change a number of characteristics, including the size of inclusions, their resonances or band gap, their concentration, and even the optical anisotropy by using inclusions of appropriate shape, and thus manufacture materials with "tunable non-linearity," which are of great importance in many applications of nonlinear optics [Flytzanis et al. (1986)].

As stated previously, scaling laws can be very useful and in many considerations essential for our understanding of the physics of the non-linearities. The approach presented above is only tentative, as experimental investigations are totally lacking. However, with the increasing use of microstructures and the requirements that prevail there, dimensionality considerations will play a very important role, and so will the scaling laws.

ah-44FR-TX1

3.0 Notes on Chemistry

3.1 Chemical Bonds

In order to understand the molecular design ideas, some basic organic chemical concepts are briefly introduced as follows:
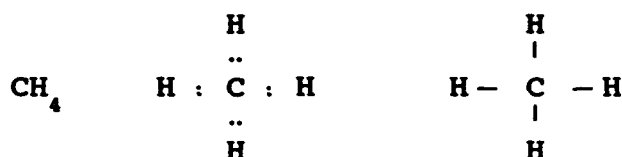
Atoms in molecules are connected by chemical bond to construct a molecule. Two major types of chemical bonds are:

1. The ionic (or electrovalent) bond, formed by the transfer of one or more electrons from one atom to another to create ions.

2. The covalent bond, a bond that results when atoms share electrons.

An example of the formation of an ionic bond is the reaction of lithium atoms and fluorine atoms. Lithium, a typical metal, has a very low electronegativity; fluorine, a nonmetal, is the most electronegative element of all. The loss of an electron (a negatively changed species) by the lithium atom leaves a lithium ion , Li^+) the gain of an electron by the fluoride atom gives a fluoride anion, F^-. Li^+ and F^- construct a LiF molecule by strong internal electrostatic forces between Li^+ and F^-. Ionic substances are usually with high melting solids, often having melting points above $1000°C$.

When two or more atoms of the same or similar electro-

ah-44FR-TX2

negativities react, a complete transfer of electrons does not occur. In these instances the atoms achieve whole gas structure by sharing electrons, covalent bonds form between the atoms and the products are cabled molecules. Molecules may be represented by electron-dot formulas or, more conveniently, by dash formulas where each dash represents a pair of electrons shared by two atoms, the molecule of methane (CH_4) is an example.

$$CH_4 \qquad \begin{array}{c} H \\ \cdot\cdot \\ H : C : H \\ \cdot\cdot \\ H \end{array} \qquad \begin{array}{c} H \\ | \\ H - C - H \\ | \\ H \end{array}$$

When two different atoms form a covalent bond, the electrons are not shared equally between them. The atom with greater electronegativity draws the electron pair closer to it, and a polar covalent bond results. An example of such a polar covalent bond is the one in hydrogen chloride. The chlorine atom, with its greater electronegativity, pulls the bonding electrons closer to it. This makes the hydrogen atom somewhat electron deficient and gives it a partial positive change (δ_+). The chlorine atom

$$\begin{array}{cc} \delta_+ & \delta_- \\ & \cdot\cdot \\ H : & Cl : \\ & \cdot\cdot \end{array}$$
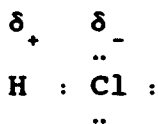
becomes somewhat electron rich and bears a partial negative charge (δ^-) because the hydrogen chloride molecule has a partially positive end and a partially negative end, it is a dipole, and it has a dipole moment. Many organic chemicals have polar covalent

48

bonds.

3.2 Atomic and Molecular Orbitals

In classical theory, all electrons of atom are moving on each circular orbits corresponding to different energies. In modern quantum mechanics theory, such electro orbits are interpreted as electron probability density, the probability of finding an electron in the space area where the orbits lie on. This electron probability density can be calculated by square of wave function ψ which is a solution of wave equation. Plots of ψ^2 in three dimensions generate the shapes of orbitals which are generally not circular. These orbits are denoted by s, p, d, ... corresponding to different angular moment or different orbit diameter in classical theory. The s and p orbitals are the most important in the formation of organic molecules.

For organic chemists the greatest utility of atomic orbitals is using them to understand how atoms combine to form molecules. When atomic orbitals combine to form molecular orbitals, the number of molecular orbitals that results always equals the number of atomic orbitals that combine. Thus in the formation of a hydrogen molecule the two atomic orbitals combine to produce two molecular orbitals. Two orbitals result because the mathematical properties of wave functions permit them to be combined by either addition or subtraction. That is, they can combine either in or out of phase. One molecular orbital, called the <u>bonding molecular</u>

49

<u>orbital</u> (ψ_{molec}), is formed when the atomic orbitals combine in the way shown in Figure 3.1.

Here, atomic orbitals combine by addition, and it means that atomic orbitals of the same phase sign <u>overlap</u>. Such overlap leads to reinforcement of the wave function in the region between the two nuclei. Reinforcement of the wavefunction not only means that the value of ψ is larger between the two nuclei; it means that ψ^2 is larger as well. Moreover, since ψ^2 expresses the probability of finding an electron in this region of space; it can be understood how orbital overlap of this kind leads to bonding. It does so by increasing the electron probability density in exactly the right place in the region of space between the nuclei. When the electron density is large here, the attractive force of the nuclei for the electrons more than offsets the repulsive force acting between the two nuclei. This extra attractive force is the "glue" that holds the atoms together.

The second molecular orbital, called the antibonding molecular orbital (ψ_{molec}^*) is formed by subtraction in the way shown in Figure 3.2. (Subtraction means that the phase sign of one orbital has been changed from (+) to (-)). Because orbitals of opposite signs overlap, the wave function interfere with each other in the region between the nuclei and a mode is produced. At the mode, $\psi = 0$ and on either side of the mode, ψ is small. If electrons were to occupy the antibonding orbitals, the electrons would avoid the region between the nuclei. There would be only a

ah-44FR-TX2

Bonding Molecuair Orbital
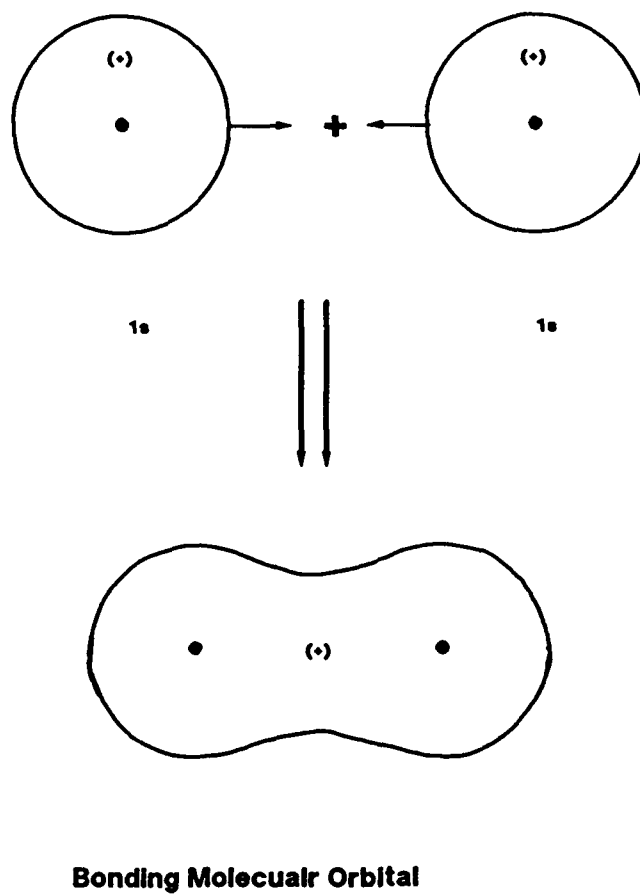
Figure 3.1 The Overlap of Two Hydrogen 1s Atomic Orbitals to
Form a Bonding Molecular Orbital

51

(+)   (-)

1s   1s

(+)   •   •   (-)

node

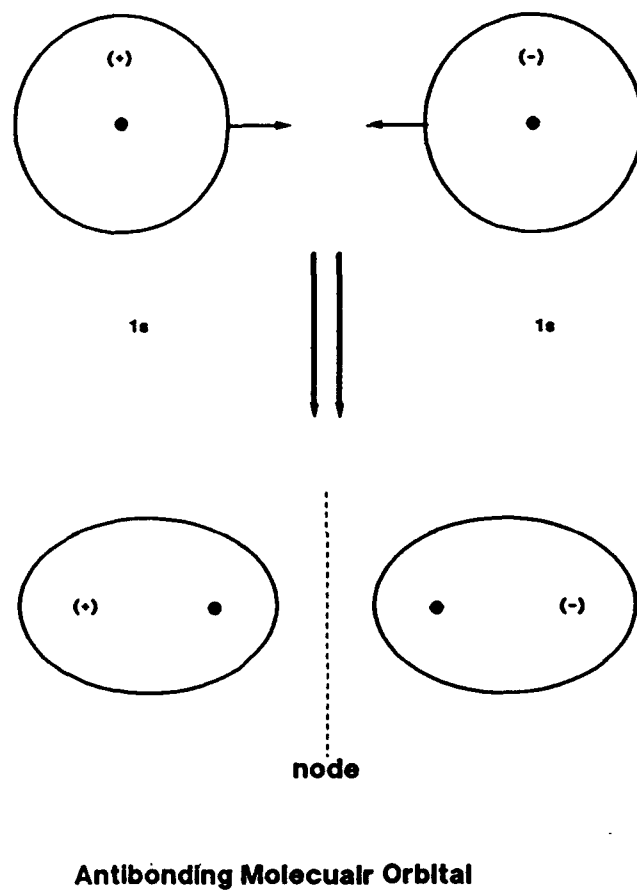**Antibonding Molecuair Orbital**

Figure 3.2 The Overlap of Two Hydrogen 1s Atomic Orbitals to
Form an Antibonding Molecular Orbital

52

small attractive force of the nuclei for the electrons. Repulse
forces (between the two nuclei and between the two electrons)
would be greater than the attractive forces. Having electrons in
the antibonding orbital would not tend to hold the atoms together;
it would tend to make them fly apart.

Molecular orbitals, like atomic orbitals, correspond to
particular energy states for an electron. Calculations show that
the relative energy of an electron in the bonding molecular
orbital of the hydrogen molecule is substantially less than its
energy in a ψ_{1s} atomic orbital. The calculations also show that
the energy of an electron in the antibonding molecular orbital is
substantially greater than its energy in a ψ_{1s} atomic orbital.

3.3 Orbital Hybridization

In this section, two very important bonds, σ bond and π bond,
which are very closely related to nonlinearity of organic
compounds, will be introduced. Based on the knowledge of
chemical bonds, the nonlinearity of molecule can be calculated
and predicted.

In a practical molecule, the molecular orbitals are very
complicated, normally a mixture of many simply molecular orbitals,
called orbital hybridization. Orbital hybridization, in this
simplest terms, is nothing more than a mathematical approach that
involves the combining of individual wave functions for s and p

orbitals to obtain wave functions for new orbitals. The new orbitals have, in varying proportions, the properties of the original orbitals taken separately. These new orbitals are called hybrid orbitals. It is possible to understand the shapes of many molecules according to their hybridized orbitals.

The theory of orbital hybridization explains the very strong bonds that are formed between carbon and hydrogen. Consider the shape of the individual sp^3 orbital shown below:
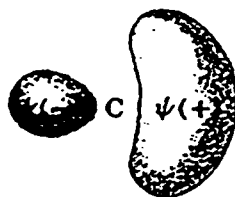
Because the sp^3 orbital has the character of a p orbital, the positive lobe of the sp^3 orbital is large and is extended quite far into space. It is the positive lobe of the sp^3 orbital that overlaps with the positive 1s orbital of hydrogen to form the bonding molecular orbital of a carbon-hydrogen bond. Because the positive lobe of the sp^3 orbital is large and is extended into space, the overlap between it and the 1s orbital of hydrogen is also large, and the resulting carbon-hydrogen bond is quite strong.

The bond formed from the overlap of an sp^3 orbital and a 1s orbital is an example of a sigma (σ) bond (see Figure 3.3). The term sigma bond is a general term applied to those bonds in which

ah-44FR-TX2
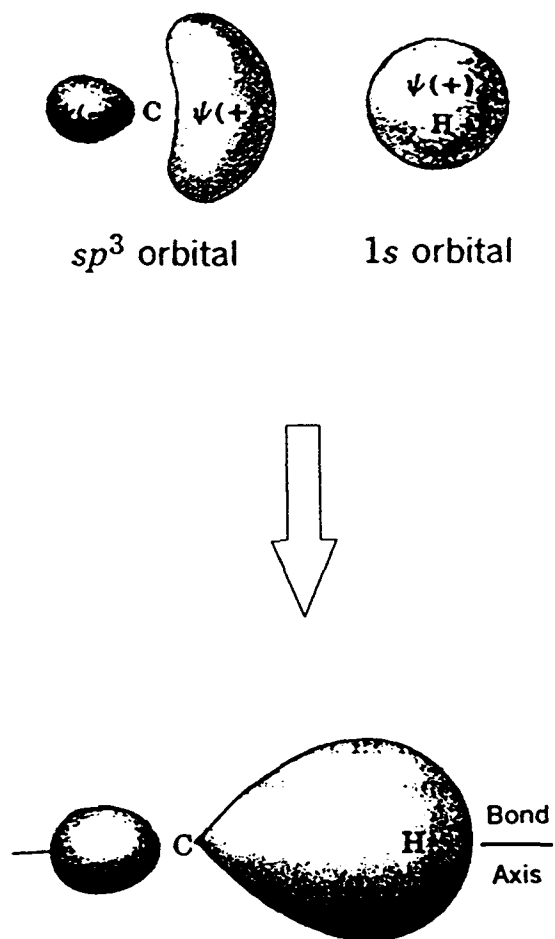
Figure 3.3 The Sigma (σ) Bond is Formed from an sp[3] Orbital and a 1s Orbital

orbital overlap gives a bond that is circularly symmetrical in cross section when viewed along the bond axis. All single bonds are sigma bonds. Because σ-bond has circular symmetry along the bond axis, rotation of groups joined by a single bond does not usually require a large amount of energy. Consequently, groups joined by single bonds rotate relatively freely with respect to one another.

To introduce, Pi(π) bond, the structure of Alkenes is taken as an example. Consider the structure of the carbon-carbon double bond in terms of orbital hybridization, the basis for this model is sp^2-hybridized carbon atoms. Formation of the sp^2 hybridized carbon atoms can be visualized in the following way. One electron from a carbon atom in its ground state is promoted from a 2s orbital to a 2p orbital. Then the 2s orbital is hybridized with two of the 2p orbitals. One 2p orbital is left unhydridized. One electron is then placed in each of the sp^2 hybrid orbitals and one electron remain in the 2p orbital.

The three sp^2 orbitals that result from hybridization are directed towards the corners of a regular triangle (with angle of $120°$ between them). The carbon p orbital that is not hybridized is perpendicular to the plane of the triangle formed by the hybrid sp^2 orbitals. So two sp^2-hybridized carbon atoms form a σ bond between them by the overlap of one sp^2 orbital from each. The remaining sp^2 orbitals of each carbon atom form σ bonds to four hydrogen atoms through overlap with the 1s orbitals

of the hydrogen atoms. These five bonds account for 10 of the 12 bonding electrons of ethene, and they are called σ-bond framework. The bond angles are quite close to the bond angles that are actually found.

The remaining two bonding electrons are located in the p orbitals of each carbon atom. The parallel p orbitals overlap above and below the plane of the σ framework. This sideways overlap of the p orbitals results in a new type of covalent bond; known as Pi(π) bond. The difference in shape of the bonding molecular orbital of a π bond is as contrasted to that of σ bond. A σ bond has cylindrical symmetry about a line connecting the two bonded nuclei. A π bond has a nodal plane passing through the two bonded nuclei P.

According to molecular orbital theory, both bonding and antibonding π molecular orbitals are formed when P orbitals interact in this way to form a π bond. The bonding π orbital results when P-orbital lobes of like sign overlap; the antibonding π orbital is formed when P-orbital lobes of opposite signs overlap.

The bonding π orbital is the lower-energy orbital and contains both π electrons (with opposite spins) in the ground state of the molecule. The region of the greatest probability of finding the electrons in the bonding π orbital is a region generally situated above and below the plane of the σ-bond framework between the two carbon atoms. The antibonding π^*

orbital is of higher energy, and it is not occupied by electrons when the molecule is in the ground state. It can become occupied, however, of the molecule absorbs light of the right frequency, and an electron is promoted from the lower energy level to the higher one. The antibonding π^* orbital has a nodal plane between the two carbon atoms.

To summarize: The carbon-carbon double bond consists of two different kinds of bonds, a σ bond and a π bond. The σ bond is formed by two overlapping sp^2 orbitals end-to-end and is symmetrical about an axis linking the two carbon atoms. The π bond is formed by a sideways overlap of two P orbitals; it has a nodal plane like a P orbital. In the ground state the electrons of the π bond are located between the two carbon atoms but generally above and below the plane of the σ-bond framework.

Electrons of the π bond have greater energy than electrons of the σ bond. The relative energies of the σ and π molecular orbitals (with the electron in the ground state) are shown in Figure 3.4. (The σ^* orbital is the antibonding σ orbital).

ah-44FR-TX2
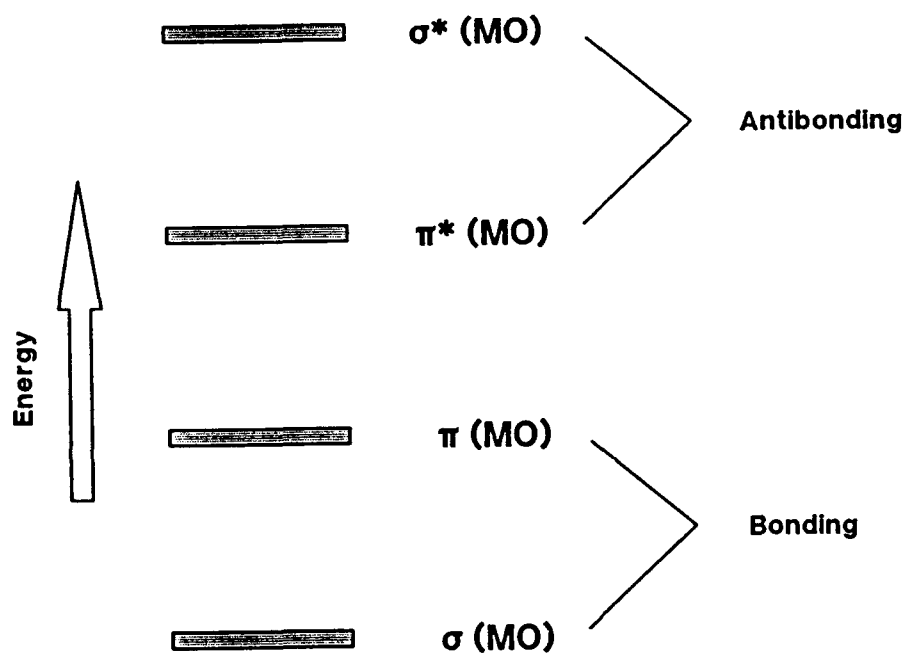
Figure 3.4 The Relative Energies of the σ and π Molecular Orbitals

4.0 Molecular Design for High Efficient Nonlinear Optical
     Materials

4.1 Theoretical Background

For the high nonlinearity efficiency, the first basic feature
is the presence of highly polarizable electronic configurations in
the molecule, such as E-Tek proposed organic molecules in this
project. Some substituents induce remarkably different electronic
behaviors on the same aromatic system. For example of the actions
of substituents on an aromatic electron system, some substituents
have a tendency to enrich their electronic population (acceptors),
while others will give away some of it (donors). Traditionally,
quantum chemists used to distinguish between long range
(mesomeric) effects, mainly π in nature, and short range
(inductive) effects, mainly σ. The nonlinear behavior of a
monosubstituted molecule can be accounted for in terms of the
π electron dipole moment. Examples of donor and acceptor
substituents are shown in Figure 4.1.

The nature of donor and acceptor groups have substantial
influence of β. One can establish a sequence of donors and
acceptors with increasing strength, as listed in Table 4.1. It
is also seen from Table 4.1 that there exists a kind of mutual
reinforcement between the donor and the acceptor. The variation
in β can exceed an order of magnitude when the donor/acceptor
combinations are changed.
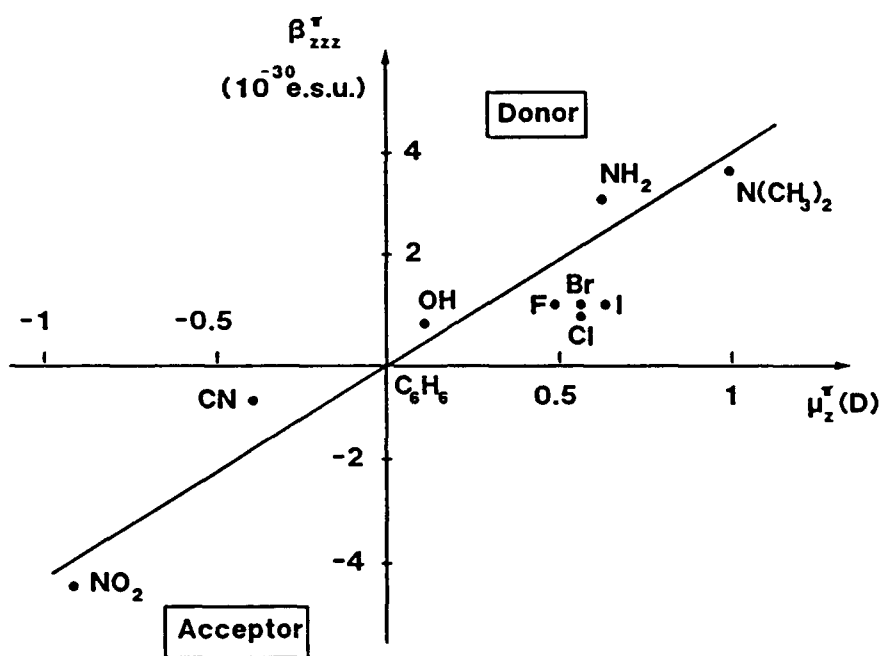
Figure 4.1 Nonlinearity of Some Monosubstituted Aromatic Molecules in Terms of Their Dipole Moments (π Electron Contributions) (After J. Badan, et al.)

Table 4.1

β (10^{-30} esu) for a Series of P-disubstituted Benzene Derivatives

Acceptor	Donor			
	CH_3	OCH_3	NH_3	$N(CH_3)_2$
CN	2.95	4.83	13.34	14.26
CHO		5.67		19.5
$COCH_3$			2.4	
NO_2	9.12	17.53	47.67	52.75

Generally, the transparence of a molecular π electron system narrows with increasing conjugation (bathochromic effect) while its nonlinear efficiency increases. The urea molecule is a small conjugated molecule transparent up to 2000 Å with a low β value. 1.3×10^{-30} esu. For 4-nitro 4'-dimethylaminostilbene the situation is opposite: absorption occurs at 5000 Å and β is 450×10^{-30} esu.

When located at opposite ends (or at conjugated positions) in a molecular system, a donor and an acceptor do more than simply add up their separate effects. A cooperative phenomenon shows up, evolving the entire disubstituted molecule, known as charge transfer (CT). Such compounds are colored (from pale yellow to red, absorption from 3000 to 5000 Å) and show high UV absorption oscillator strength. Figure 4.2 helps understand the enhancement of optical nonlinearity in such a system.

From the viewpoint of application, we need to optimize the organic systems to get the best nonlinear optical efficiency, which means not only that the high nonlinearity is required, but also that the transparent band be in the visible region as well as fast response time. Based on the design strategies described in the beginning of this section, E-Tek designed eight new organic molecules in this Phase I R&D project. These molecules are listed in Table 1.3. These molecules are short conjugated molecules, so the blue-shifted transparent band and fast response time are expected. The intramolecular charge-transfer characteristic makes

ah-44FR-TX2

ground state　　　　excited state

g　　　　　　　e

Mulliken resonant states (limits)

I　　　　II　　　　III

time

π electron
polarization
μ-μ $_o$

μ $_o$
g

state I ← weak　　　→ state III enhanced
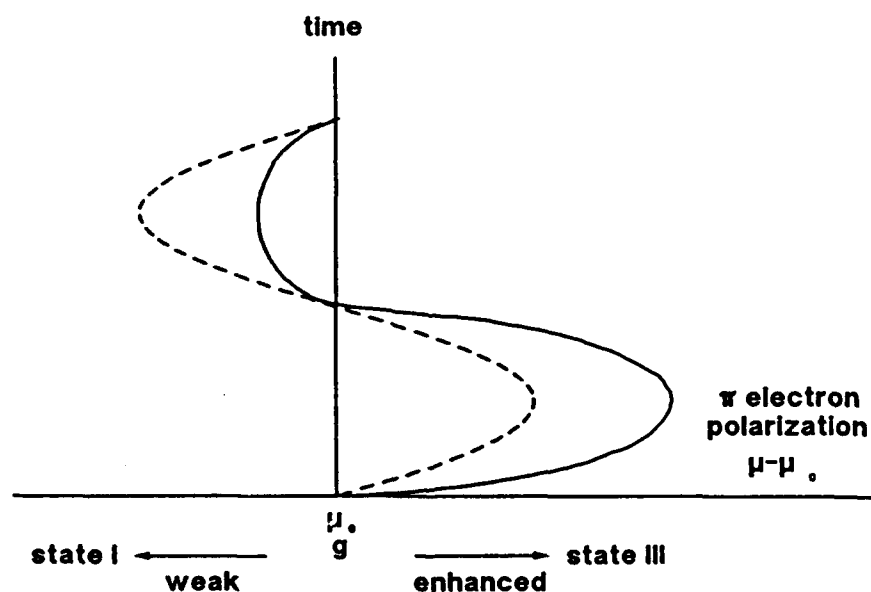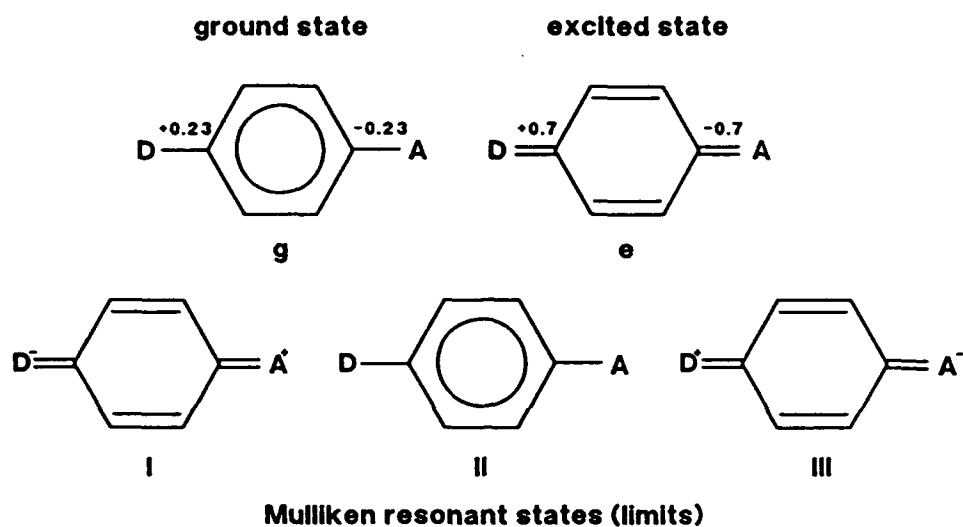
Figure 4.2　Origin of the Nonlinearity of Charge-Transfer Molecules
for a Two-Level-Like Disubstituted Aromatic Molecule.
The Donor (D) and Acceptor (A) Cooperate to Distort the
Linear Response (Dotted Lines) of a Nonsubstituted
Benzene Ring (Below)　(After J. Badan, et al.)

42-2-8

it possible for them to have relatively large nonlinearities. For example, the fourth compound 4-aminobenzophenone (ABP) listed in Table 1.3. Its chemical molecular structure is written below:
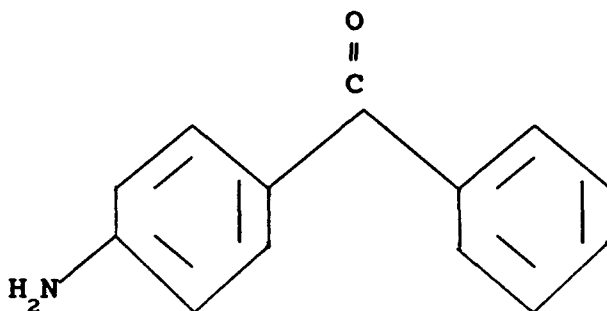
This structure has strong charge-transfer interaction along the two-fold rotational axis of the benzene ring arising from the positioning of electron-donating amino substituent para to the carbonyl group. In addition, ABP is transparent through the visible and the near infrared, i.e., the cutoff wavelength for a solution (4×10^{-4}M) of ABP in tetrahydrofuran was 394nm.

Following the same line of thought, CMV1, DVDA and MNP were designed.

The last four candidates were developed based on the very prospective new nonlinearity material 3-methyl-4-methoxy-4'-nitrostilbene (MNONS) which shows one of the longest powder second-harmonic generation signals ever observed (1250 x urea). The MNONS may be of potential interest for various nonlinear optical applications, provided large single crystals can be grown. The large powder SHG signal is due in part to charge transfer

ah-44FR-TX2

excitons which result from strong intermolecular interactions in the crystal structure.

For convenience of analysis, the molecular structure of MNONS is written below. High microscopic second-order

$$H_3CO \text{——} \underset{\underline{\quad}}{\bigcirc}\overset{CH_3}{} \text{——} CH = CH \text{——} \underset{\underline{\quad}}{\bigcirc} \text{——} NO_2$$
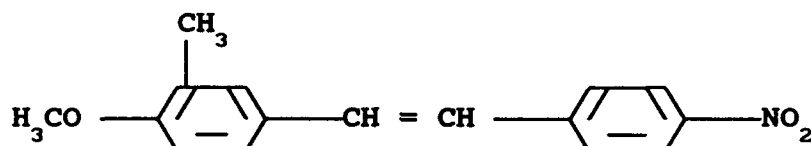
polarizabilities have been observed in molecules that possess low-lying charge-transfer resonance states. In the molecule of MNONS, H_3CO and NO_2 groups act as donor and acceptor, respectively. In their excited states, H_3CO and is positively charged and NO_2 is negatively charged. Field-induced mixing of the excited polar state into the ground electronic configuration makes the main contribution to the large nonlinearity. The methyl group associates with the the molecule through hyperconjugation, which increases the number of contributing π-type electrons, the conjugation length, and the number of resonating structures with charge migration in the same direction. These combine to yield the large molecular nonlinearity. On the third position of the aromatic ring, there is another group CH_3 which provides significant influence on conjugation strength and path, therefore, on the melting point, wavelength limit.

The MNONS has a large nonlinear optical coefficient, but the

transparency cutoff wavelength is 510 nm. Furthermore, its low melting point indicates that the damage threshold of this crystal may be lower than others. E-Tek's design goals on the new materials are not only to keep high nonlinearity but also to increase the melting point (threshold), to reduce the wavelength limit. The molecular structure of the four newly designed materials are listed below:

3-acetamido-4-methoxy-4'-nitrostilbene (ACMONS) ($C_{17}H_{16}N_2O_4$)

$$H_3CO-\underset{\underset{}{}}{\overset{\overset{NHCOCH_3}{|}}{\bigcirc}}-CH=CH-\bigcirc-NO_2$$
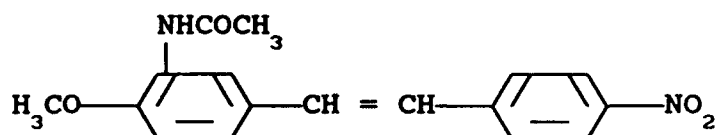
3-amino-4-methoxy-4'-nitrostilbene (AMMONS) ($C_{15}H_{14}N_2O_3$)
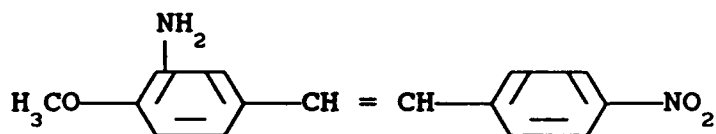
$$H_3CO-\underset{\underset{}{}}{\overset{\overset{NH_2}{|}}{\bigcirc}}-CH=CH-\bigcirc-NO_2$$

3-Hydroxy-4-methoxy-4'-nitrostilbene (HMONS)

$$H_3CO-\underset{\underset{}{}}{\overset{\overset{OH}{|}}{\bigcirc}}-CH=CH-\bigcirc-NO_2$$

3-methoxy-4-hydroxy-4'-nitrostilbene (MHONS)

$$HO \longrightarrow \overset{\displaystyle OCH_3}{\underset{\displaystyle}{\bigcirc}} \longrightarrow CH = CH \longrightarrow \bigcirc \longrightarrow NO_2$$
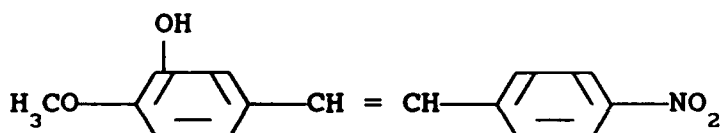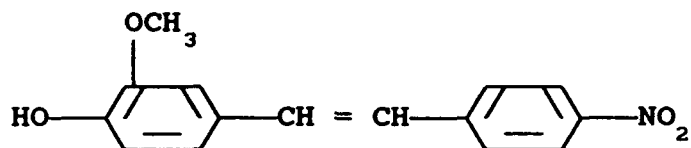
These four structures keep the basic configuration of MMONS
for which it is expected to have high nonlinearities. For ACMONS,
AMMONS and HMONS the CH_3 group at the 3rd position of the aromatic
ring is replaced by other groups $NHCOCH_3$, NH_2, NSC which are
donors also.

ah-44FR-TX2

5.0 New Organic NOM Synthesization, Purification and Physicochemical Property Characterization

In this and the next chapters, we will report our experimental research results. The synthematic experiment flowchart is shown in Figure 5.1.

After a detailed investigation, we finally selected four NOMS from the eight candidates for further experimental investigation in Phase I R&D. These four NOMs are shown in Figure 5.2. It is shown that the NOMs are delocalized π electrosystem with electron donors and acceptors.

$$H_3 \text{—} \langle \text{—} \rangle \text{—CHO} + \text{HOOCH}_2\text{C} \text{—} \langle \text{—} \rangle \text{—NO}_2 \rightarrow H_3\text{CO} \text{—} \langle \text{—} \rangle \text{—CH=CH} \text{—} \langle \text{—} \rangle \text{—NO}_2 + CO_2 + H_2O$$

(with HO on first and third rings)
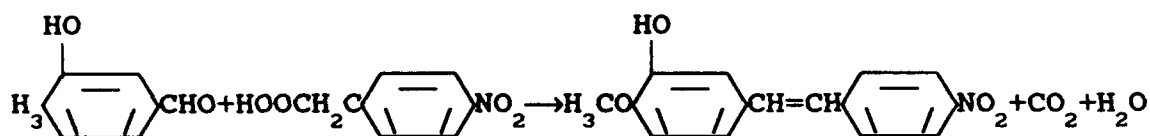
5.1 Synthesization and Purification

5.1.1 Synthesis Approaches, Equipment and Procedures of CMVI

5.1.1.1 Synthesis Approach[1]

The chemical reaction equation for synthesizing CMVI is:

$$\text{(bicyclic N–H structure)}\text{—CHO} + \text{CNCH}_2\text{CO}_2\text{C}_2\text{H}_5 \longrightarrow$$
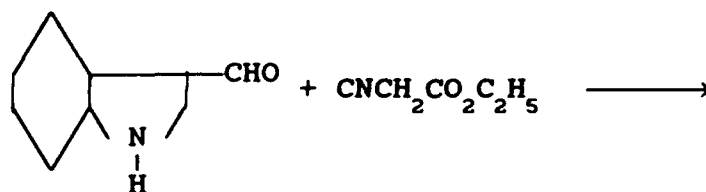
1. R.B. Van Order and H.G. Lindwall, J. Org. Chem., 10, 128, 1945.

Systematic Experiment Flowchart

Investigate The Synthesis Methods

↓

Select Raw Materials

↓

Synthesization Process

↓

Purification

↓

Elemental Analysis

↓

Structure Determination

↓

Melting Point Measurement

↓

Transparent Band Determination

↓
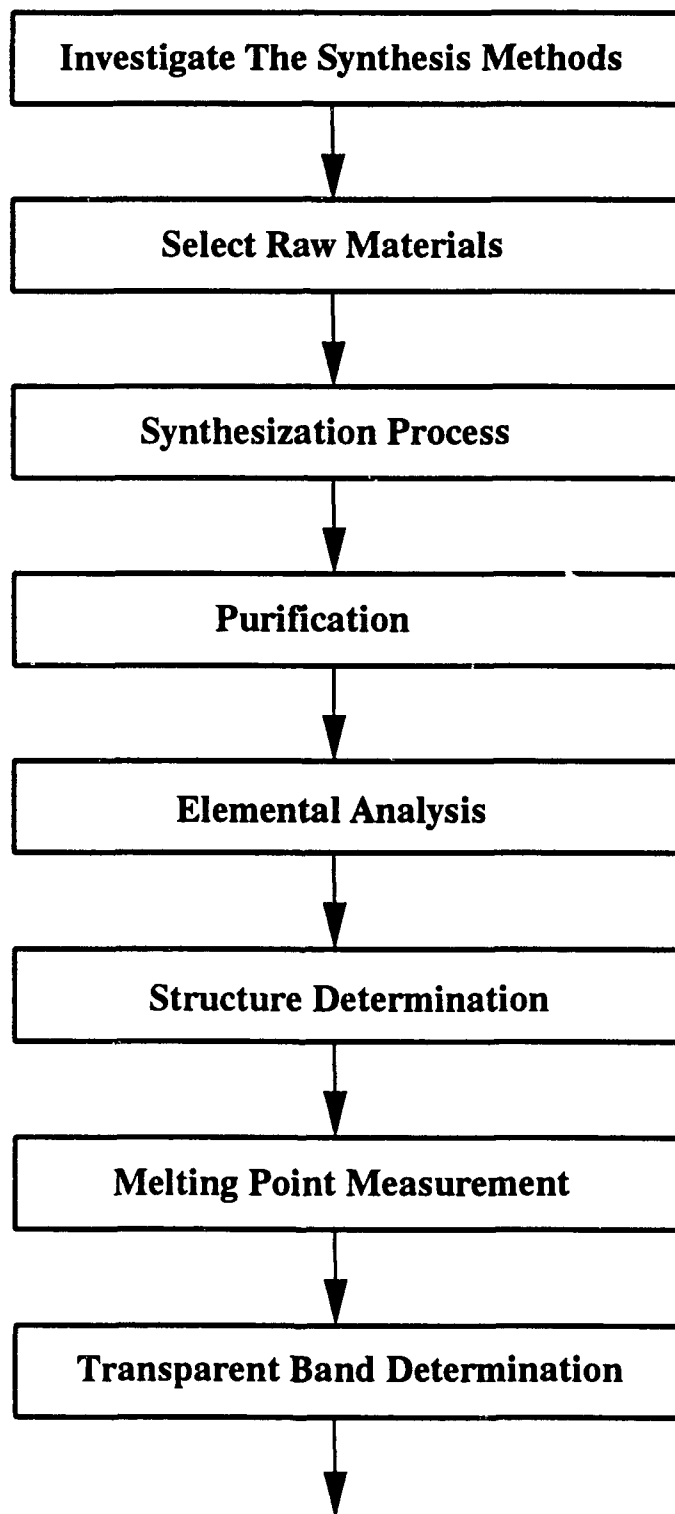
Figure 5.1 Systematic Experiment Flowchart

61-44pst2

Systematic Experiment Flowchart (Con't)

$x^{(2)}$Estimation By Power Effect Test

$x^{(3)}$And Response Time Test In Solvent

Crystal Growth Investigation

Device Fabrication Investigation

Device Application Investigation
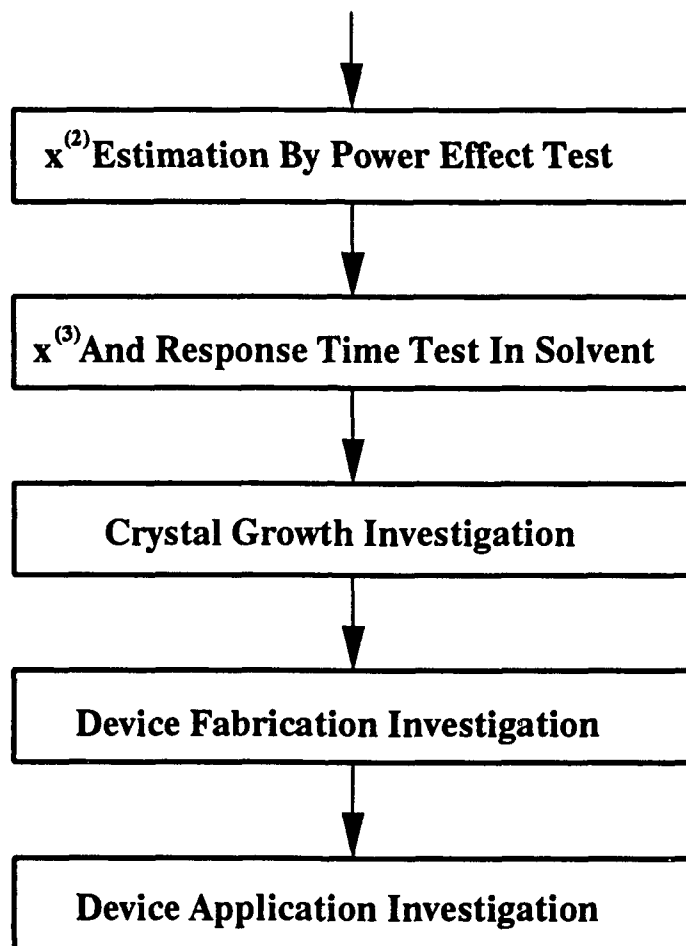
Figure 5.1 Systematic Experiment Flowchart (Con't)
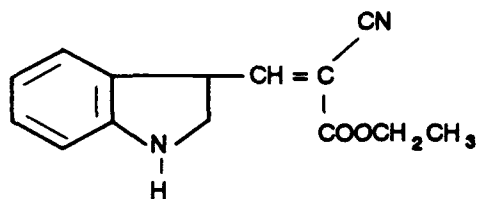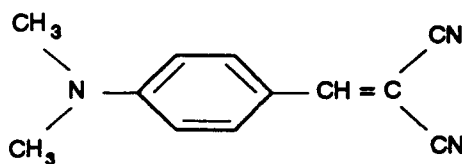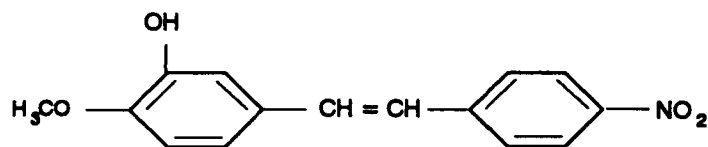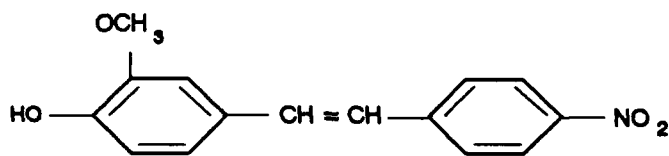
Figure 5.2 The Four Selected NOMS Further Experimental Investigation

$$\text{Indole-CH}=\text{C} \begin{subarray}{l} \diagup \text{CN} \\ \diagdown \text{COOCH}_2\text{CH}_3 \end{subarray} + \text{H}_2\text{O}$$
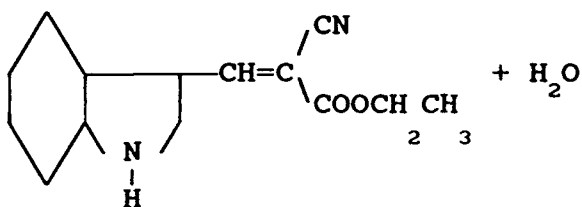
Required raw materials are:

Indol-3-aldehyde	99%, 14.5 g
Ethyl cyanoacetate	99%, 11.3g
Pipeidine (catalyst)	0.5 ml
Alcohol	500 ml

5.1.1.2   Equipment

- Temperature stabilized magnetic stirrer
- 250 ml round bottom boiling flask
- Buchner style funnel
- 250 ml filtering flask (for purifying material)
- Condenser pipes
- Porcelain mortar

5.1.1.3   Synthesis and Purify Procedures

Collect 14.5 gram of Indol-3-aldehyde and 11.3 gram of ethyl cyanoacetate; mix them and stir for 30 minutes at room temperature using temperature stabilized magnetic stirrer. Add 0.5 ml pipeidine into mixture while stirring. The created materials are solid. Grind the solid into powder in a mortar, then rinse powder

ah-44FR-TX3

using mixture of boiling water and acetic acid glacial (PH = 4), filter solution immediately, rinse it again using cool alcohol to receive 22 gram crude outcome. Re-crystallize the outcome in alcohol to receive light yellow crystals.

5.1.2 Synthesis Approaches, Equipment and Procedures of DVDA[1]

5.1.2.1 Synthesis Approach

The chemical reaction equation for synthesizing DVDA is:

$$(CH_3)_2N—\langle\ \rangle—CHO + (CN)_2 CH_2 \longrightarrow$$

$$(CH_3)_2N—\langle\ \rangle—CH=C(CN)_2 + H_2O$$
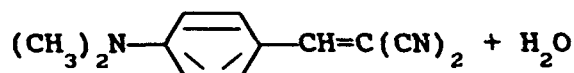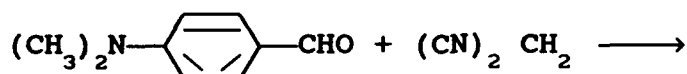
Required raw materials are:

p-dimethylaminobenzaldehyde	99%, 7.5 g
Malonitrile	99%, 3.3 g
Pipeidine (Catelyst)	0.3 ml
Alcohol	500 ml

5.1.2.2 Equipment

- Temperature stabilized magnetic stirrer

---

1. L. Horner, K. Klupfel, Ann., 591, 69, 1955 (Ann. = Annalen der chemie)

- 250 ml round bottom flask

- Buchner style funnel

- Condenser pipe

- Mortar

- 250 ml filtering flask

5.1.2.3 Synthesis and Purify Procedures

Collect 7.5 gram of p-dimethylaminobenzaldehyde and 3.3 gram of malonitrile, place them in a round bottom flask; stir and mix them in a flask which is in a 65°C water both. When materials become liquid, add 0.3 ml pipeidine to speed up chemical reaction. The outcomes are solid. Grind this solid into powder in a mortar, add a little mixture of boiling water and acetic acid glacial to rinse powder; then rinse it again using cool alcohol. Filter outcome to have 9.3 gram of orange-red crude material. Re-crystallize the outcome in alcohol to receive final product of DVDA in orange-red crystals.

5.1.3 Synthesis Approaches, Equipment, Procedures of HMONS[1,2]

(3-hydroxy-4-methoxy-4'-nitrostilbene).

1. Migridichian, V. (1957), Organic Synthesis, Vol. II 957-958. New York: Reinhold
2. J.C.S. (1942), p. 112.

5.1.3.1 Synthesis Approaches

The chemical reaction equation is:

$$H_3CO\!-\!\!\langle \text{OH} \rangle\!-\!CHO + HOOCH_2C\!-\!\langle \rangle\!-\!NO_2 \xrightarrow{\text{pipeidine}}$$

$$H_3CO\!-\!\!\langle \text{OH} \rangle\!-\!CH{=}CH\!-\!\langle \rangle\!-\!NO_2 + CO_2 + H_2O$$
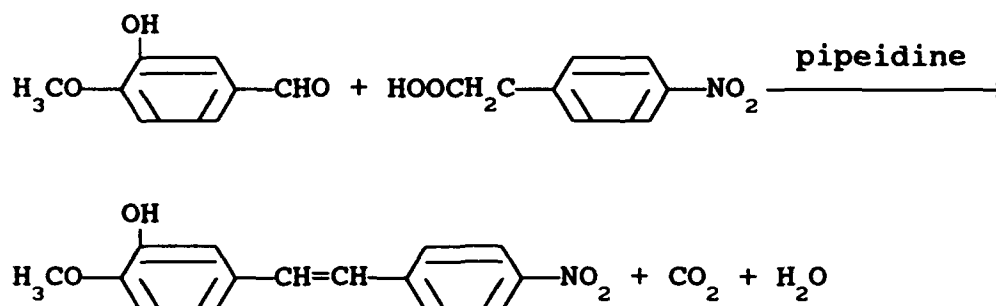
Required raw materials are:

3-hydroxy-4-methoxybenzaldehyde   99%, 15g
     (Aldrich Company)

4-nitrophenylacetic acid   99%, 18g
     (Aldrich Company)

Pipeidine   (Catalyst)   1 ml

Phridine   (for purifying)   500 ml

5.1.3.2 Equipments

- Temperature stabilized magnetic stirrer
- 250 ml round bottom boiling flask
- Buchner style funnel
- Condensers

- 250 ml filtering flask (for purifying materials).
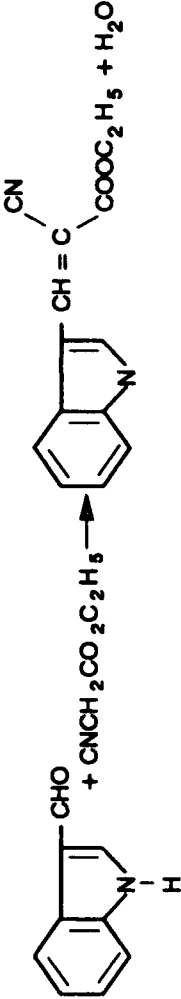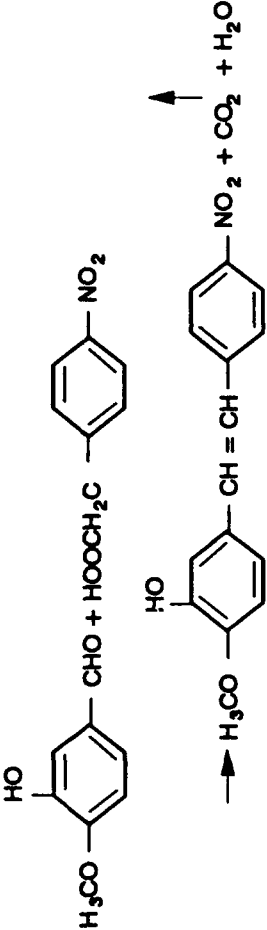
5.1.3.3 Synthesis and Purify Procedures

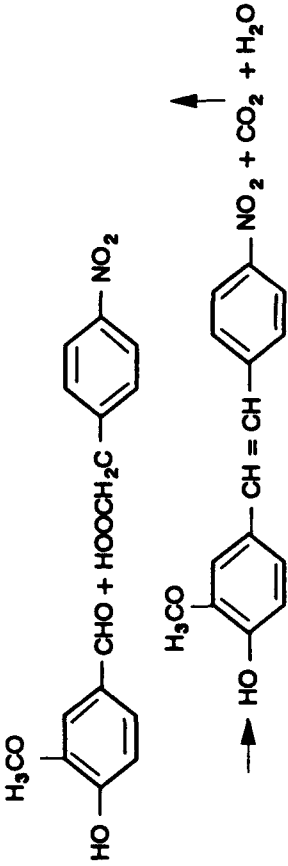Collect 15 gram (0.1 Mol.) of 3-hydroxy-4-methoxydenzaldehyde and 18 gram (0.1 Mol.) 4-nitrophenylacetic acid to mix together, then place the mixture in a round bottom flask. Set condenser on the flask. Make cool water to pass through the condenser then heat flask while stirring chemical mixture using temperature stabilized magnetic stirrer. At temperature 160°C, both 3-hydroxy- 4-methoxydenzaldehale, and 4-nitrophenylacetic acid are totally melted. Drop 1 ml of pipeidine (the catalyst which speeds up the reaction between two raw materials). Keep temperature at 160°C, materials are evaporating to condenser and going back to flask under cooling effect of the water surround condenser. This processing lasts for six hours. The materials in the flask become black. Then remove heater, cool solution in the flask down, get black solid. This solid includes remaining raw materials and created compounds. Procedures of purifying created material are as follows:

Place all materials in a flask; add 75 ml phridine and heat flask a little bit until all things dissolved in phridine. Pour the solution into a beaker, then evaporate most of the pyridine. Cool down the solution, filter it through a filtering flask, obtain a dark yellow HMONS. Repeat the purifying procedures twice until yellow color, sliced crystal powders are obtained.

77

5.1.4 Synthesis Approaches, Equipment and Procedures of MOHNS

5.1.4.1 Synthesis Approaches

The chemical reaction equations for synthesizing MOHNS is

$$OH-\underset{H_3CO}{\bigcirc}-CHO + HOOCH_2C-\bigcirc-NO_2 \xrightarrow{\text{pipeidine}}$$

$$OH-\underset{H_3CO}{\bigcirc}-CH=CH-\bigcirc-NO_2 + CO_2 + H_2O$$
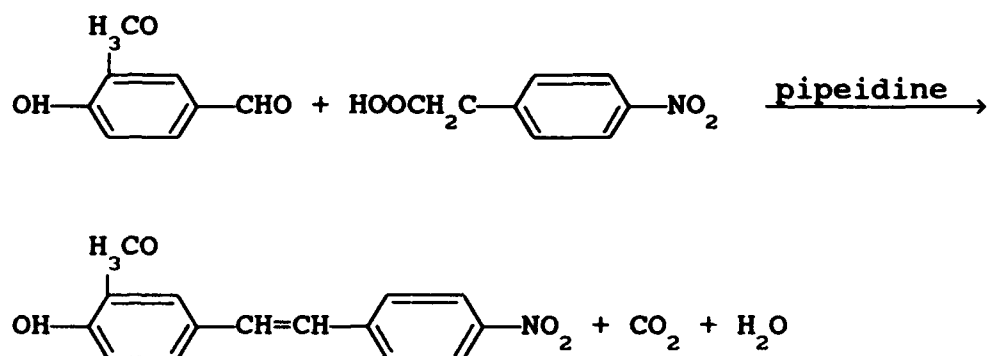
Required raw materials are:

3-methoxy-4-hydroxylbenzaldehyde (Aldrich Company)	99%, 15 g
4-nitrophenylacetic acid (Aldrich Company)	99%, 18 g
Pipeidine (catalysit)	1 ml
Phridine	500 ml

5.1.4.2 Equipment

- Temperature stabilized magnetic stirrer
- 250 ml round bottom boiling flask
- Buchner style funnel

- 250 ml filtering flask (for purifying material)
- Condensers

5.1.4.3   Synthesis and Purify Procedures

Collect 15 gram (0.1 Mol.) 3-methoxy-4-hodryxylbenzaldehyde and 18 gram (0.1 Mol.) 4-nitrophenylacetic acid. Mix them and pour them into a round bottom flask with condenser on. Heat flask while stirring mixture using temperature stabilized magnetic stirrer. When temperature rises to 120°C, both raw materials totally melt. Add 1 ml of pipeidine (the catalyst which speeds up the reaction between two raw materials). Keep temperature at 120°C for six hours, materials in chemical reaction go up to condenser and down back to flask under cooling effect of water surround the condenser. Cool whole solution down then obtain black solid of raw created materials. Purifying procedures are as follows: Add 75 ml pyridine into this black solid and heat them a little bit until the solid is totally dissolved. Evaporate most pyridine from the solution, then filter the rest solution using filtering flask after solution was cooled down. The created materials are brown-red. Repeat purifying procedures twice and finally obtain the golden-yellow sliced crystal powder.

The synthesization and purification experiments are summarized in Table 5.1.

5.2   Elemental Analysis and Structure Determination

After these new NOMS, CMVI, DVDA, HMONS and MOHN have been

ah-44FR-TX3

Table 5.1 New Material Synthesization and Purification

New Materials	Synthesis Reaction	Purification	Sample Color	Mark
CMVI ($C_{14}H_{11}N_2O_2$)	indole-CHO + $CNCH_2CO_2C_2H_5$ → $CH=C(CN)COOC_2H_5 + H_2O$	Recrystallization in Alcohol	Light Yellow	[1]
DVDA ($C_{12}H_{11}N_3$)	$(CH_3)_2N$-C$_6$H$_4$-CHO + $(CN)_2CH_2$ → $(CH_3)_2N$-C$_6$H$_4$-$CH=C(CN)_2 + H_2O$	Recrystallization in Alcohol	Orange	[2]
HMONS ($C_{15}H_{13}NO_4$)	H_3CO/HO-C$_6$H$_3$-CHO + $HOOCH_2C$-C$_6$H$_4$-NO_2 → H_3CO/HO-C$_6$H$_3$-$CH=CH$-C$_6$H$_4$-$NO_2 + CO_2 + H_2O$	Twice Recrystallization in Pyridine	Light Yellow	[3][4]
MOHNS ($C_{15}H_{13}NO_4$)	H_3CO/HO-C$_6$H$_3$-CHO + $HOOCH_2C$-C$_6$H$_4$-NO_2 → HO/H_3CO-C$_6$H$_3$-$CH=CH$-C$_6$H$_4$-$NO_2 + CO_2 + H_2O$	Twice Recrystallization in Pyridine	Golden Yellow	[3][4]

[1] R.B Van Order and H.G. Lindwall, J. Org. Chem., 10, 128 (1945).
[2] L. Horner, K. Klupfel, Ann., 591, 69 (1955).
[3] V. Migrdichian (1957), Organic Synthesis, Vol. II 957-958, New York: Reinhold.
[4] J.C.S. (1942), P. 112

synthesized and purified, we have to determine that the compounds we get are exactly the same as what we designed. So the elemental analysis and structure determination have been carried out.

An elemental analyzer has been used for the elemental analysis of the four compounds, and the measurement results have been summarized in Table 5.2.
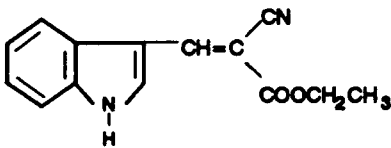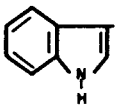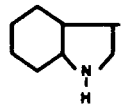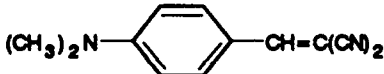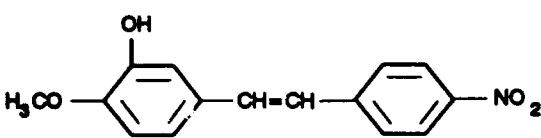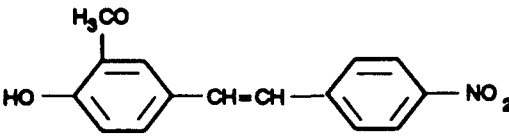
Table 5.2
Compositions of Synthesized Materials

Name	Formula	Composition Analysis					
		Theoretically			Experimental		
		C	H	N	C	H	N
CMVI	$C_{14}H_{11}N_2O_2$	70.00	5.00	11.67	70.27	5.12	11.72
DVDA	$C_{12}H_{11}N_3$	73.10	5.58	21.32	73.01	5.43	21.41
HMONS	$C_{15}H_{13}NO_4$	66.42	4.80	5.17	66.36	4.60	5.36
MOHNS	$C_{15}H_{13}NO_4$	66.42	4.80	5.17	66.80	5.00	5.11

After the compositions of the four organic NOMS have been confirmed, we have also determined the chemical structures of these four NOMS, using ^{1}H NMR (proton nuclear magnetic resonance) FT-06A. The experimental results are listed in Table 5.3.

The original signal curves are shown in Figures 5.3 to 5.6.

Table 5.3

Chemical Structure Determination

Number	Name	Structure	Displacement δ (ppm)
1	CMVI		1.31-1.50 (3H, t, $-COOCH_2CH_3$) 4.23-4.50 (2H, d, $-COOCH_2CH_3$) 7.26-8.64 (6H, m, $CH=C-$) 9.31 (1H, S,)
2	DVDA	$(CH_3)_2N$—⬡—$CH=C(CN)_2$	3.13 (6H, S, $(CH_3)_2-N-$) 6.62, 6.74, 7.43, 7.74, 7.85) 5H, qu, —⬡—$CH=C$)
3	HMONS		3.93 (3H, S, $-OCH_3$) 5.56 (1H, -OH) 6.88 - 7.15 (5H, M, $C_6H_3C_2H_2-$) 7,52, 7.63, 8.14, 8.24 (4H, q, $-C_6H_4NO_2$)
4	MOHNS		3.97 (3H, S, $-OCH_3$) 5.75 (1H, S, -OH) 6.97 - 7.13 (5H, M, $C_6H_3C_2H_2-$) 7.52, 7.63, 8.14, 8.25 (4H, q, $-C_6H_4NO_2$)

82
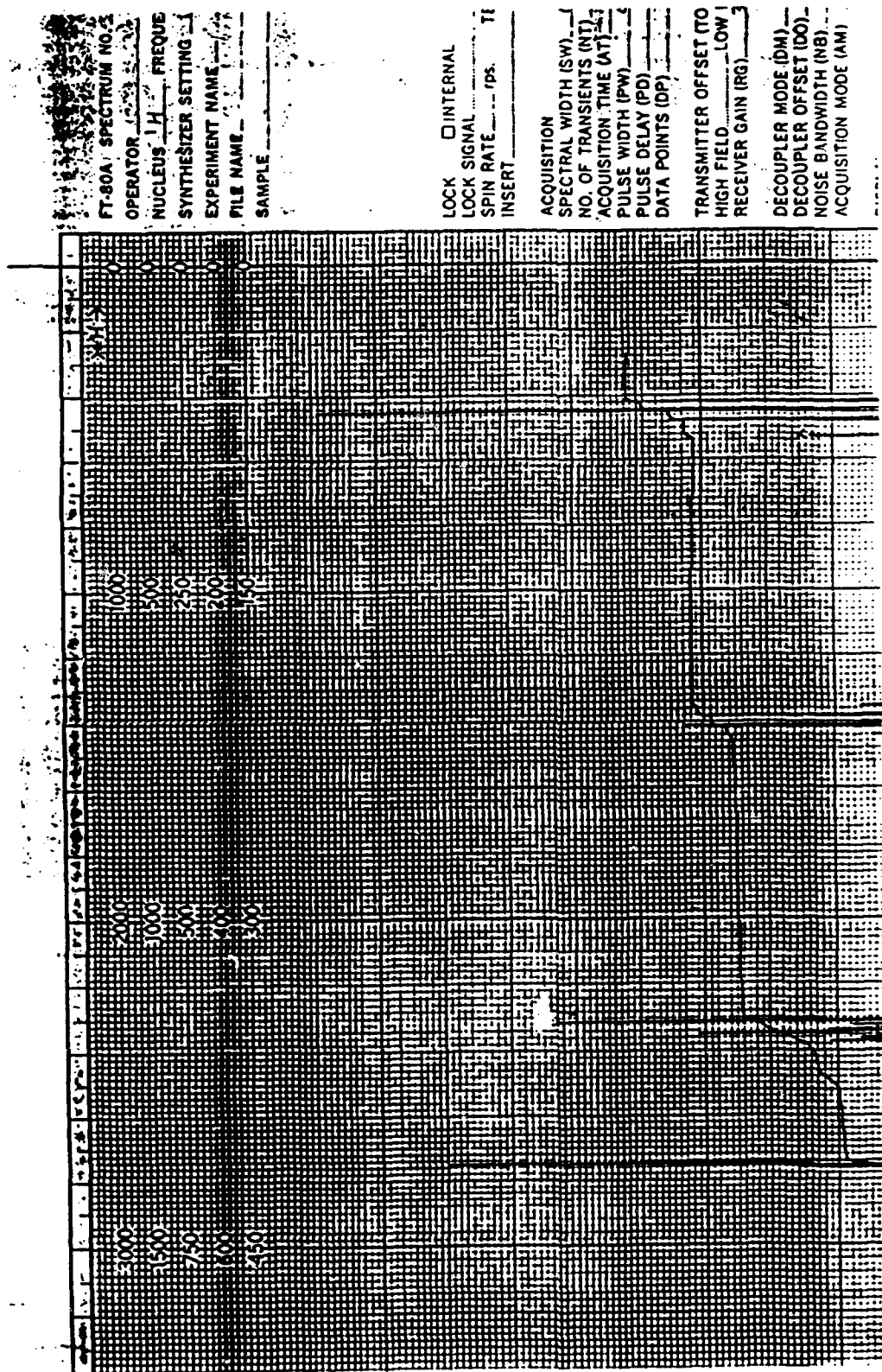
Figure 5.3 ^{1}H NMR Spectrum of CMVI
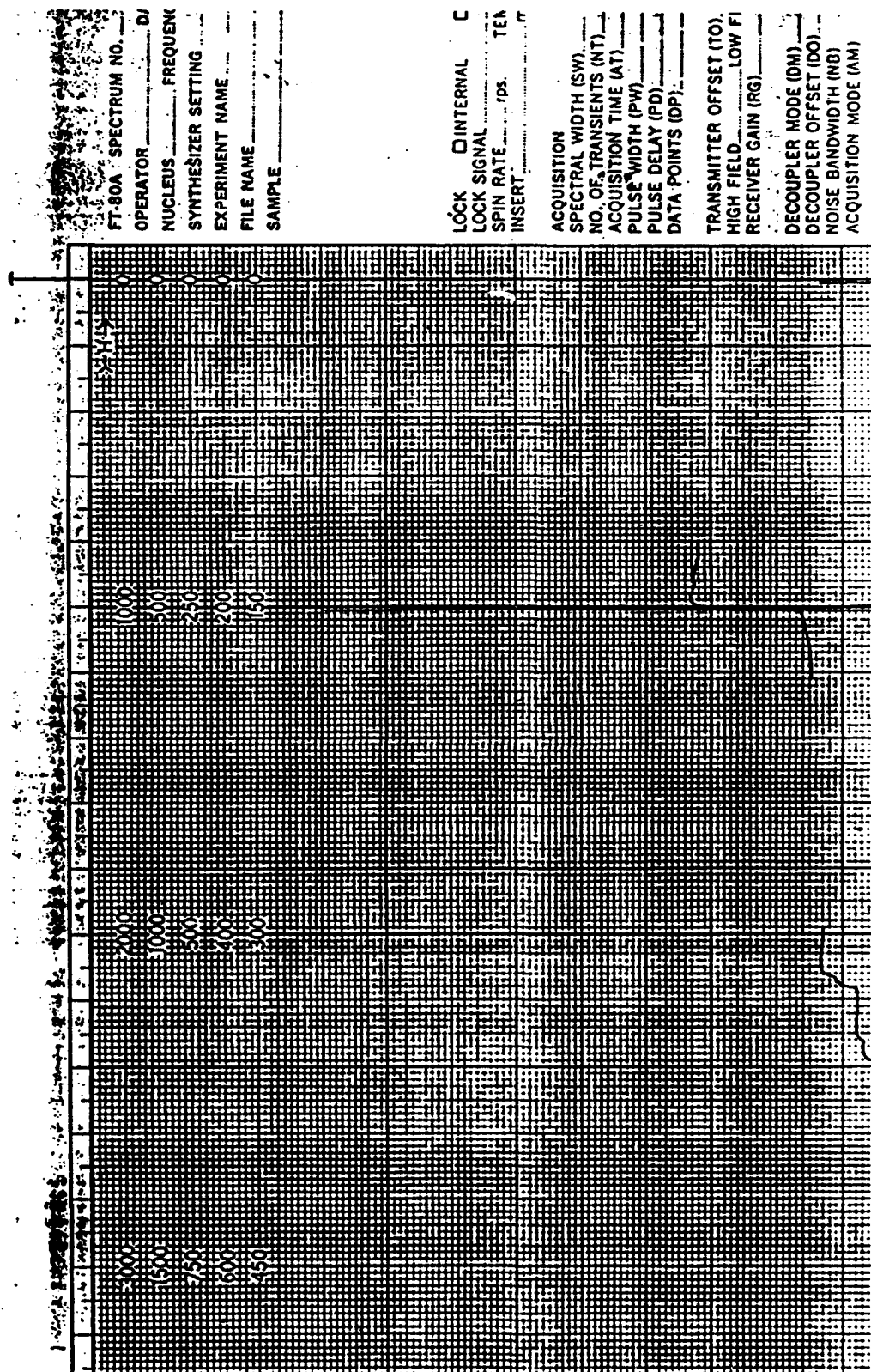
Figure 5.4 ¹H NMR Spectrum of DVDA

84
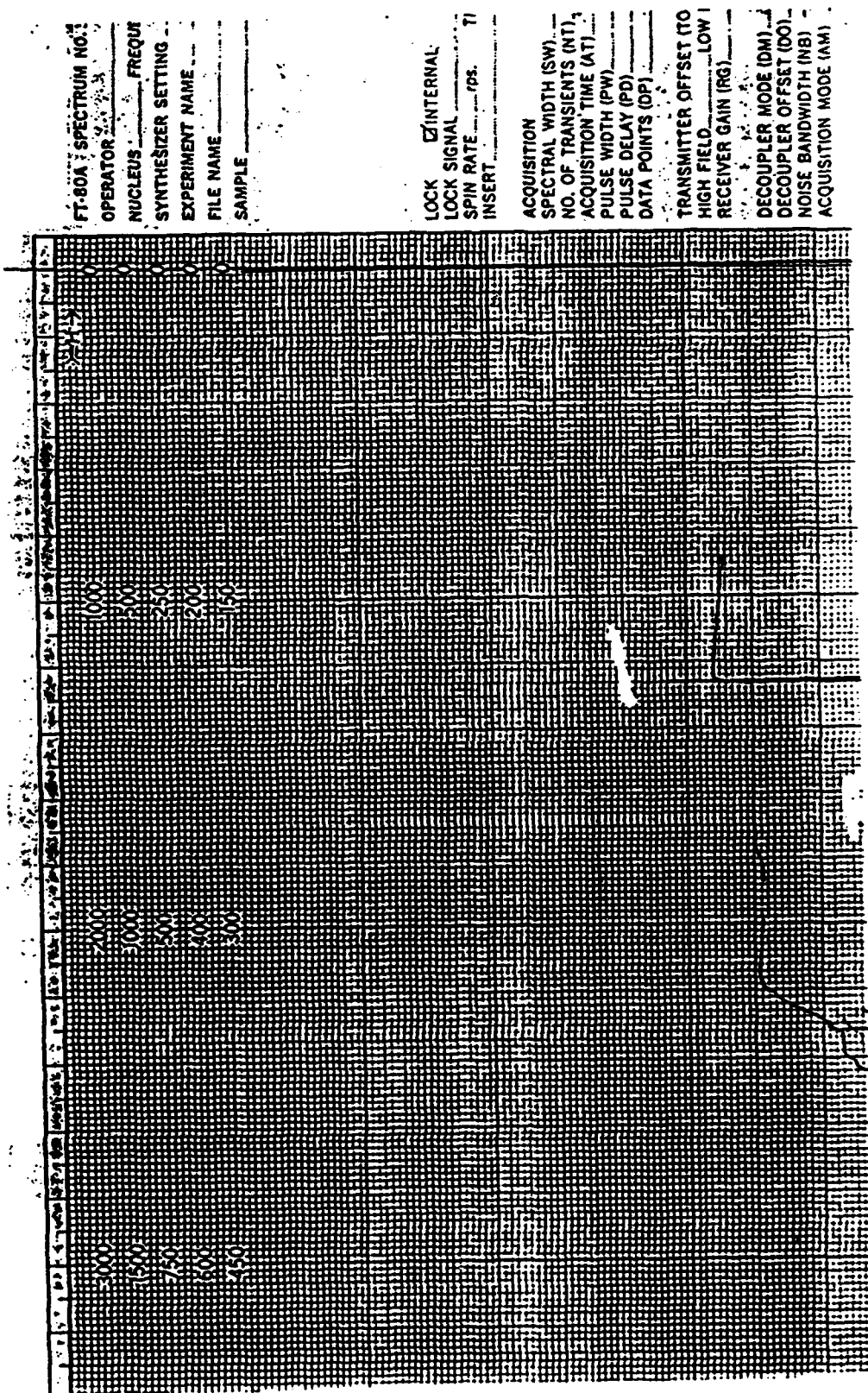
Figure 5.5 ^{1}H NMR Spectrum of HMONS
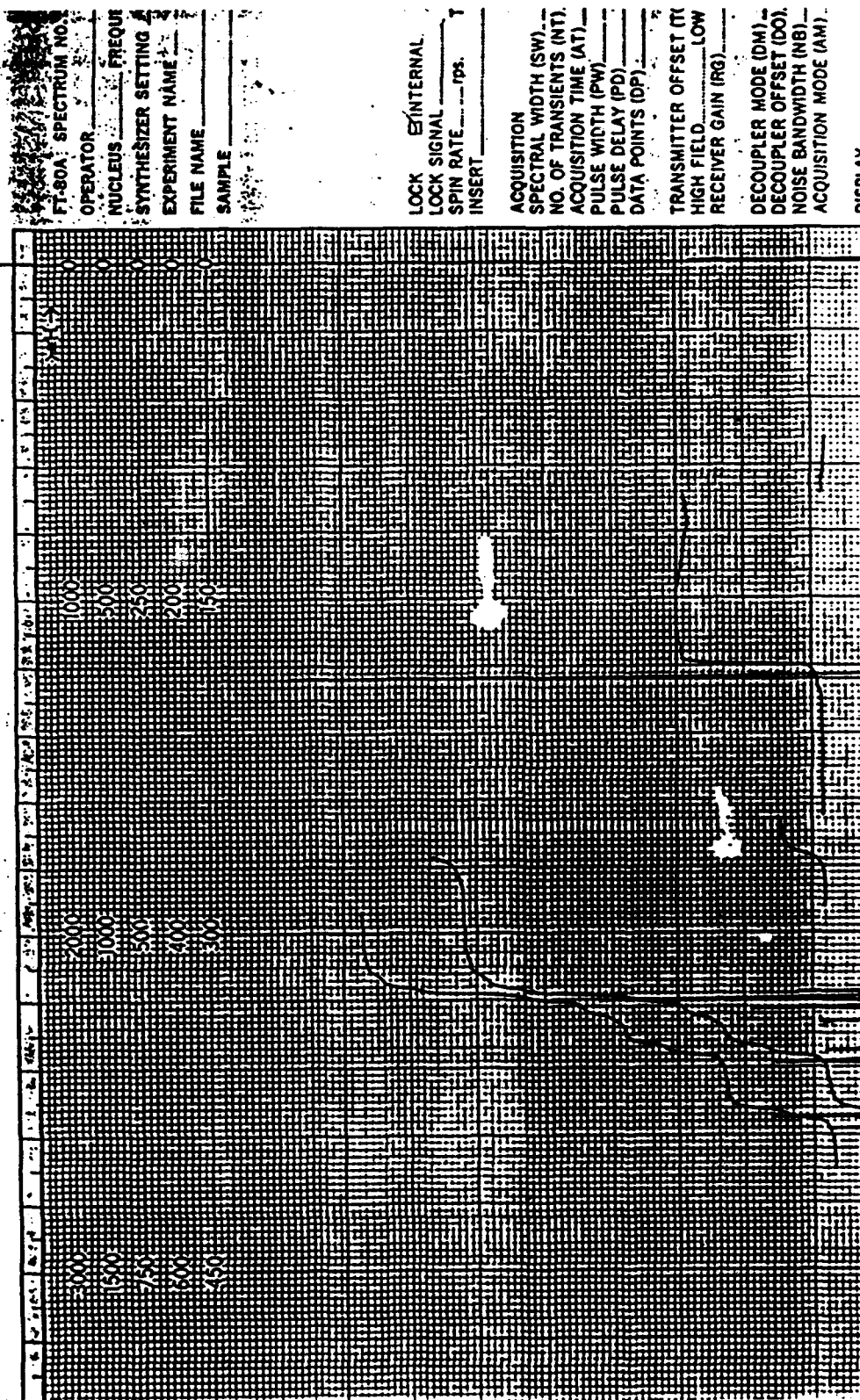
Figure 5.6 ^{1}H NMR Spectrum of MOHNS

5.3 Melting Points and Absorption Spectra Measurements

5.3.1 Melting Point Measurement

Melting point of NOMS are related to their damage thresholds The measurements of melting points are performed by a differential scanning calorimeter of DSC-4. The results are listed in Table 5.3.

The original measurement curves of CMVI, DVDA, HMONS and MOHNS are shown in Figures 5.7, 5.8, 5.9 and 5.10.

5.3.2 Absorption Spectra

Absorption spectra of synthesized materials are determined by a wideband spectrometer UV-3000. Absorption edges were determined when the transmittance of 1×10^{-4} M alcohol solution of material is 95%. The experimental results are listed in Table 5.4.

Table 5.4
Absorption Spectra of Synthesized Materials

Number	Name	Absorption Edge (Cut-Off) nm
1	CMVI	435
2	DVDA	485
3	HMONS	485
4	MOHMS	495
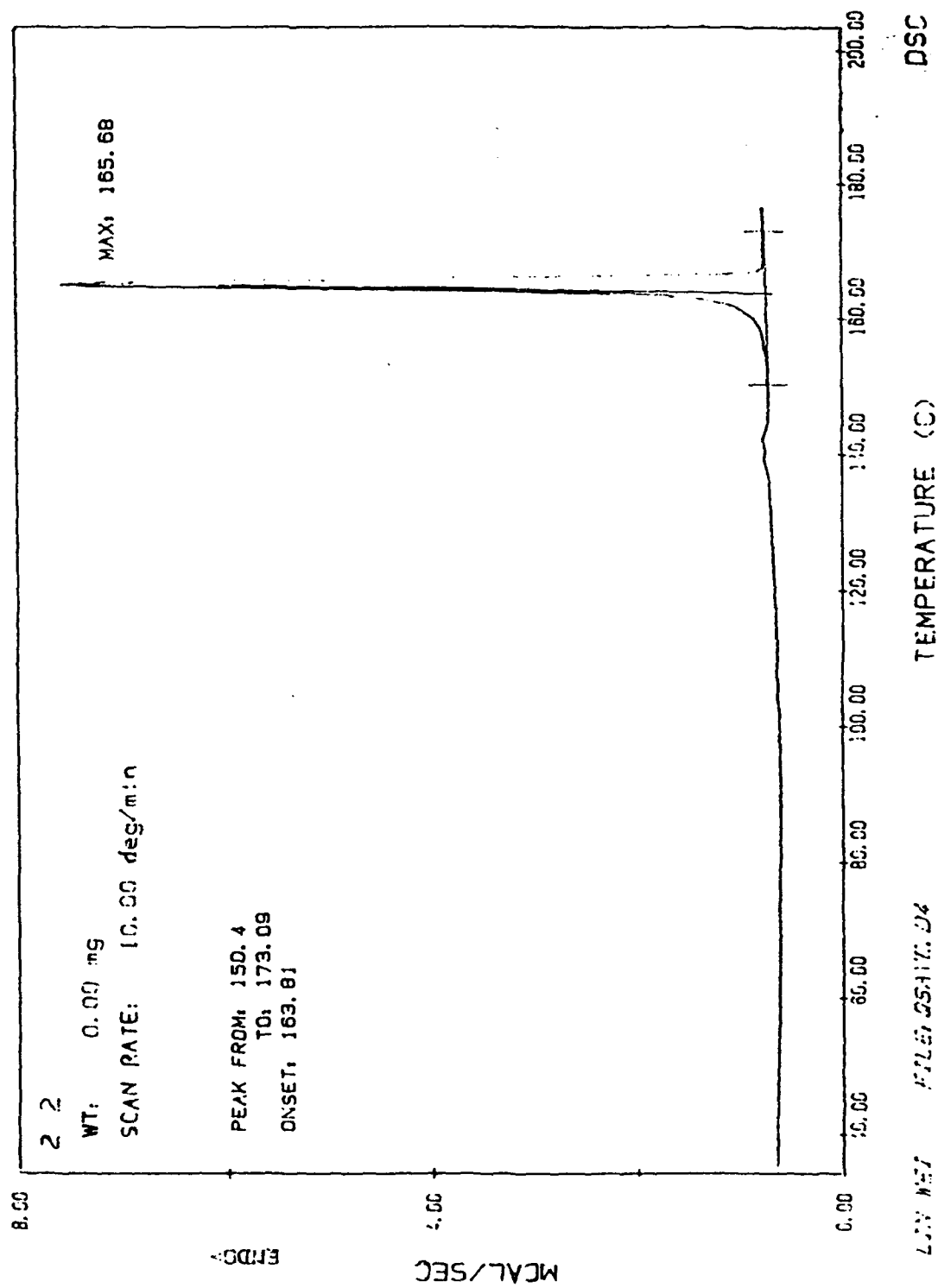
ah-44FR-TX3

Figure 5.7 Spectrum of CMVI by Differential Scanning Calorimeter
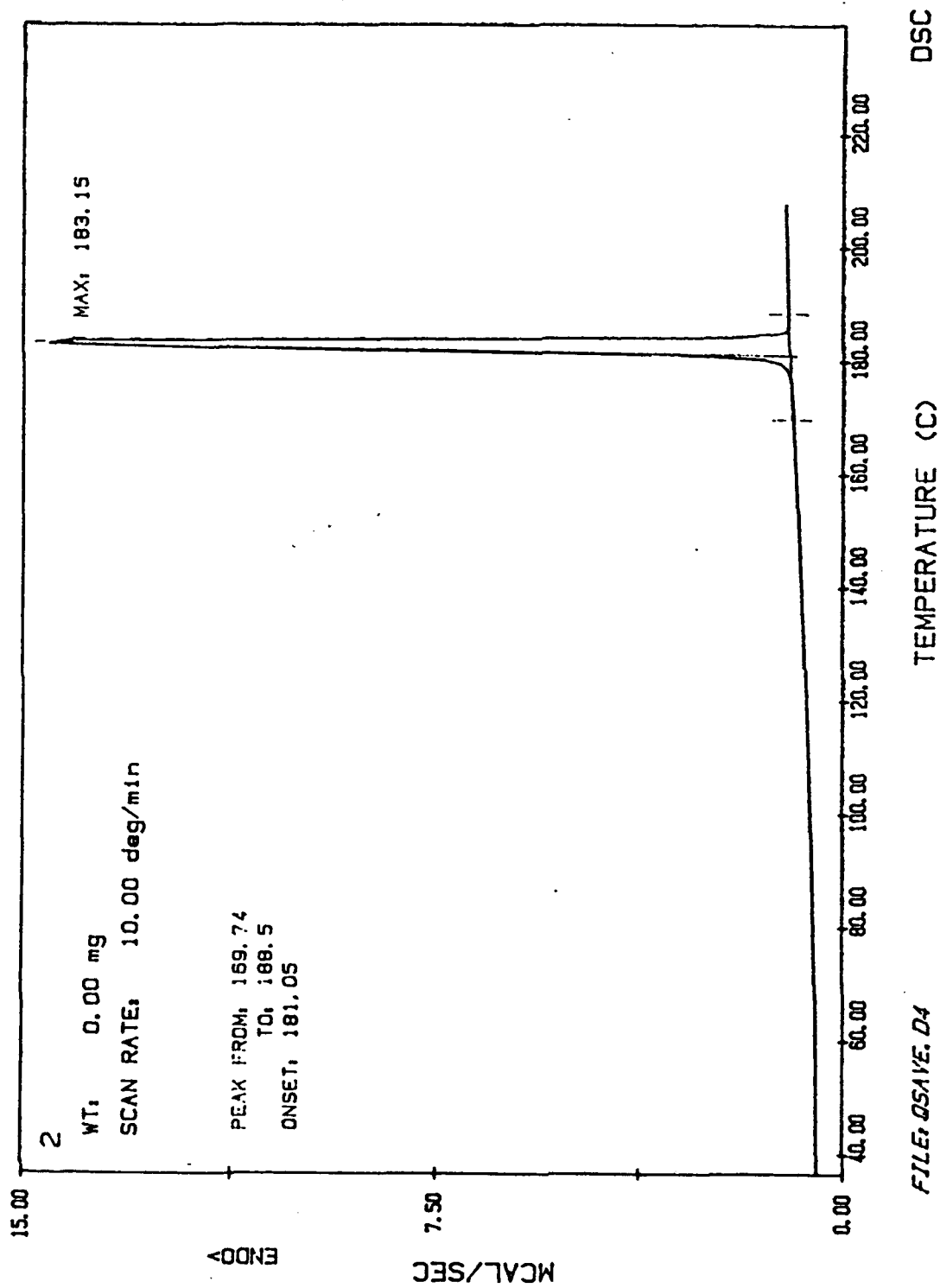
Figure 5.8 Spectrum of DVDA by Differential Scanning Calorimeter
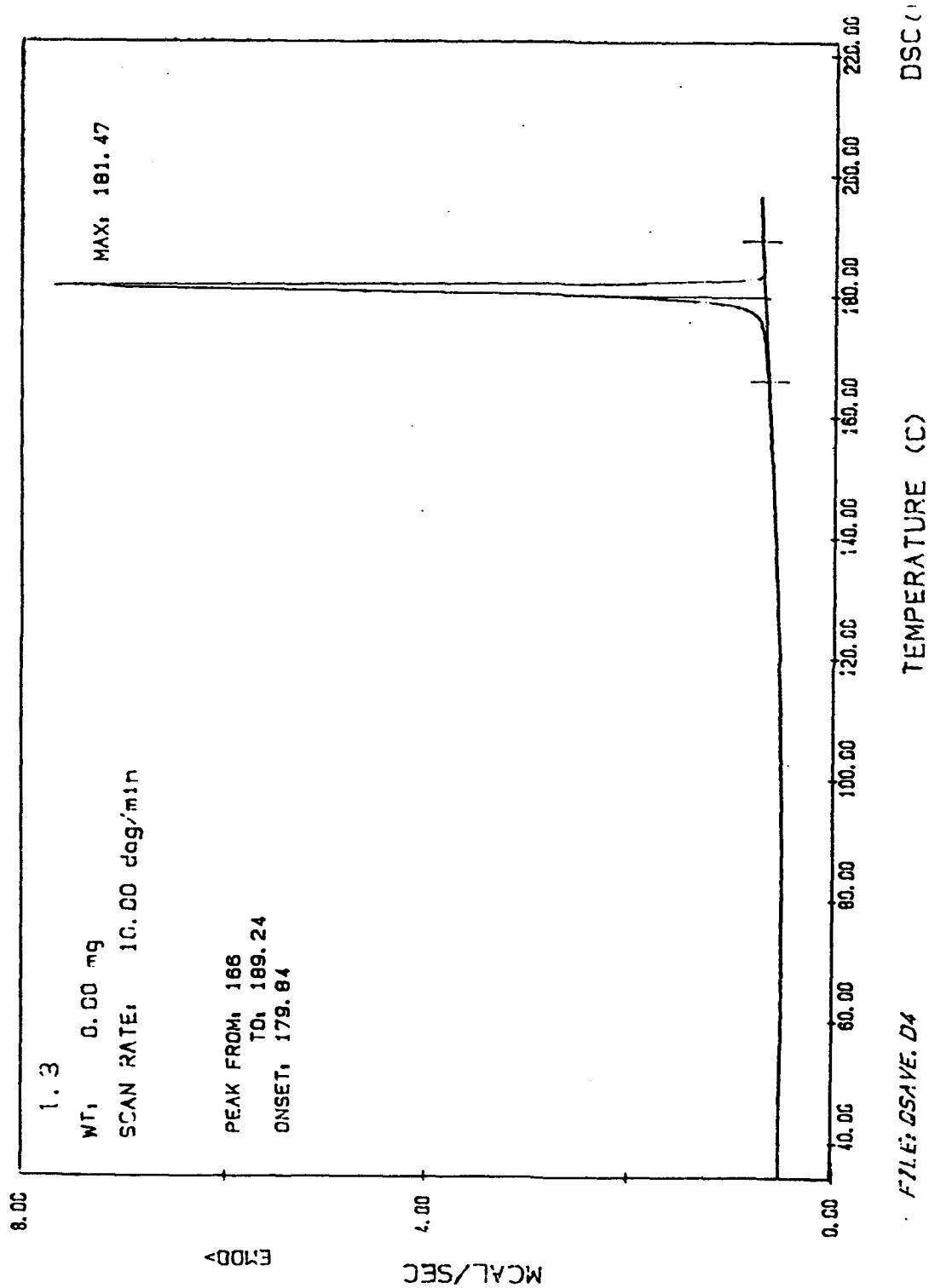
Figure 5.9 Spectrum of HMONS by Differential Scanning Calorimeter

MOHNS

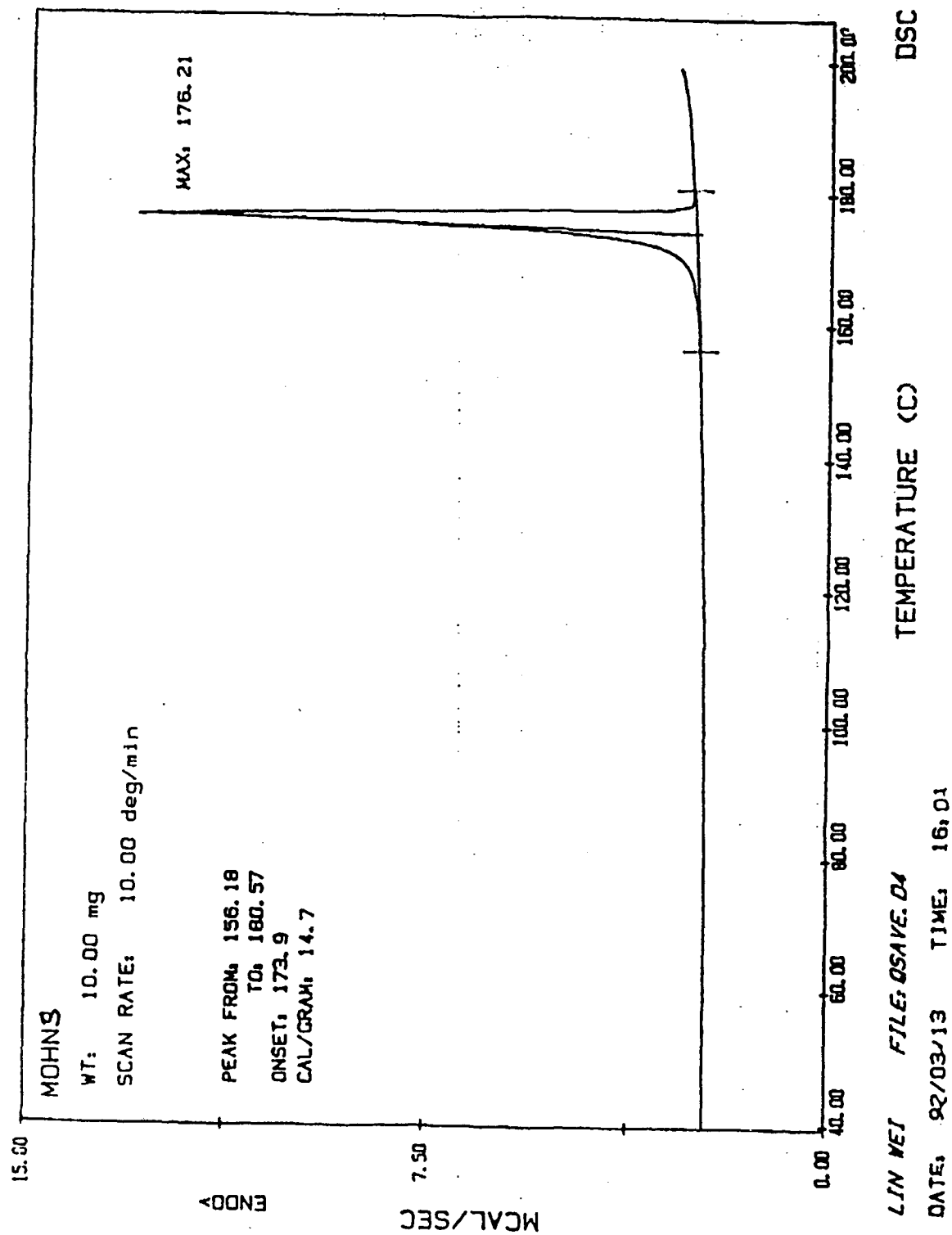WT: 10.00 mg
SCAN RATE: 10.00 deg/min

PEAK FROM: 156.18
        TO: 180.57
ONSET: 173.9
CAL/GRAM: 14.7

MAX, 176.21

15.00

7.50

ENDO▼

MCAL/SEC

40.00   60.00   80.00   100.00   120.00   140.00   160.00   180.00   200.00

TEMPERATURE (C)

0.00

DSC

LIN WEI   FILE: QSAVE.04

DATE: 92/03/13   TIME: 16:01

Figure 5.10 Spectrum of MOHMS by Differential Scanning Calorimeter

The original curves of absorption spectra are shown in Figures 5.11, 5.12, 5.13 and 14.

The synthesized new materials are shown in Figure 5.15.

5.4 Summarization of Measurement Results

The summarized experimental results are listed in Table 5.5.

ah-44FR-TX3
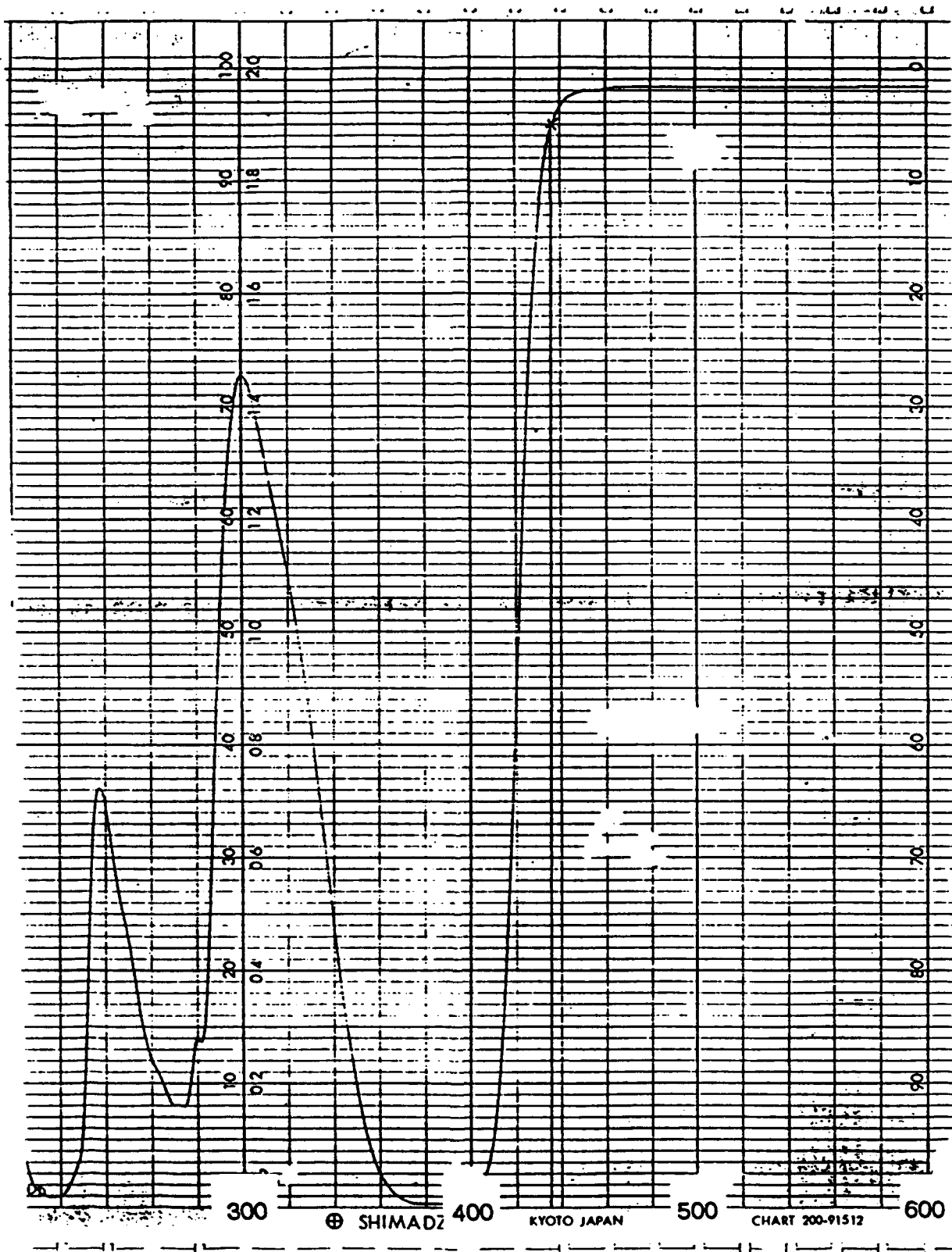
Figure 5.11 Absorption Spectrum of CMVI by UV Spectrometer
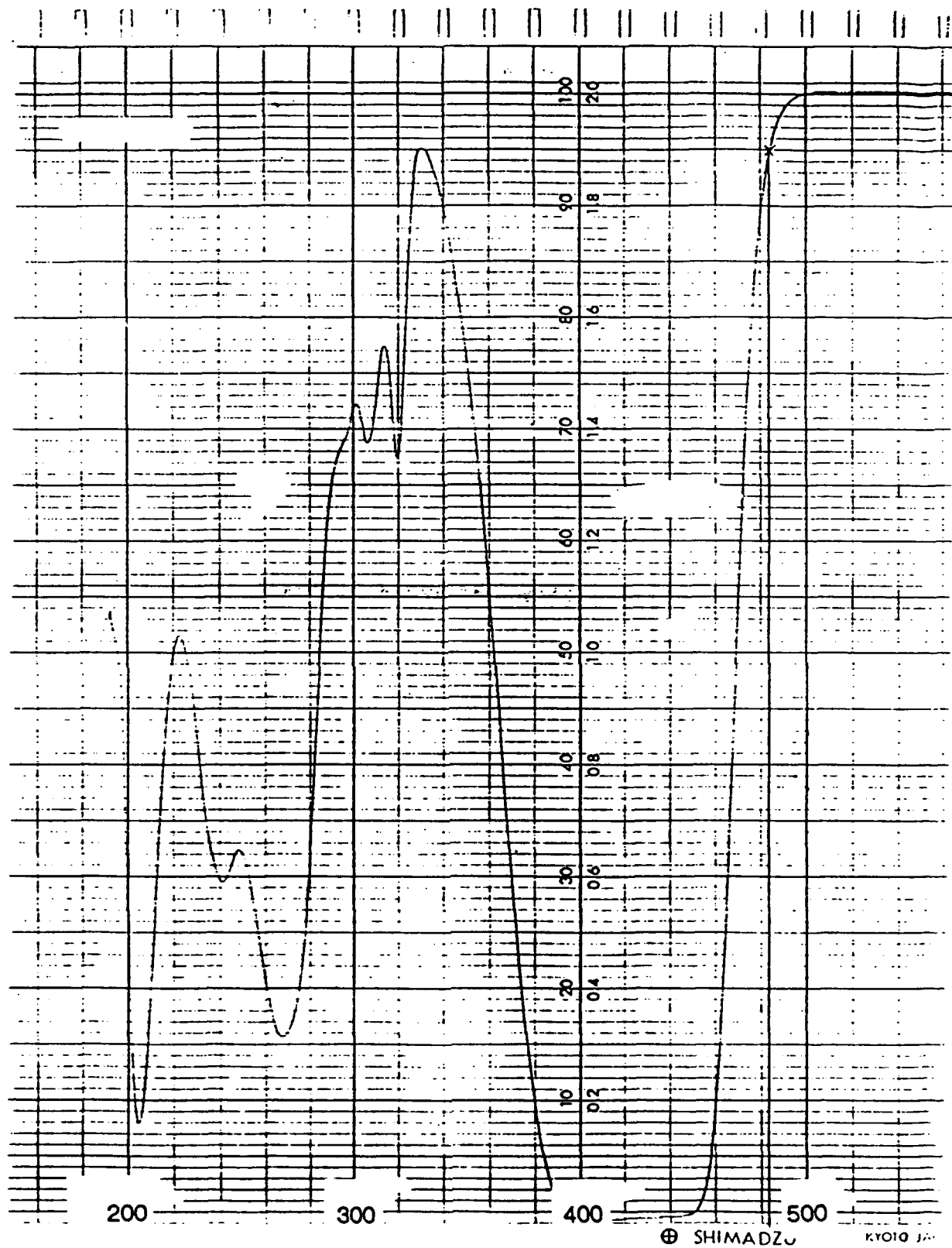
Figure 5.12 Absorption Spectrum of DVDA by UV Spectrometer
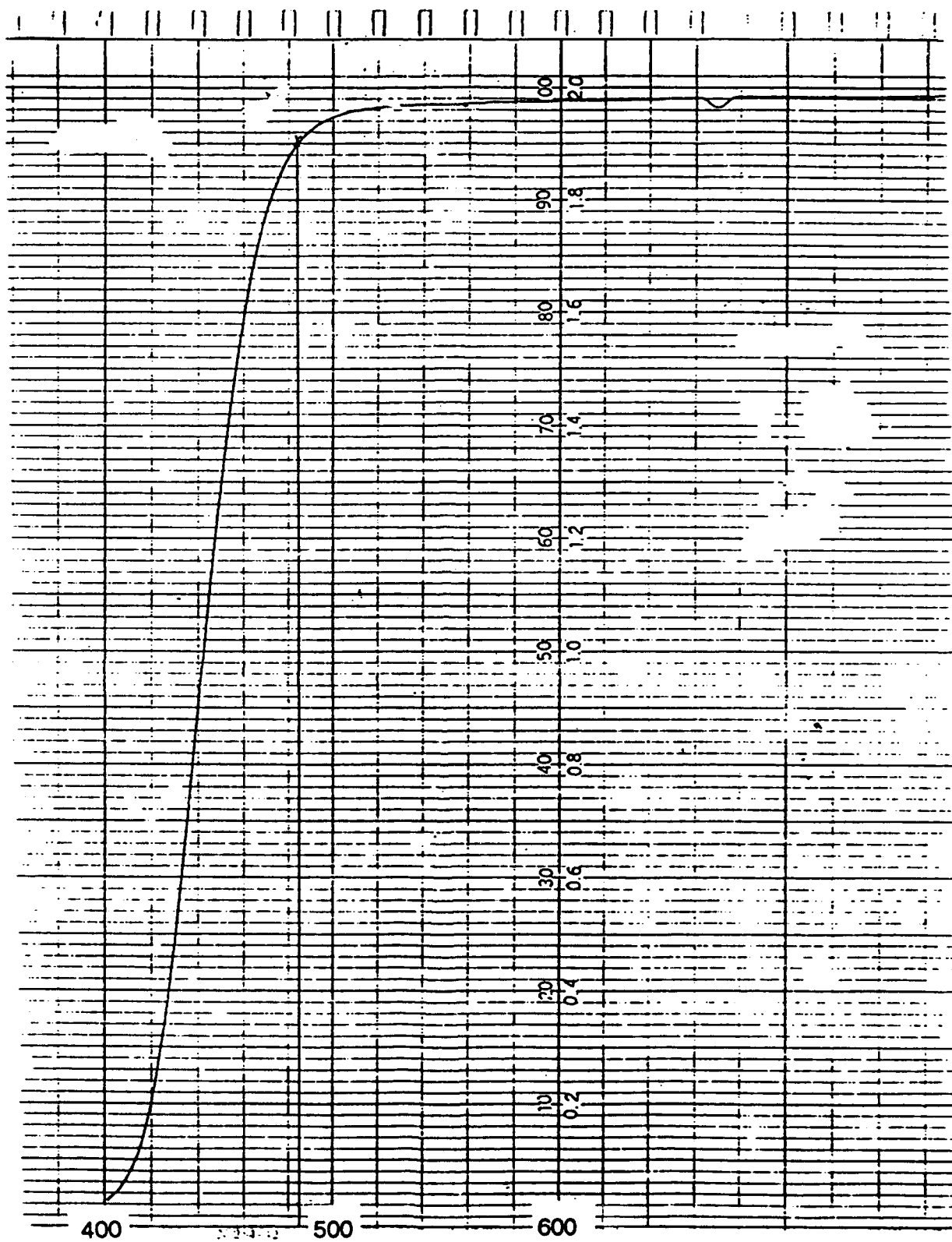
Figure 5.13 Absorption Spectrum of HMONS by UV Spectrometer
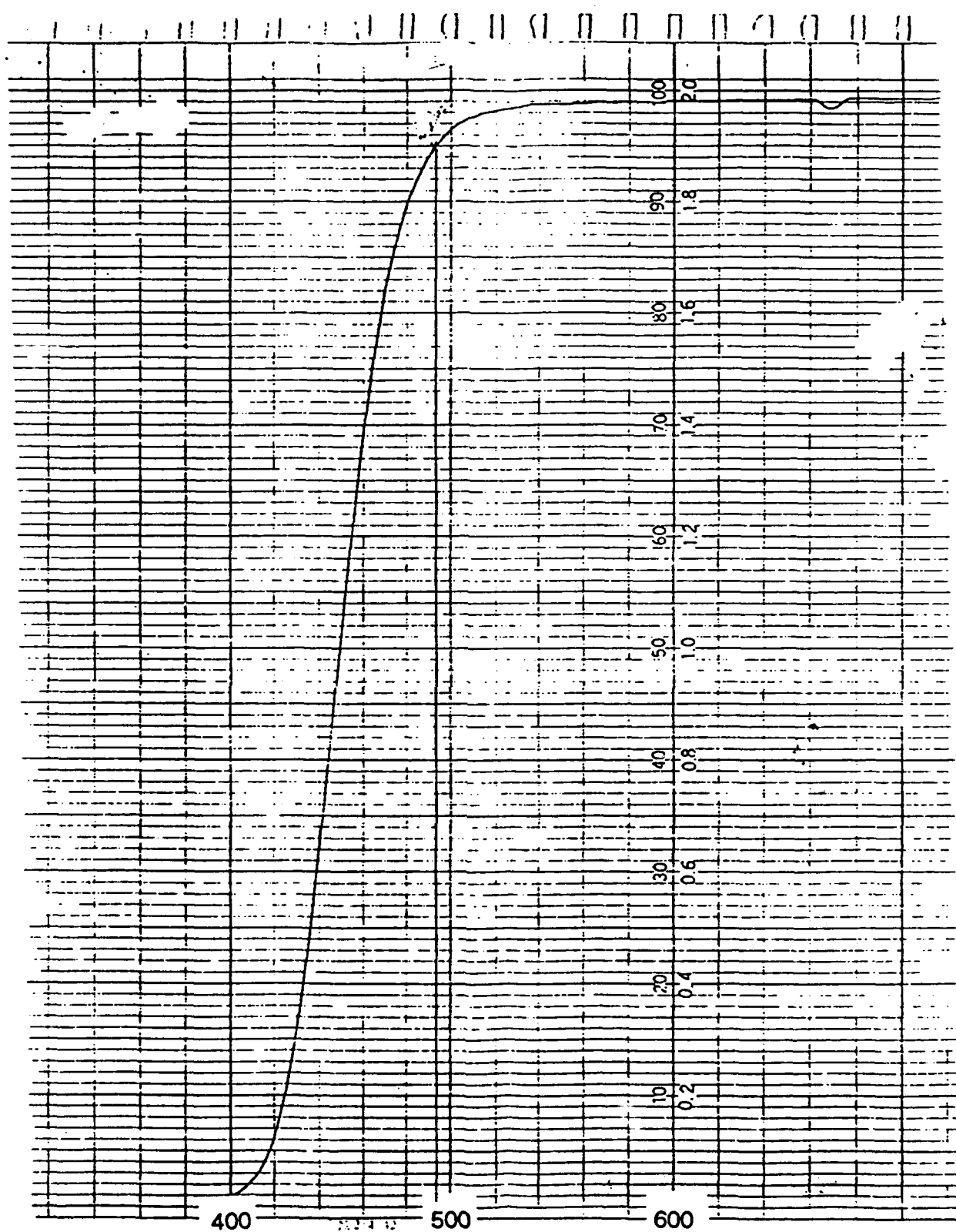
Figure 5.14 Absorption Spectrum of MOHNS by UV Spectrometer

Table 5.5
Experimental Results of Synthesized Materials

Number	Name	Composition Analysis						Color	Melting Points (C°)	Absorption Edge
		Theoretical (%)			Experimental (%)					
		C	H	N	C	H	N			
1	CMVI	70.00	5.00	11.67	70.27	5.12	11.72	Light Yellow	163.8-165.7	435
2	DVDA	73.10	5.58	21.32	73.10	5.43	21.41	Orange Red	181.1-183.2	485
3	HMONS	66.42	4.80	5.17	66.36	4.60	5.36	Yellow	179.8-181.5	485
4	MOHNS	66.42	4.80	5.17	66.80	5.00	5.11	Golden Yellow	172-173	495

Figure 5.15 The Four Synthesized Organic NOMs

6.0 Optical Nonlinearity Characterization

The four selected organic NOMS have been successfully synthesized and purified (98% purified) and the basic physicochemical properties of these four materials have been fundamentally measured, see Chapter 5.0. The optical nonlinearity characterization of these four organic NOMS has been sumarized in this chapter.

6.1 Demonstration of Second Order Optical Nonlinearity $\chi^{(2)}$ by Using SHG in Powder

A general method for demonstrating the second order optical nonlinearity in molecule level is to use the so called "powder effect" technique - which is the *Second Harmonic Generation* (SHG) in NOM powder form. The fabrication of NOM powder is described as follows:

- Drying the four new materials of CMVI, DVDA, HOMNS and MOHNS after purification,

- Grinding the purified new materials into powder in an agate mortar (see Figure 6.1),

- Filtering the Grinded new materials by using a two-layer sifter with an up screen hole dia. of 98 μm, lower screen hole dia. of 76 μm,

- The remainder (see Figure 6.2) between the two screens are samples to be used for $\chi^{(2)}$ demonstration by second
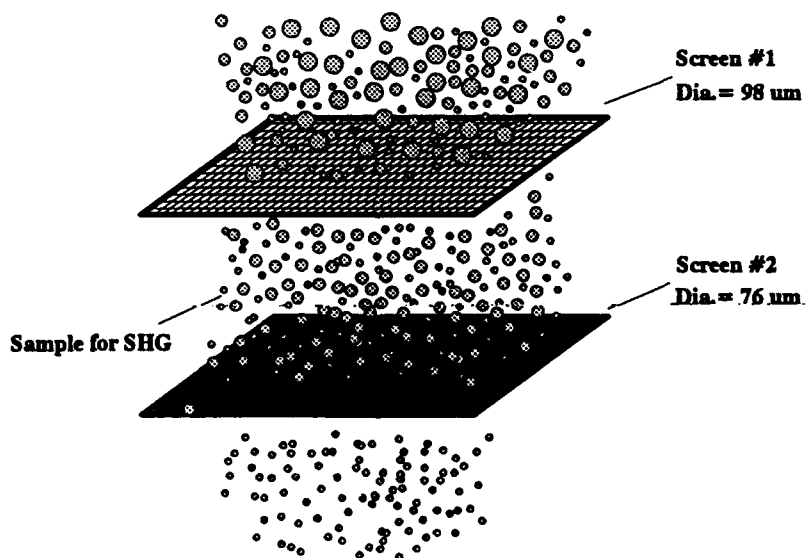
ah-44FR-TX3
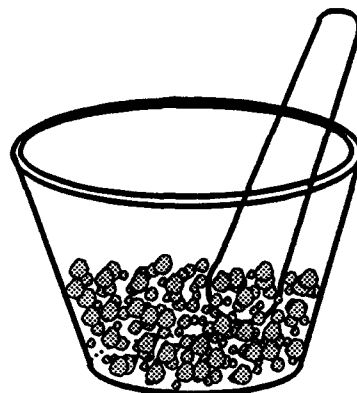
Figure 6.1 Grinding Sample In An Agate Mortar

Screen #1
Dia. = 98 um

Screen #2
Dia. = 76 um

Sample for SHG

Figure 6.2 Powder Filtering With A Two-Layer Sifter

61-powder

harmonic generation (SHG) powder effect. Their sizes are 76 – 98 μm.

Place prepared powder samples in a SHG sample box of diameter 9 mm, thickness 1 mm. The second order nonlinearities in powder have been demonstrated by using a Q-switched Nd-YAG laser, with wavelength 1064 nm, and 1 kw peak power to measure the SHG output after these samples. The experimental setup is shown in Figure 6.3. The measurement results are shown in Table 6.1. And the green light output (532 nm, SHG of 1.06 μm Nd:YAG laser) are shown in Figures 6.4, 6.5 and 6.6.

Table 6.1
SHG Intensity of These NOM Powders

Number	Name	Size	Color	SHG (532 nm) Intensity
0 (Standard)	Urea	76 – 98	White	1
1	CMVI	76 – 98	Light Yellow	2.5
2	DVDA	76 – 98	Orange Red	4
3	HMONS	76 – 98	Yellow	0
4	MOHNS	76 – 98	Golden Yellow	9

6.2 Characterization of Third Order Optical Nonlinearities $\chi^{(3)}$

We have performed a preliminary study on the four organic materials, namely MHONS, HMONS, DVDA and CMVI, all in solution in ethanol. The method we have used is the Z-scan technique, which

ah-44FR-TX3
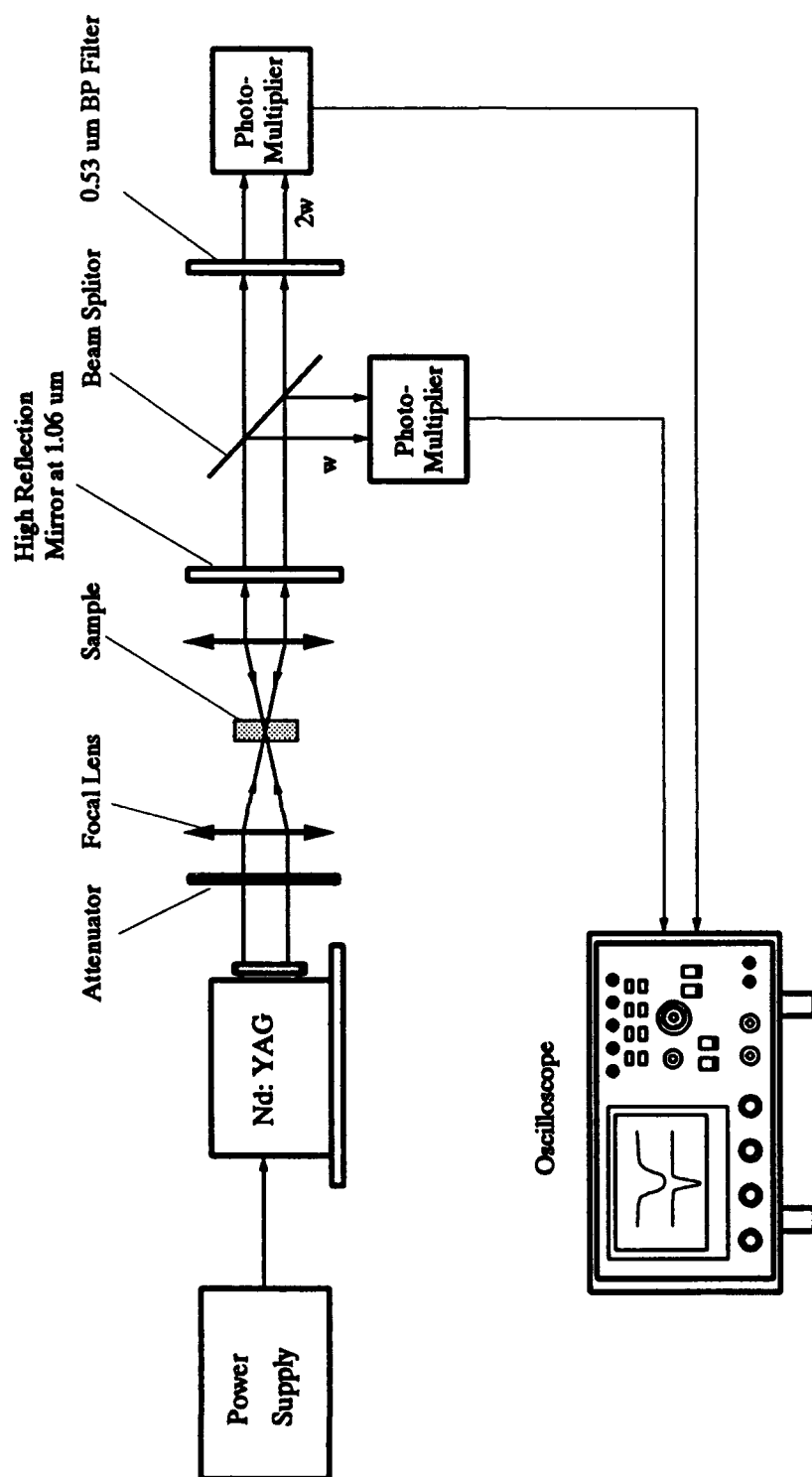
Figure 6.3 The Schematic Diagram of SHG Signal Analysis

Figure 6.4 SHG Signal (532 nm, Green) from a Q-Switched Nd:YAG Laser in CMVI Powder
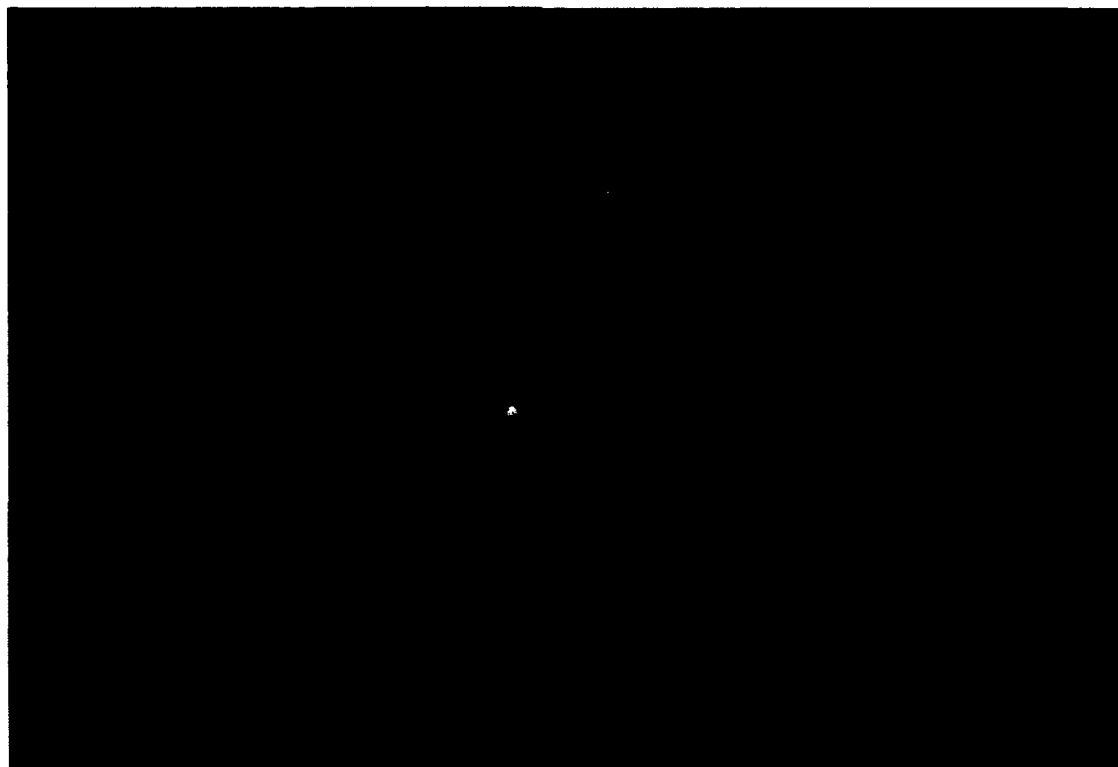

Figure 6.5 SHG Signal (532 nm, Green) from a Q-Switched Nd:YAG Laser in DVDA Powder
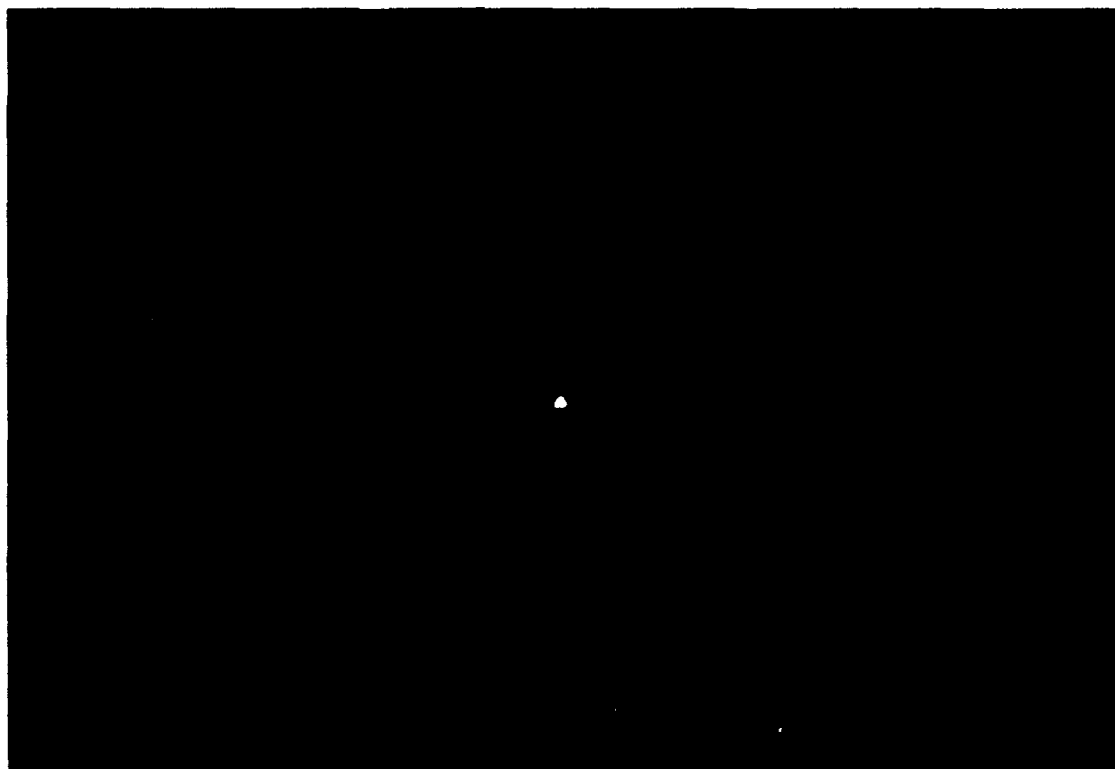
Figure 6.6 SHG Signal (532 nm, Green) from a Q-Switched Nd:YAG Laser in MOHNS Powder

measures both the sign and magnitude of nonlinear index changes, along with nonlinear absorption. These methods were performed with 30 psec pulses at the fundamental and second harmonic wavelengths of a modelocked Nd:YAG laser, i.e. 1064 nm and 532 nm. such pulsewidths are short enough to avoid thermal and electrostrictive nonlinearities which can mask the true bound electronic nonlinear refraction. However, the experiment would have to be repeated at other pulsewidths to be certain that the nonlinearities are due to ultrafast bound electronic nonlinearities rather than excited state effects. This will be elaborated on in the following section.

6.2.1 Z-Scan Technique

The Z-scan technique is based on the transformation of phase distortions to amplitude distortions during beam propagation. The Z-scan experimental apparatus is as shown in Figure 6.7 where the sample is moved along the propagation direction z while keeping the input pulse energy fixed. A qualitative physical argument that explains the transmittance variations in the Z-scan experiment can be given as follows. Starting the scan from a distance far away from the focus (negative z), the beam irradiance is low and negligible nonlinear refraction occurs leading to linear transmittance. We normalize the linear transmittance to unity. As the sample is brought closer to the focus, the beam irradiance increases leading to self-lensing in the sample. A negative self-lensing prior to focus tends to collimate the beam and reduce the diffraction leading to a smaller beam at the aperture and an
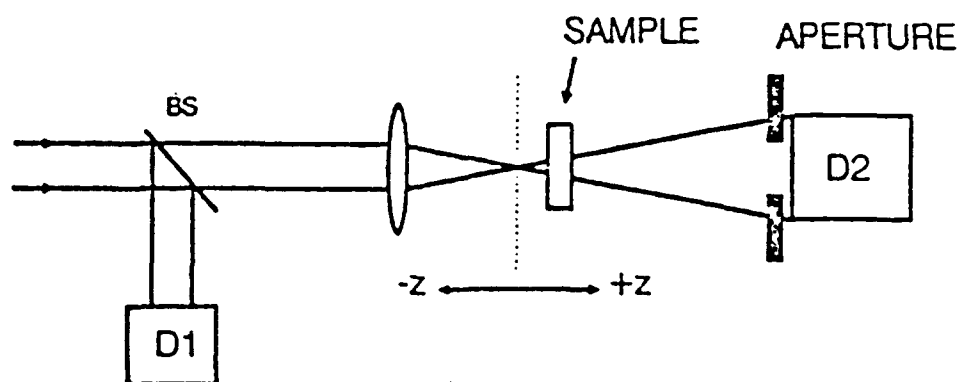
Figure 6.7 Z-Scan Experimental Geometry

increased transmittance. As the scan continues and the sample crosses the focal plane to the right (positive z), the same self-defocusing effect will tend to augment diffraction and reduce the aperture transmittance. A pre-focal transmittance maximum (peak) and a post-focal transmittance minimum (valley) are, therefore, the Z-scan signature of a negative nonlinearity while a positive one, following the same analogy, will given rise to an opposite valley-peak configuration, as depicted in Figure 6.8. With a small phase shift and a thin sample, the peak and valley are symmetrically positioned about the focal plane and are separated by a distance $\Delta Z_{p-v} \propto 1.7 z_0$. Numerical simulations have shown that the difference between peak and valley transmittances, ΔT_{p-v} is linearly related to the nonlinearly induced phase shift, $\Delta \Phi_\sigma$.

$$\Delta T_{p-v} = 0.406 (1-S)^{0.25} |\Delta \Phi_0|$$

This feature makes rapid determination of nonlinear refraction very straightforward.

The effects of nonlinear absorption may be independently seen by fully opening the aperture, rendering the experiment insensitive to nonlinear refraction. The nonlinear absorption causes a decrease in transmission near the focus, assuming reverse saturable absorption, such as two-photon absorption (2PA). Such a result is shown in Figure 6.9(a). Partially closing the aperture gives a combination of refractive and absorptive signals as shown in Figure 6.9(b). However, for small transmission changes, the
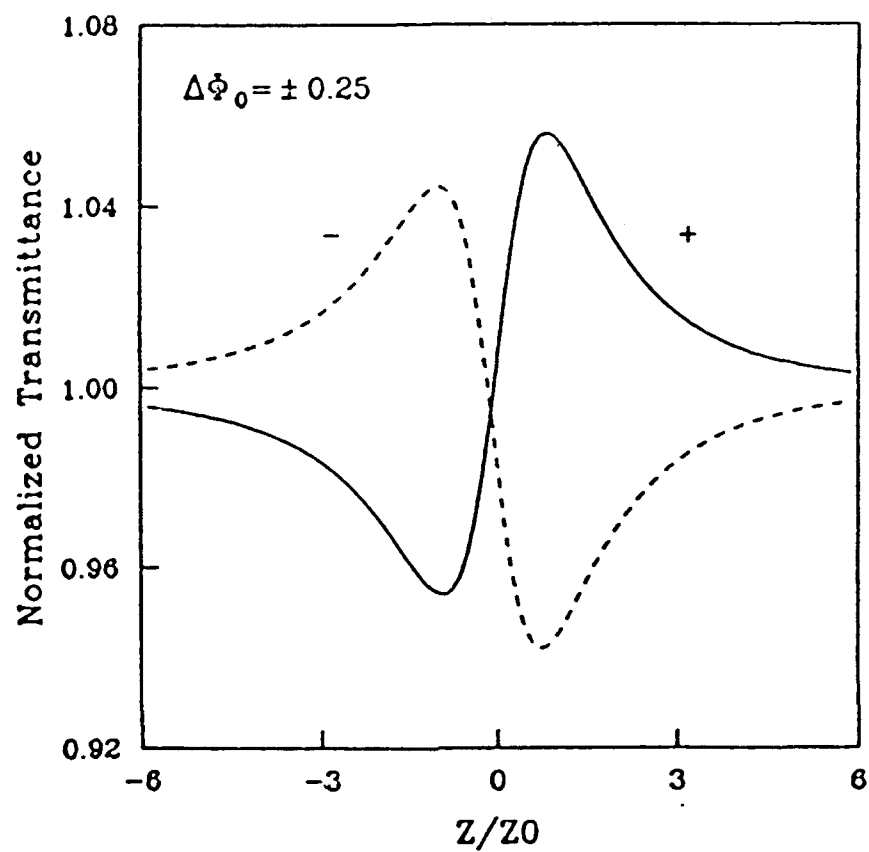
107

ah-44FR-TX3

Figure 6.8 Theoretical Plots of Z-Scan for Positive and Negative Nonlinear
Refraction

108

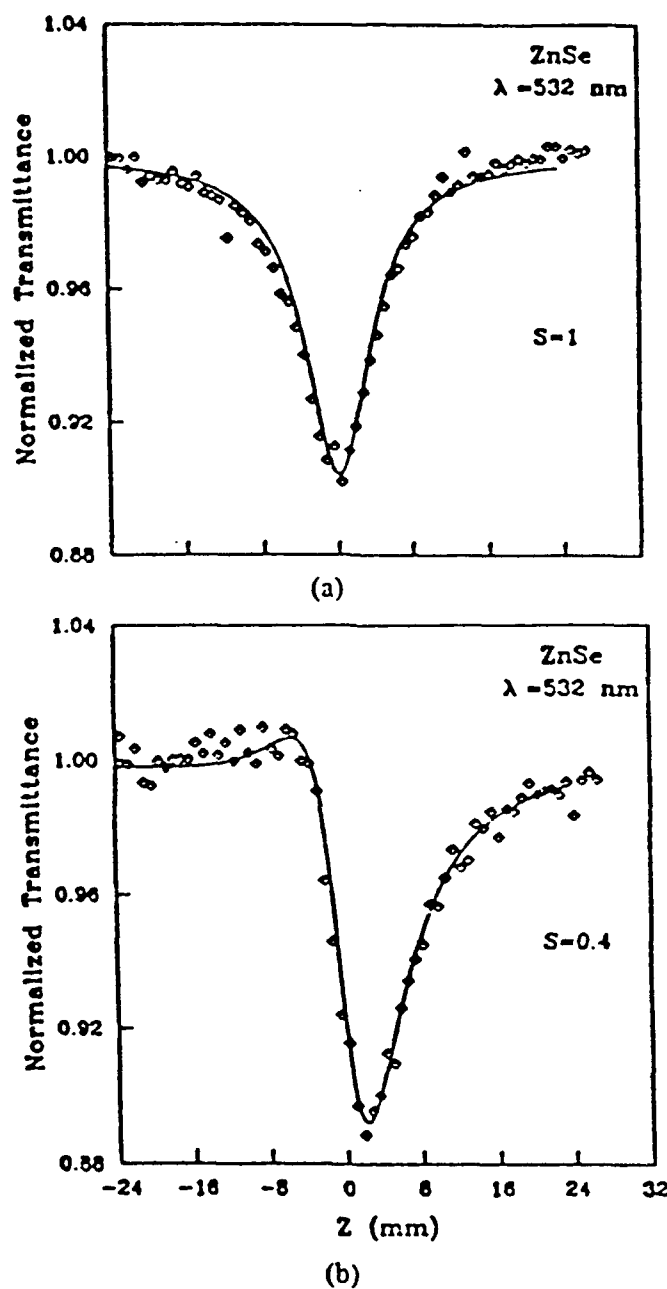Figure 6.9 (a) Open Aperture Z-Scan for the Two Photon Absorber ZnSe at
λ = 532 nm, (b) Closed Aperture Z-Scan.

refractive component is returned simply by dividing the closed aperture data by the open aperture data. The resulting signal has a ΔT_{p-v} that is within 1% of that which would be obtained if no absorption had been present. Such a result is shown in Figure 6.10.

6.2.2 Measurement of Organic Nonlinear Materials

The four samples MHONS, HMONS, DVDA and CMVI were dissolved in ethanol to concentrations of 10^{-2} M or as high as could be obtained without aggregation of the molecules. This could be seen to occur in HMONS and DVDA, so they were further diluted to 5×10^{-3} M. The experiments were performed using a picosecond Q-switched and modelocked Nd:YAG laser, which produces 25 psec (FWHM) at a wavelength of $\lambda = 1.064$ μm. Frequency doubling in KDP gives 17 psec pulses at $\lambda = 532$ nm. Z-scans were performed at both of these wavelengths for all four samples. The Z-scan data are shown in Figures 6.11, 6.12, 6.13 and 6.14. For each each material and wavelength, measurements were made at several irradiances, up to ≈ 15 GW/cm^2 in order to check the order of the nonlinearity. For example if we are measuring $\chi^{(3)}$ such as 2PA or n_2 effects, the nonlinear phase shift must be linearly rated to the input irradiance. In all our measurements, this was found to be the case.

The results obtained are quoted in terms of n_2 and β, defined as
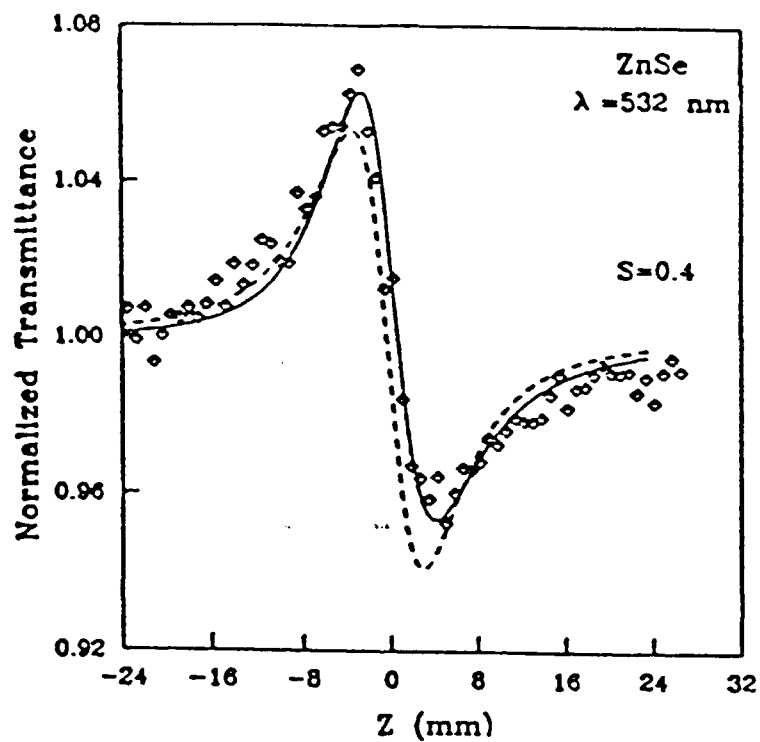
$$n = n_o + \frac{n_2 |E|^2}{2},$$

Figure 6.10 Divided Z-Scan for ZnSe, Obtained by Dividing the Data of
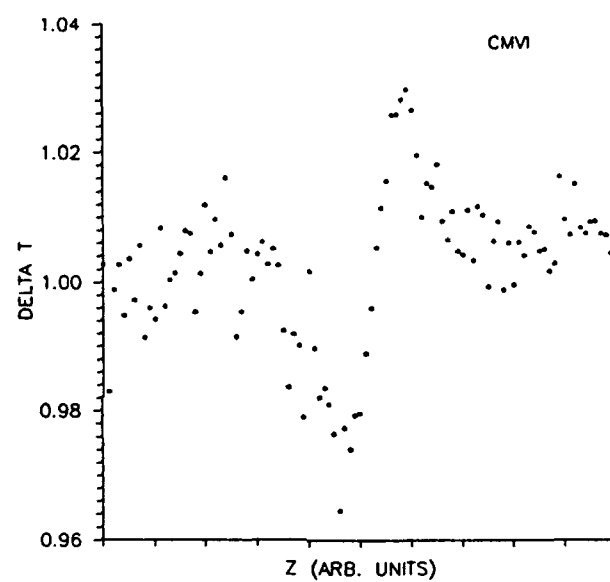Figure 6.9(a) by the Data of Figure 6.9(b).

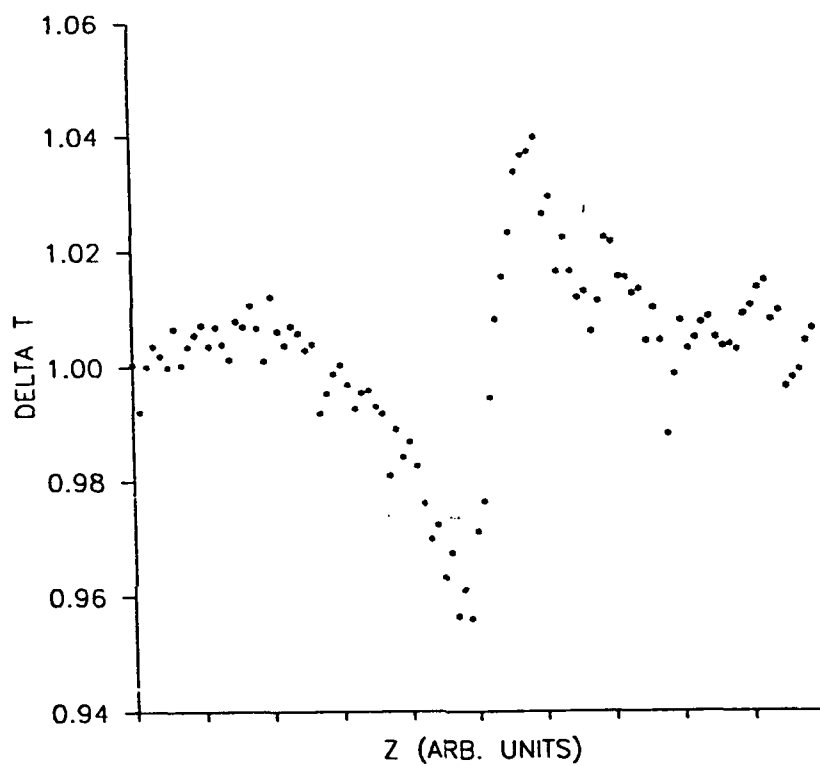Figure 6.11 Z-Scan of CMVI at 532 nm and an Irradiance of 8 GW/cm^2

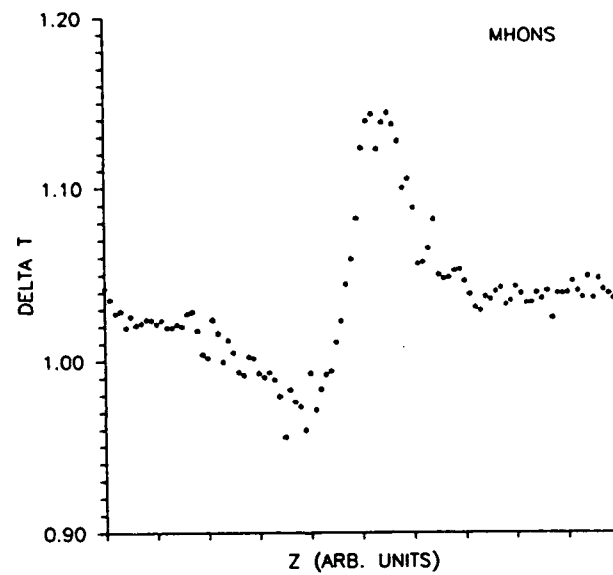Figure 6.12 Z-Scan of DVDA at 532 nm and an Irradiance of 8.7 GW/cm^2

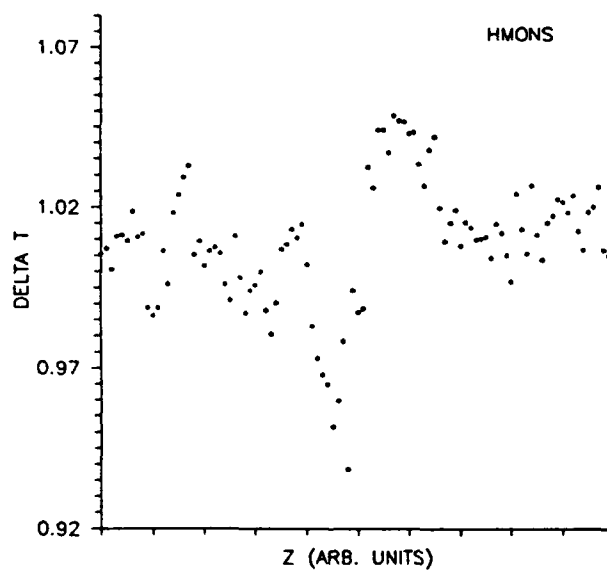Figure 6.13 Z-Scan of MHONS at 532 nm and an Irradiance of 6.8 GW/cm^2

114

Figure 6.14 Z-Scan of HMONS at 532 nm and an Irradiance of 8.8 GW/cm^2

$$\frac{dI}{dz} = -\beta I^2$$

Typically, n_2 is expressed in $cm^2/statvolt^2$ (often just written as "esu") and β, the 2PA coefficient, in cm/GW. We will conform to this standard of notation. The results are summarized in Table 6.2. It should be noted that no attempt has been made to determine if these nonlinearities are truly 2PA and the bound electronic Kerr effect.

6.2.3 Discussion

(i) Nonlinear Absorption

The absence of nonlinear absorption at 1.064 μm is as expected, as this wavelength shows weak linear absorption and there are few states at the two photon energy to couple into. Thus both 2PA and excited state (two-step) absorption are not expected or observed. The nonlinear absorption in the MHONS is quite large. As stated previously, it is ambiguous as to whether this is true two-photon or excited state absorption. If this were deemed to be of interest, pulsewidth dependent studies could be performed to determine this.

(ii) Nonlinear Refraction

This data should be interpreted by substracting off the value of n_2 for pure ethanol. The data shows the nonlinear refraction

ah-44FR-TX3

Table 6.2 Third-Order Nonlinearity Characterization of These Four Materials

SAMPLE	λ Cutoff	Concentration	$\lambda = 532\ nm$ $\tau_p \sim 17\ ps$		$\lambda = 1.064\ nm$ $\tau_p \sim 25\ ps$	
			n_2 (esu)	Nonlinear Abs. β (cm/GW)	n_2 (esu)	Nonlinear Absorption
Ethanol (sovent)	-	-	1.4×10^{-13}	0	9×10^{-14}	0
MHONS	495 nm	10^{-2} M	3.6×10^{-13}	0.5	1×10^{-13}	0
HMONS	485 nm	5×10^{-3}M	1.6×10^{-13}	0.09	Not measurable	0
DVDA	485 nm	5×10^{-3}M	1.4×10^{-13}	0	1.1×10^{-13}	0
CMVI	435 nm	10^{-2} M	1.4×10^{-13}	0	1.2×10^{-13}	0

to be small in all four materials, perhaps with the exception of MHONS. This again could be due to excited states with refractive "cross sections" larger than the ground state cross sections. Thus, once again, the study of MHONS at different pulwewidths would seem to be the most interesting way to proceed with further studies.

ah-44FR-TX3

7.0 Investigation of Device Application and Fabrication

The beauty of utilizing organic NOM is that these materials cam be fabricated into a variety of types of devices, for example, incorporating the organic molecules in a transparent polymer to form a thin film of the polymer. It is also possible to grow these highly polarized materials into amorphous or polycrystalline solids. In addition to crystalline materials, the nonlinear organic polymers are now being used to make a new family of active waveguide devices, and could allow the cost-effective manufacture of much higher-bandwidth optical modulators.

The traditional way to fabricate NOM devices is to grow the materials into crystals. E-Tek's engineers have this experience and have conducted further investigation to grow the NOM single crystals in different forms.

- Bulk crystal growth using Bridgman method is shown in Figure 7.1.
- Single crystal growth in a cored fiber is shown in Figure 7.2.
- Film single crystal growth is shown in Figure 7.3.

Several methods could be applied to forming NOM polymers. They are:

- Monomer-doped polymer (complex)
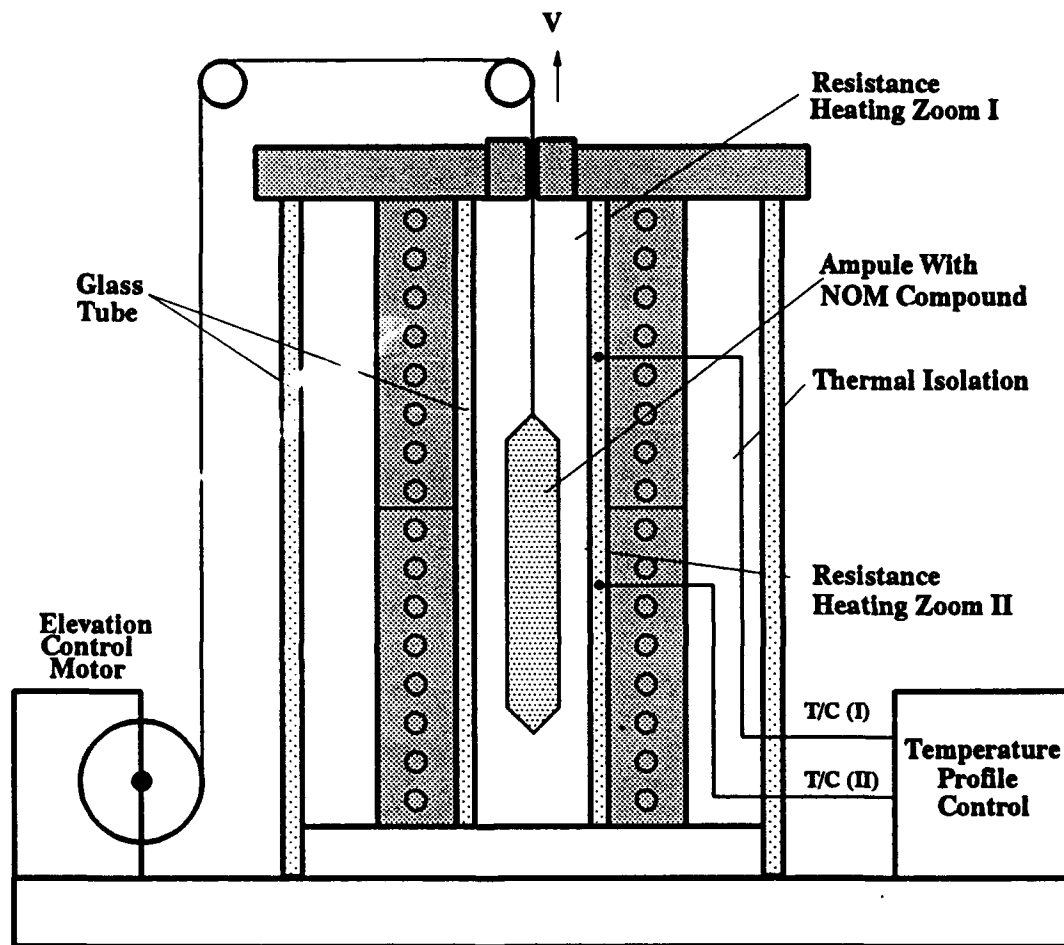- Monomer-pendant polymer (compound)

119

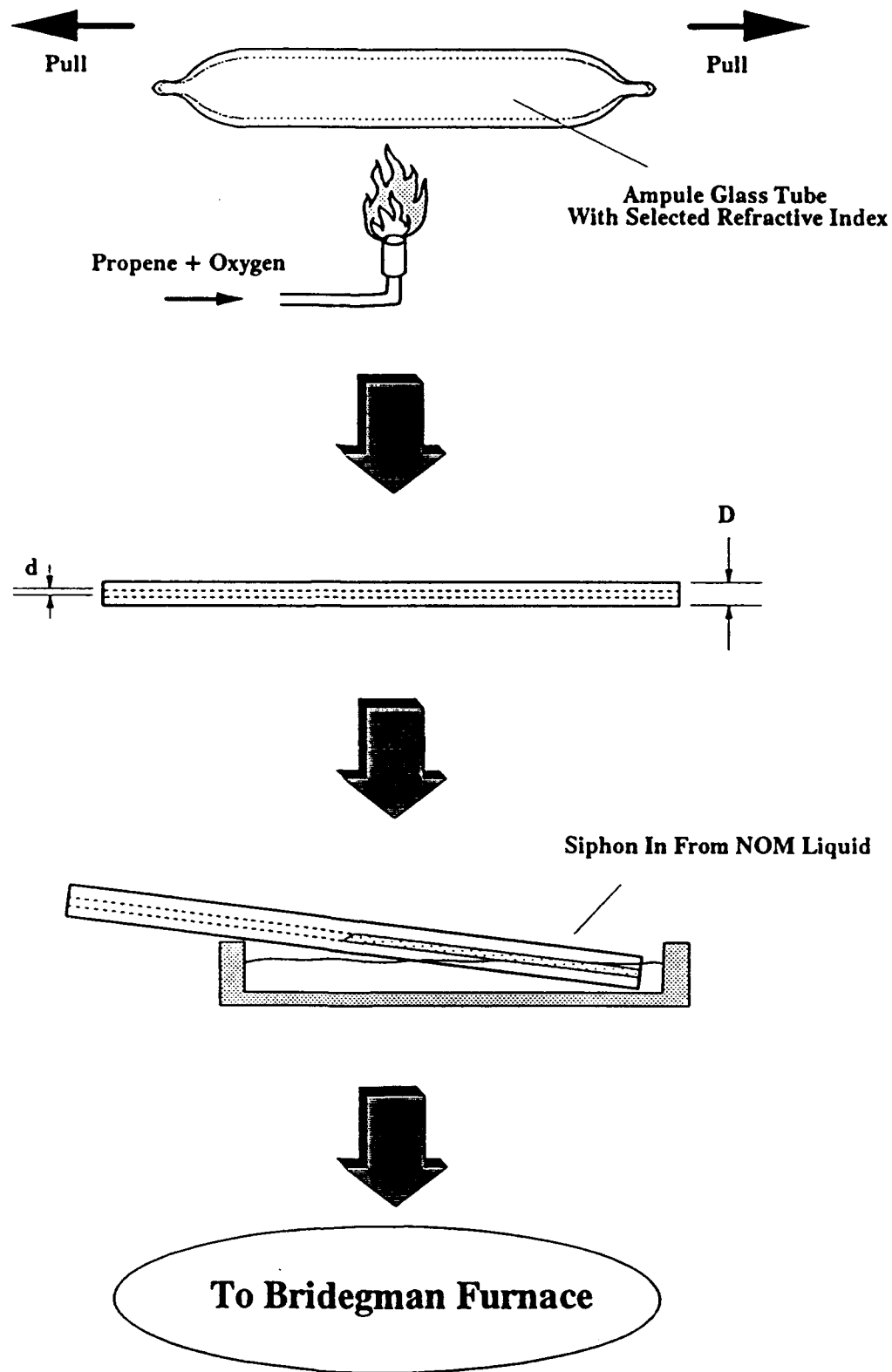**Figure 7.1 Single Crystal Growth Using Bridgeman Method**

61-44crystal

Figure 7.2 Crystal Growth in a Cored-Fiber

NOM Film

Rotating Direction

Heat Conductor

T/C

V

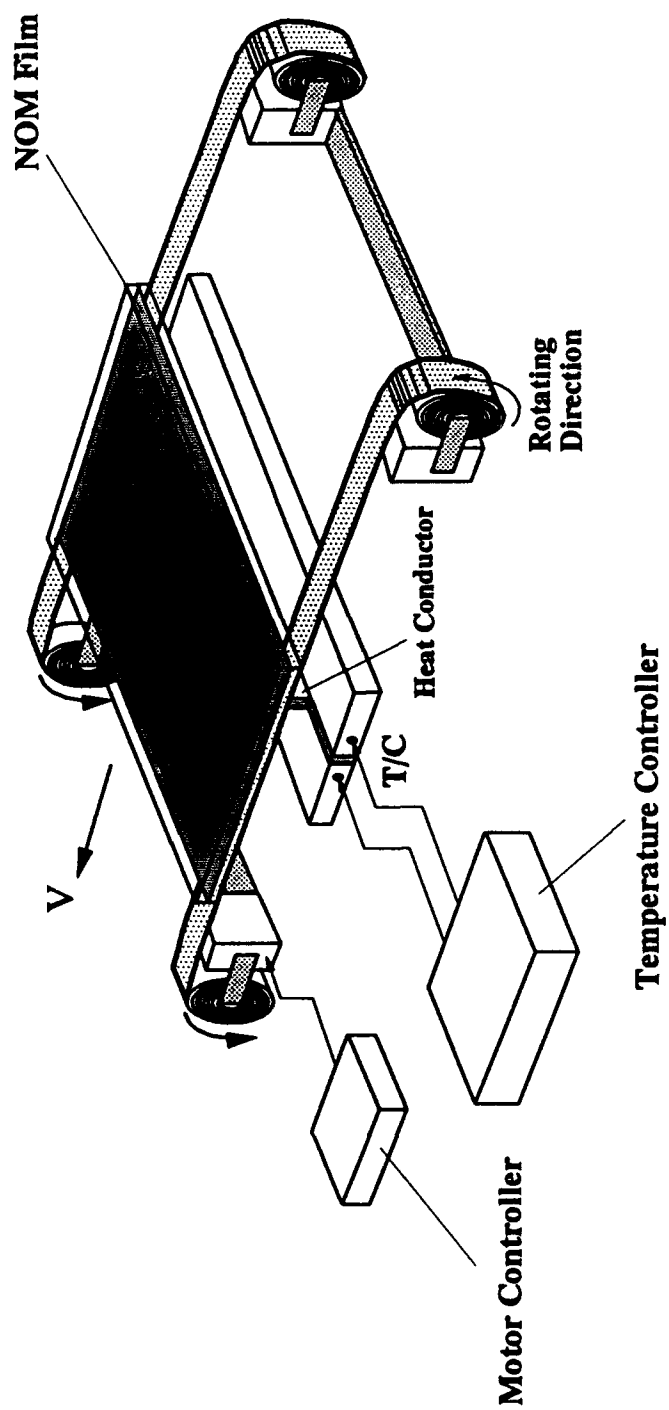**Temperature Controller**

Motor Controller

Figure 7.3 Single Crystal Thin Film Fabrication

61-44nn

- π-conjugated (self-polymerization)

Organic polymers exhibit better mechanical properties than organic thin-film crystals (fully conjugated small molecules). The π-electron conjugated organic polymers are of potential importance in relation to optical devices, such as optical switches and logic gates, because of their large nonlinearities $\chi^{(3)}$.

Polymers of long conjugated molecules have a tendency to possess high third-order optical nonlinearities, due to the resonate effects. However, tradeoffs include increased absorption in the longer wavelengths in the visible light region and longer response times. So E-Tek engineers are currently concentrating on researching and developing new organic molecules which possess high optical nonlinearities and will then later fabricate them into NOM polymer form.
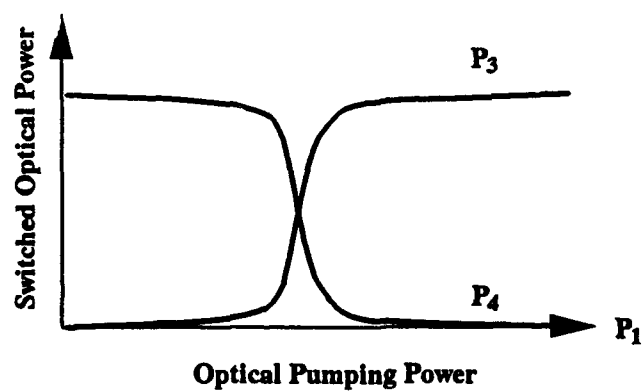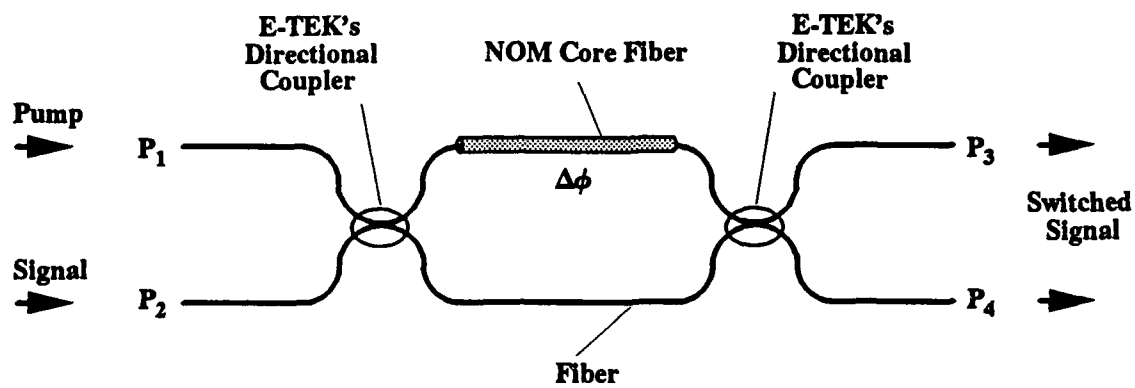
High efficient third-order nonlinear optical materials have many applications:

- Optical switch,
- Optical logic gate,
- High speed multiplexer,
- Reconfigurable interconnector,
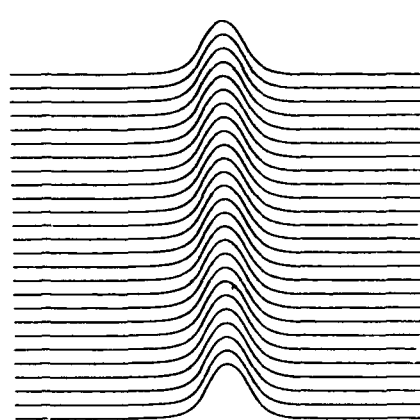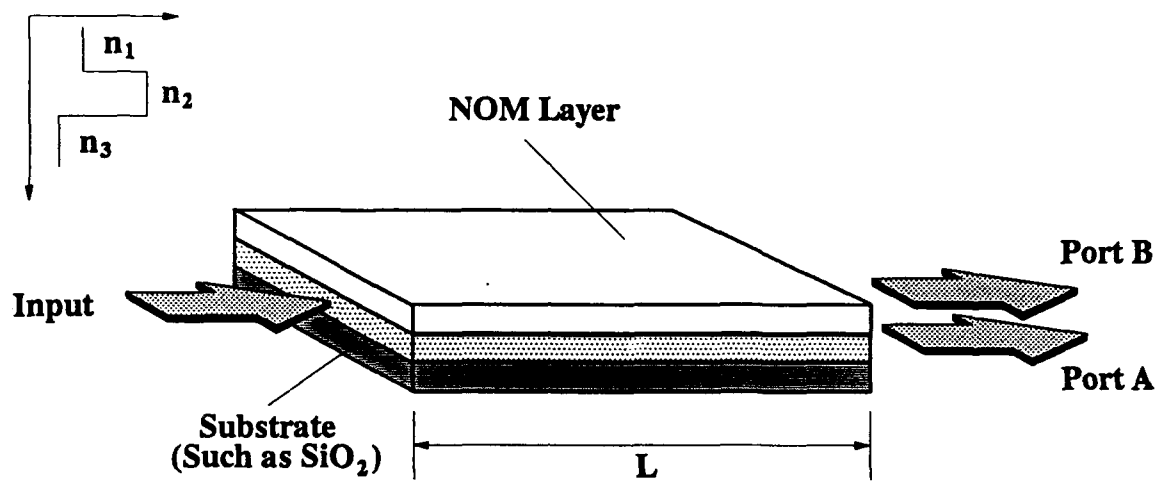- Bistable memory, and
- Power limiter.

However, using inorganic bulkcrystals has many shortcomings, including:

- High cost,

- Fabrication and processing complexity,

- Poor compatibility with other electronic devices,

- Velocity matching required for high-speed and wide-band operation,

- High optical power required due to low nonlinear susceptibility,

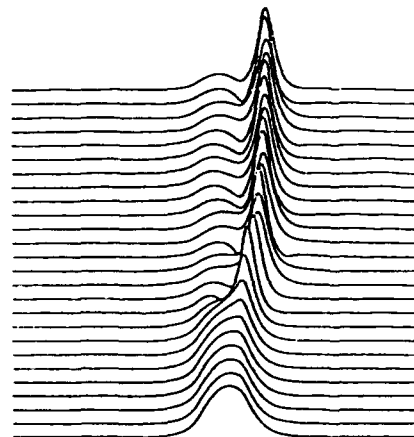- Difficult to implement all-optic devices/components/ circuits.

For example, the single crystal in cored-fiber maybe utilized in a Mach-Zehnder Interferometric Fiber Type All-Optic Switch (see Figure 7.4). The slab waveguide type of All-Optic Switch Using Multilayer NOM films (see Figure 7.5).

ah-44FR-TX3

Pump → P₁

Signal → P₂

E-TEK's Directional Coupler

NOM Core Fiber

$\Delta\phi$

E-TEK's Directional Coupler

P₃ →

Switched Signal

P₄ →

Fiber

$$\Delta\phi = 2\pi\Delta n(\lambda_p)L/\lambda_s$$

Figure 7.4 All Optical Switch
(Fiber Mach-Zehnder Interferometric Type)

n₁
n₂
n₃

NOM Layer

Input

Substrate
(Such as SiO₂)

L

Port B

Port A

A: Low Power Input

B: High Power Input

Forming Method:

- Ion Exchange (for n_2)
- Deposition (for NOM Layer)
- Single Crystal Growth in Film (for NOM Layer)

**Figure 7.5 All Optical Switch
(SLAB Wave Guide Type)**

61-SLAB

8.0 Summary and Recommendation

8.1 Summary

Organic materials with high third-order nonlinearities, high damage threshold, broad transparent bands and fast response times are highly prospective candidates for all optical devices. The technical objectives of this Phase I R&D project are to design, synthesize new organic NOMs, characterize their physicochemical properties and demonstrate their optical nonlinearities and response times. In this Phase I R&D project, four newly designed materials have been synthesized. Their optical nonlinearities, melting points (damage threshold) and absorption spectra have been obtained. The estimated optical nonlinearities in molecular level are not exceptionally big. However, the melting points of these four materials are higher than most of the other organic NOMs such as DAN $166°C$ and MMONS $109°C$, and the absorption edges of these four materials are all lower than 495 nm.

The R&D results obtained during Phase I project have demonstrated, both theoretically and experimentally, our approach of design, research and development of new high-efficient organic NOMs.

The experimental results will enrich the design theory of new optical material. Additionally, each of the new materials may lead to commercially viable optical crystal and devices.

ah-44FR-TX3

8.2 Accomplishment of Phase I R&D

E-Tek Engineers have performed Phase I R&D tasks, including the invention of innovative designs, development of synthesis approaches, and experimental measurements. These design and fabrication guidelines will lead to the success of Phase II further investigation on new materials and device fabrication. A comparison of Phase I proposed tasks with Phase I actual achievement is summarized in Table 8.1.

ah-44FR-TX3

Table 8.1 Proposed Phase I Tasks and Actual Achievements

Proposed Phase I Task	Task Accomplished	Highlights of Phase I Achievement
• Theoretical study, design and investigate the possible compounds	Yes	• Theoretically investigate design principle for new materials. • Design eight possible components and investigate several other components.
• Set up equipment for chemical and physical experiments	Yes	• Set up chemical equipment for synthesizing the four new material • Set up experimental system for optical nonlinearity demonstration • Set up experimental system for melting point, absorption spectra.
• Synthesize newly designed materials	Yes	• Synthesize four newly designed materials. • Purify these materials to above 98%. • Determine molecular structure.
• Measure physical and chemical parameters of new materials	Yes	• Determine chemical composition of four materials. • Measure melting points of these materials. • Measure absorption spectra of these materials.
• Demonstrate of second-order optical nonlinearity in powder	Yes	• Prepare samples into powders of 70 μm - 100 μm. • Demonstrate the second harmonic generation in new materials.
• Characterize the third-order optical nonlinearity and response time	Yes	• characterized by Z-scan technique.
• Investigate device fabrication	Yes	• Single crystal • Polymer
• Investigate of device application	Yes	• Mach-Zehnder Interferometric all optical switch. • Slab waveguide type all optical switch.

129

ab-64444FR-TB1

Acknowledgement

ah-44FR-TX3